Modeling Steam Locations During a Steam Injection Process for Subsurface Gasoline Spill

Contents

Modeling Steam Locations During a Steam Injection Process for Subsurface Gasoline Spill

Kent M. Kenneally

Abstract

Thermal modeling was performed to determine the location of subsurface steam zones during a steam injection process to remove gasoline. The principal model used was the Marx-Langenheim relation. There was good agreement between the model's predicted location and actual location obtained from field data at specified points. Model results and an overall energy balance offer excellent agreement of a total injected steam volume of 166,000 m^3.

1. Introduction and Background

1.1 Project and Site Description

A steam injection remediation process has been successfully completed at the Lawrence Livermore National Laboratory. Beginning February 4, 1993, steam was injected below and above the water table in an effort to clean up gasoline contaminated soil within water-bearing zones. The gasoline was distributed 20 m to 35 m below the surface. Estimates of the spill size vary from 23,000 to 64,000 liters.

Six injection wells were placed around the perimeter of the area contaminated by gasoline; they were constructed to allow separate injection above and/or below the water table. Two recovery wells were located near the center of the zone. Twelve temperature wells were placed throughout the site in order to monitor the underground steam zones. A scale drawing of the site can be seen in Figure 1.1.

Steam was first injected for 37 days in combination with an electrical heating process. Electrical heating assisted in volatizing contaminants located in lower permeable zones. A final pass of steam injection alone began June 2, 1993, and continued for 29 days. A total of 23,000 liters of gasoline was removed.

Modeling of the steam growth was done both during and after steam injection. The principal method used was the popular Marx-Langenheim relation. Preliminary results during injection helped to increase injection rates in wells whose steam zones had not reached the extraction wells. At the conclusion of steam injection, the model was used to produce a movie in which the daily growth of the steam zones could be observed for the entire process.

This report will discuss the Marx-Langenheim model in detail, especially how field data was input to best agree with the model's assumptions and limitations. The accuracy of the model is then determined by comparing the predicted steam zone locations with actual field data from the temperature monitoring wells. An overall energy balance will then be used to further verify model predictions.

The following section in this chapter will give an overview of the steam injection process. Results from a previous steam injection field study conducted in July 1991 will also be briefly discussed.

1.2 The Steam Injection Process

Figure 1.2 is a schematic representation of a steam injection process. Hot steam injected into the subsurface will initially condense when contacting the ambient underground soil. With further injection, a steam zone will develop and will push the condensate radially outward. A large portion of the subsurface contaminant will be moved ahead of this condensation front. Remaining contaminants will be vaporized by the continually flowing steam. Once the steam zone reaches the extraction wells, "steam breakthrough" occurs; and contaminants in the liquid and vapor phase are then removed.

1.3 Results of a Previous Steam Injection Field Study

Before attempting the full scale cleanup effort described above, a pilot test was conducted to test monitoring techniques and to ensure that steam zone growth could be controlled. The site chosen for this test was an uncontaminated "Clean Site" of similar geology located adjacent to the gasoline spill site at the neighboring Sandia National Laboratory.

This site consisted of only one injection well and one extraction well. Steaming began on July 23, 1991, and concluded on August 16, 1991, establishing a total steam zone volume of about 8000 m^3. Specifics can be found in the report by Chung (1992). General conclusions were that the Marx-Langenheim model gave accurate predictions of steam zone location compared with data from temperature monitoring wells. As discussed by Chung, the inherent error of the model gives a predicted volume subject to an uncertainty of +/- 29%. Estimated actual steam volume, however, was well within this error range. Such good agreement was the reasoning behind the continued use of the Marx-Langenheim model for the full-scale cleanup effort.

2. Description

2.1 Derivation of the Marx-Langenheim Model

Figure 2.1 shows a simplification of the steam injection schematic discussed earlier. The steam is assumed to be of constant thickness, h, radially expanding outward with time, with a surface area, A(t).

An overall energy balance gives

$$\dot{m}_s \bar{h} = \dot{Q}_{loss} + \overline{\rho c_p} \Delta T h \frac{d}{dt}(A(t)) \tag{2.1}$$

where $\dot{m}_s$ is the steam injection rate, $\bar{h}$ is the available heat of the steam, 2666 kJ/kg (Incropera and Dewitt), and $\dot{Q}_{loss}$ is the rate of thermal energy lost to the overburden and underburden regions which are at ambient temperature. The overall heat capacity, $\overline{\rho c_p}$, is given by

$$\overline{\rho c_p} = \left[(1-\Phi)\rho_r c_{p,r} + S_w \Phi \rho_w c_{p,w}\right] \tag{2.2}$$

where Φ is the porosity, 0.39 (Bishop, 1992); ρ_r is the rock grain density, 2650 kg/m^3; $c_{p,r}$ is the specific heat of the rock, 1152 J/kg-K; S_w is the initial reservoir water saturation, 0.3; ρ_w is the density of water, 1000 kg/m^3; and $c_{p,w}$ is the specific heat of water, 4187 J/kg-K (property values from Incropera and Dewitt).

The above energy balance (2.1) gives the temperature distribution as ΔT, the difference between the injected steam temperature and the ambient ground temperature. This is a fundamental assumption of the Marx-Langenheim model. Figure 2.2 illustrates this assumption compared to an actual temperature distribution.

The expression for $\dot{Q}_{loss}$ is given by (Lake, 1989),

$$\dot{Q}_{loss} = 2\int_0^t \frac{k\Delta T}{\sqrt{\alpha\pi(t-u)}} \frac{dA}{du} du \tag{2.3}$$

where k is the overburden thermal conductivity, 1.3 W/m-K; and α is the overburden thermal diffusivity, 1.01E-6 m^2/s (Incropera and Dewitt). Equation (2.3) expresses the rate of heat loss at time t as a function of the rate of growth of the heated area.

Substituting (2.3) into (2.1) then gives

$$\dot{m}_s\bar{h} = 2\int_0^t \frac{k\Delta T}{\sqrt{\alpha\pi(t-u)}}\frac{dA}{du}du + \overline{\rho c_p}\Delta T h\frac{d}{dt}(A(t)) \tag{2.4}$$

Equation (2.4) is an integral-differential equation for A(t) which is solved with the initial condition A(0) = 0. The most direct method of solution is through a Laplace transform. The transformed solution to (2.4) is

$$A(\xi) = \frac{\dot{m}_s\bar{h}}{2C_1\sqrt{\pi}\xi^{3/2} + C_2\xi^2} \tag{2.5}$$

where ξ is the transform variable, $C_1 = k\Delta T/\sqrt{\alpha\pi}$, and $C_2 = \overline{\rho c_p}\Delta T h$. The inverse transform of (2.5) with $\dot{m}_s\bar{h}$ constant is

$$A(t) = \left[\frac{m_s\bar{h}\overline{\rho c_p}h\alpha}{4k^2\Delta T}\right]\left[e^{y^2}erfc(y) + \frac{2y}{\sqrt{\pi}} - 1\right] \tag{2.6}$$

where

$$y = \left[\frac{2k}{\overline{\rho c_p}h\sqrt{\alpha}}\right]\sqrt{t}.$$

One feature of the Marx-Langenheim theory is that the above result (2.6) is independent of shape of the heated zone; the only constraint being a zone of constant height. Because the actual shape of the expanding surface area is different for each well, the steam volume is assumed to be a radially expanding cylinder with constant height in order to simplify the analysis. This was done in the previous "Clean Site" analysis (Chung, 1992), and proved to be a good first-order approximation. The growing radius, r(t), for each steam zone is therefore given by

$$r(t) = \sqrt{\frac{A(t)}{\pi}} \tag{2.7}$$

2.2 Field Data Used in the Model

The following sections will describe how steam injection rates and steam zone thicknesses are obtained and used in the Marx-Langenheim relation.

2.2.1 Obtaining Steam Injection Rates

Figure 2.3 shows the Venturi arrangement used to determine the steam injection rate for each of the injection wells. A Validyne differential pressure transducer was used to determine flow rates. A current output was desired rather than a voltage output so as to avoid voltage drop losses that would occur in the long data cables leading to the computer.

The illustrated plumbing arrangement was chosen for several reasons. Steam is too hot a fluid for contact with the pressure transducer. Carefully filled water lines free of air bubbles transmitted the pressure variations with little damping. Water could easily be added to the system through the bottom valves (see Fig 2.3). Simultaneously closing the quick-turn upper shutoff valves effectively isolated the pressure transducer from the steam flow, preventing steam from entering the plumbing lines. The transducer zero could then be checked by opening the bypass valve - with no pressure difference, the output when properly calibrated is 4 mA.

During normal operation, the linear output of the pressure transducer varies between 4 and 20 mA. This corresponds to differential pressures between 0.0 Pa and 55,160 Pa (0.0 psi and 8.0 psi) for the particular diaphragm used. The linear relation between milliamp output and differential pressure is therefore given by

$$\Delta p = 3447.5x - 13790 \tag{2.8}$$

where x is the milliamp output (4-20 mA) and Δp, the differential pressure, is measured in Pa.

In order to determine how the differential pressure varies with steam flow rate, Bernoulli's Equation applied along the Venturi (Fig. 2.3) gives:

$$\frac{V_1^2}{2} + p_1 v = \frac{V_2^2}{2} + p_2 v . \tag{2.9}$$

Solving for the differential pressure gives,

$$\Delta p \equiv p_1 - p_2 = \frac{\left(\frac{A_1}{A_2}\right)^2 - 1}{2v} V_1^2 = C_1 V_1^2 \rho \tag{2.10}$$

where C_1 is an arbitrary constant. The entering velocity is therefore

$$V_1 = \sqrt{\frac{\Delta p}{C_1 \rho}} . \tag{2.11}$$

Multiplying the above equation by ρA_1 and changing the arbitrary constant gives the mass flow rate along the pipe to be

$$\dot{m}_s = \sqrt{C_2 \Delta p \rho} . \tag{2.12}$$

If the steam is assumed to be an ideal gas,

$$\dot{m}_s = C_3 \sqrt{\frac{P \Delta p}{T}} . \tag{2.13}$$

Based on manufactured calibration of the Venturi giving a known flow rate of 0.383 kg/s steam corresponding to Δp = 7465.2 Pa (with P = 530.9 kPa and T = 427.6 K), the arbitrary constant C_3 can be determined so that the expression for steam flow rate becomes

$$\dot{m}_s = 1.258 \cdot 10^{-4} \sqrt{\frac{P \Delta p}{T}} \tag{2.14}$$

where $\dot{m}_s$ is in kg/s, P and Δp are in Pa, and T is in degrees Kelvin (K).

Figures 2.4 - 2.7 show the injection rates for the twelve wells (six lower and six upper) for both passes of steaming. Pass 1 steaming was between Day 1 and Day 37. Pass 2 steaming was between Day 10 and Day 39. The injection technique was noticeably different for the two passes: the first pass had long intervals, between 10-14 days, where all of the lower wells were on, followed by all of the upper wells, concluding with the lower wells again; the second pass had shorter intervals of only a few days when only 2 or 3 wells were on, alternating between upper and lower zones throughout the month.

2.2.2 Determining Steam Zone Thickness

With knowledge of the steam injection data, the Marx-Langenheim method also requires an estimate of the steam zone thickness. Determining the subsurface temperature would identify the hot steam thickness. A temperature measurement system was developed by the Environmental Restoration Laboratory in which temperature profiles of all twelve of the monitoring wells could be determined simultaneously. The temperature sensor used measured the thermal radiation of the inner wall of the well. This sensor was attached to a probe which was remotely controlled. All of the probes were lowered so as to log the temperature data at a rate of about 0.1m/s. Data was collected during every day of steaming. Representative temperature profiles can be seen in Figures 2.8 - 2.15.

Figures 2.8 - 2.10 show the initial growth of steam in the lower zone of TEP 9 through Day 15. The thickness increased from 7 m to 12 m. Injection into the upper zone then began, and Figure 2.11 shows that on Day 22 there is the addition of an upper zone 3 m thick. Such is the manner in which upper and lower steam zone thicknesses are obtained for the model.

Underground heating is not only limited to these upper and lower zones, however. With the presence of hot zones due to upper and lower steaming, the area between these zones will also gradually become heated due to thermal conduction. For example, Figure 2.11 shows the cool region between the hot zones. But in just one week, this cool region was heated by conduction, as seen in Figure 2.12.

After the first steaming pass, the ground settled for two months before the start of the final pass. As shown by the temperature profile in Figure 2.13, conduction played a significant role during this time in that uniform heating as thick as 25 m was evident in zones. As shown in Figures 2.14 and 2.15, these zones mostly retained their uniformity during Pass 2, with the entire zone increasing temperature during the injection process. Steam zone thickness, therefore, did not vary significantly for Pass 2. This is very different from the method of steam spreading in the first pass, where initial growth was limited to only the higher permeable zones.

2.2.3 Applying the Data to the Model

Sections 2.2.1 and 2.2.2 described how the necessary data was obtained. The Marx-Langenheim model has certain inherent assumptions and limitations, and the following section will describe how the data was input to best agree with these constraints.

In order to review, the major assumptions of the Marx-Langenheim model are listed here (Boberg, 1988):

a) One-dimensional flow in a homogeneous sand.
b) Constant physical properties and fluid saturations.
c) Constant injection temperature and rate.
d) Ground assumed to be either at the injected steam temperature or the ambient ground temperature. (See Fig. 2.2).

The first assumption for the model is that the subsurface is homogeneous. While not the case at the Livermore site, the previous application of this model showed that this discrepancy did not cause any increased error beyond the inherent uncertainty of the model, +/- 29% (Chung, 1992).

Also conflicting with the assumptions of the model, the injection rates during both passes were not constant. A good approximation, however, is to time average the varying injection rates (Boberg, 1988). This was possible for the first steam pass in which there were long intervals of varying injection rates. Time averaging of the lower injectors was even done for the two week period in which

only the upper zones were steamed - thereby averaging in zero flow in the lower zone for these two weeks which caused a shrinking of the calculated steam area. This does physically correspond to collapsing and shrinking of the steam zone, although only in a very abstract manner, for the model (with a steady injection rate assumption) in no way accounts for such a steam zone collapse.

During the second steam pass, such time averaging was not possible due to the very intermittent injection scheme. Time averaging a typical process where steaming was on for 4 days and off for 15 days would not be physically accurate at all. The assumption was therefore made that area calculations were additive, or that steam injected in a well which had been shut down for a while simply expanded from its previous location.

The Marx-Langenheim model also assumes a constant steam zone thickness. As discussed previously in Section 2.2.2, such was generally the case during Pass 2. However, Pass 1 steaming initially grew in high permeable zones, with conductive heating effectively broadening the thickness with time. In addition, steam thickness will also vary with distance from the injector, particularly in a heterogeneous subsurface. Steam zone thicknesses obtained from the temperature profiles were therefore time averaged for the first steam pass.

It also was determined which temperature wells provide profiles that best predict the local steam zone thickness for each injection well. The first consideration was that the temperature well be nearby the injector. Preference was given to temperature wells that were located between the particular injection well and the extraction wells. Since this analysis was started after initial steaming had begun, it was also decided, if applicable, to avoid temperature wells that were seeing negligible steam.

Based on the above considerations, Table 2.1 shows which temperature well was used for each injector to determine steam zone thickness (the same TEP well is used to determine both the upper and lower zones):

The last topic to be discussed concerning model application involves determining the temperature variation across the steam front. As stated in the assumptions, the Marx-Langenheim model assumes a step temperature variation. The

difference between the injected steam temperature and the ambient ground temperature is ΔT. For the first steam pass, the ambient ground temperature was 20°C. With 110°C steam, ΔT was therefore 90°.

Determining ΔT was slightly more complicated for Pass 2. After settling for 2 months after the first pass, the subsurface hot zone was on average 80°C. When starting the second steam pass (again with 110°C steam), a ΔT of 30°C was used while the calculated steam front location was within the hot zone retained from Pass 1. If subsequent Pass 2 steaming were to extend the front beyond the previous hot zone, the original ΔT of 90° was used for calculating the additional area.

3. Results

The following section refers to Figures 3.1 - 3.24 which show representative results of the daily steam zone location. As discussed in Section 2.1, the Marx-Langenheim relation predicts the area of the steam zone, A(t), having a constant height, h. Not knowing the shape of this predicted area, an estimate was made that a regular radial expansion would be illustrated for qualitative use. Such a simplification gives an "overlapping" of steam zones which do not occur in reality. This area is actually expanded along the zone boundary. With no idea how this occurs, however, the radial estimate gives an idea of the relative position of the steam zones. Comparisons of a theoretical, overall steam volume to the volume predicted by the Marx-Langenheim model will be given in Section 4.2.

3.1 Steam Zone Radii Predictions

Figures 3.1-3.11 show the calculated steam radii for selected days during Pass 1. Figures 3.1-3.4 correspond to the first 14 days of lower zone steaming. Figures 3.5-3.8 show the upper zone steaming, with Figure 3.8 showing the final extent of the upper zone on Day 28. Figures 3.9-3.11 show the final growth of the lower zone concluding on Day 37.

The lower injector of well IW819 failed after approximately Day 10, and such is the reasoning for the dotted circle around this well. Injection wells IW813, IW815, and IW820 did not inject enough steam so as to reach the extraction wells.

Figures 3.12-3.18 show the steam location in the lower zone during Pass 2. The larger dotted lines outline the location of the hot zone from Pass 1. The interior, solid circles represent the progress of the re-establishing steam zone. The dotted lines are removed around each well if the injection rate for Pass 2 establishes a larger steam zone than before. Figures 3.19-3.24 show the steam growth in the upper zone during Pass 2. The final extent of the steam in Pass 2, concluding on Day 39, can be seen in Figures 3.18 and 3.24, for the lower and upper zones, respectively.

Compared with the Pass 1 steam radii, larger steam zones due to Pass 2 were formed in the lower zone from wells IW813 and IW814, and in both the upper and lower zones from wells IW815 and IW820. While this added growth was able to have the IW820 steam zone reach the extraction wells, the IW813 and IW815 steam zones still remained too small after steaming was completed.

4. Discussion

The following sections will discuss the accuracy of the predicted results. Fixed thermocouple data will be used to compare actual steam location at the various temperature wells with the location predicted by the model. A simplified energy balance will then be made to compare the calculated steam volume with that predicted by the Marx-Langenheim relation (Equation 2.6). Finally, the accuracy of the model's heat loss to the overburden and underburden will be discussed by noting the actual temperature distribution obtained from the temperature profile data.

4.1 Comparison to Fixed Thermocouple Data

In order to determine the accuracy of the model, comparisons were made using fixed thermocouple data. Each temperature (TEP) well had 4 fixed thermocouples located at depths of 24.4 m, 29.0 m, 33.5 m, and 39.6 m. Daily fixed-TC readings were taken in all of the TEP wells before and after both steam

passes. Such data can be seen in Figures A.1 - A.22 in the Appendix. It is rather evident when steam reaches a TEP well given the typical sharp increase in temperature for at least one of the thermocouples.

Tables 4.1 and 4.2 show the correlation between the actual steam location and the predicted location using the Marx-Langenheim model. The fixed-TC data for TEP's 1-11 (TEP 807 fixed-TC data not available) will show the day when steam was observed in any of the 4 TC's for each particular TEP. The model data will give the day when the predicted radius reaches the TEP. Multiple entries for several of the TEP wells are due to steam reaching the well from different steam injectors and/or from upper and lower steaming zones.

Table 4.1 shows that for Pass 1, there is good agreement between the actual and predicted steam location for the interior TEP wells (TEP 7 - TEP 10). The agreement, however, is not as good for the exterior wells. For example, the predictions for steam reaching TEP 2 were on Days 6 and 21, but steam did not actually reach TEP 2 until Days 12 and 33. Although a noticeable difference in days, Figures 3.2 - 3.4 show that the modeled radial expansion near TEP 2 from Day 6 through Day 14 was only 4 meters.

TEP 4 had steam on Day 22; although the model did not predict any steam fully reaching this well (Table 4.1), Figures 3.7 and 3.8 show steam within 7 meters on Day 23 and within 3 meters on Day 28. Thus discrepancies in days do not necessarily mean poor prediction of the growing steam radius, especially for zones that grow rather slowly.

The most critical requirement is that the model predict "steam breakthrough" accurately, when the steam zones reach the extraction wells. Because the interior wells (which are near the extraction wells) gave good agreement, the model seems promising for predicting the location of the Pass 1 steam zones.

Table 4.2, which shows the data for Pass 2 steaming, gives excellent agreement for interior and exterior wells, thereby giving good breakthrough predictions.

4.2 Energy Balance to Compare Steam Volume

The following equation was the energy balance used to derive the Marx-Langenheim relation in Section 2.1.

$$\dot{m}_s\bar{h} = \dot{Q}_{loss} + \overline{\rho c_p}\Delta T h\frac{d}{dt}(A(t)) \tag{4.1}$$

Integrating this over all time from the beginning of Pass 1 to the end of Pass 2 gives an "overall" energy balance of the entire process, including the 81 days during which no steaming occurred. This "settling" time between steaming passes can be characterized as a period in which conduction dominates over the other thermal processes which occur during steaming. In order to get an estimate of a theoretical, "overall" steam volume, the following simplified energy balance will be used to compare the steam volume predicted by the Marx-Langenheim model:

$$M_s\bar{h} = \overline{\rho c_p}\Delta T h A_s \tag{4.2}$$

where M_s is the total mass of injected steam, $11.73 \cdot 10^6$ kg (Siegel, 1993); ΔT is the average difference between steam zone temperature and the ambient for the overall process, 80°C; h is the final height of the entire steam zone, 20 m; and A_s is the estimated resulting steam zone surface area. Note that the above equation does not have a heat loss term for the overburden and the underburden. The reasoning for this is that to a first approximation, the heat lost to these ambient regions is balanced by the conductive heating which expanded the steam zone primarily during the "settling" period between steam passes. Solving the above equation for the final theoretical steam volume gives

$$\frac{M_s\bar{h}}{\overline{\rho c_p}\Delta T} = hA_s = V_{steam} = 166200 \text{ m}^3 \tag{4.3}$$

The calculated Marx-Langenheim steam volume can be obtained from

$$V_{M-L} = \sum_{i=1}^{6} \pi r_i^2 h \tag{4.4}$$

where r_i is the outermost predicted radius for each of the 6 injection wells (either from the lower or upper zone); and h is the final steam zone height, 20 m. This result is given by

$$V_{w-i} = 162900 \text{ m}^3 \tag{4.5}$$

Thus the energy balance calculated volume gives excellent agreement (within 2%) with the Marx-Langenheim prediction.

Figure 4.1 shows the final theoretical steam volume expressed as a cylinder with a radius of 51.4 m. Because the theoretical volume and the sum of the Marx-Langenheim volumes about each well match so well, this gives a reasonable estimate of the overall hot surface area of the site.

4.3 Discussion of Marx-Langenheim's Thermal Loss Term

The Marx-Langenheim model is unique from other simple, analytical models in that it accounts for energy loss to the overburden and the underburden. Since the previous sections show how the Marx-Langenheim relation gave very good predicted results, this section will describe how the model's Q_{loss} term accurately describes actual thermal processes taking place as shown by the temperature profiles.

Figure 2.15 shows the final temperature profile taken during the last day of steaming for TEP 9. Between the hot zone of 15 m and 35 m, the temperature is relatively constant. Between depths of 10-15 m and 35-40 m, however, the temperature can be seen to decay to the ambient.

The Marx-Langenheim theory gave a Q_{loss} term according to Equation (2.3). This term is derived by assuming the following temperature distribution (Lake, 1989):

$$T(z,t) = T_{\infty} - \Delta T erf\left(\frac{z\sqrt{\rho c_r}\sqrt{\alpha}}{2k\sqrt{t}}\right) \tag{4.6}$$

where temperature is a function of the depth coordinate, z, and time, t.

The above equation predicts the temperature decay above and below the hot zone with an error function. Actual decay is seen in Figure 2.15. The model therefore gives good correlation between its thermal loss assumptions and what actually was observed in real temperature distributions.

5. Conclusions

The chosen techniques for applying the Marx-Langenheim model to the Lawrence Livermore site gave good results. These include:

- Time averaging varying injection rates
- Time averaging varying steam zone thicknesses during Pass 1
- Changing the temperature difference, ΔT, during Pass 2 when steam exceeds the estimated zone from Pass 1.

The daily radii generated by the model can be used to accurately predict steam zone breakthrough for both steam passes. Comparisons between fixed thermocouple and temperature profile data give good agreement for predicting steam location. The total injected steam zone volume was also confirmed with excellent agreement from an overall energy balance of the process.

Acknowledgements

I would like to gratefully acknowledge the assistance and direction provided by my advisor, Professor Kent S. Udell, during this project. I am also thankful for the direction and troubleshooting expertise offered by Ron Goldman. Many thanks also to those at the Gas Pad, particularly Robin Newmark, Bill Siegel, and Paul Gronner. I finally wish to thank all who helped in the temperature logging experience, especially Ron, Cessy Alacatar, Troy Jones, Dave Kayes, Mike Itamura, Erik Boucher, and Paul Konkola. Best wishes to Dave and Cliff Yuan with their future field study work.

References

Bishop, D., "Dynamic Stripping Characterization Report," *Dynamic Underground Stripping Project Clean Site Interim Engineering Report*, (1992).

Boberg, T.C., Thermal Methods of Oil Recovery, John Wiley & Sons, Inc., 1988.

Chung, Craig S., "A Field Study of a Steam Injection Process That Can Be Used in the Recovery of Subsurface Gasoline Spills", Master's Research Report, University of California at Berkeley, May 1992.

Incropera, F.P. and D.P. Dewitt, Fundamentals of Heat and Mass Transfer, John Wiley & Sons, Inc., 1981.

Lake, L.W., Enhanced Oil Recovery, Prentice Hall, 1989.

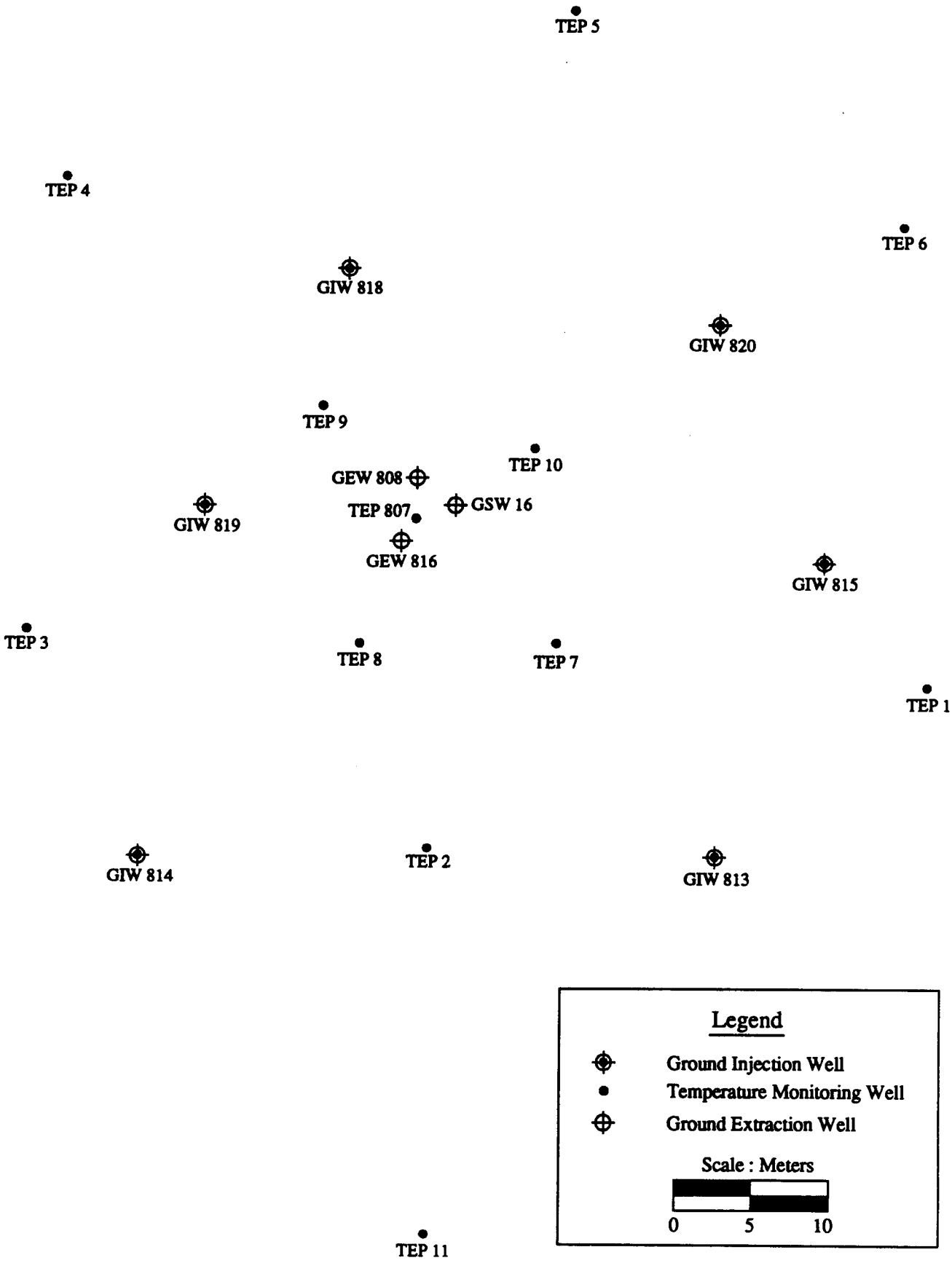

Figure 1.1: Contaminated Field Site at Lawrence Livermore National Laboratory

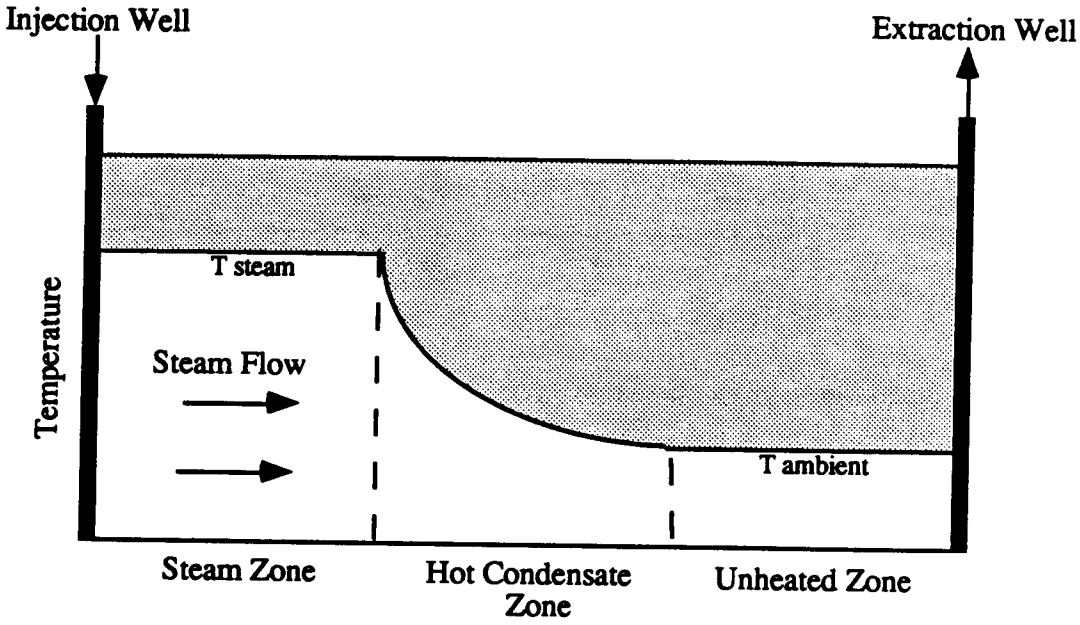

Figure 1.2: Schematic zones in a steam injection process.

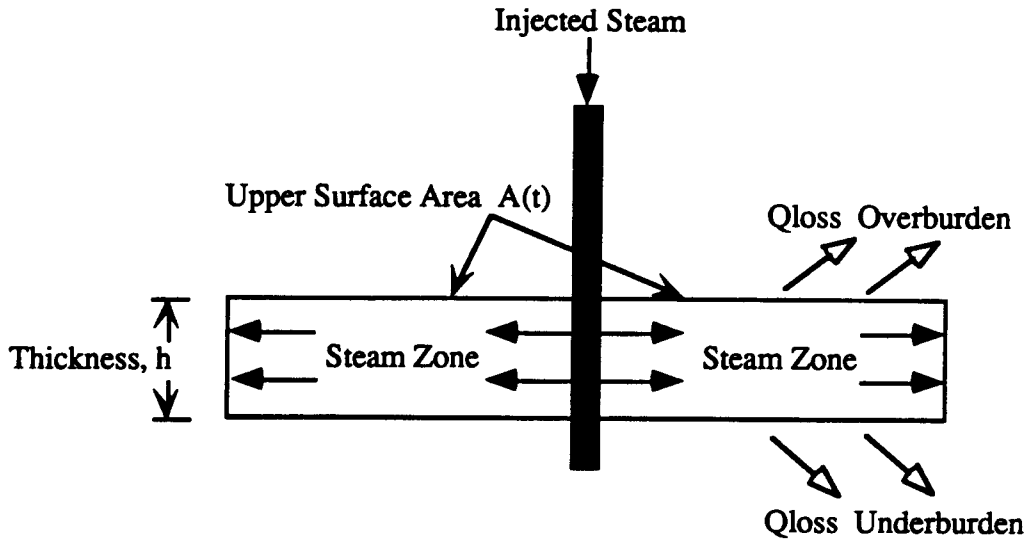

Figure 2.1: Steam injection schematic as represented by the Marx-Langenheim model.

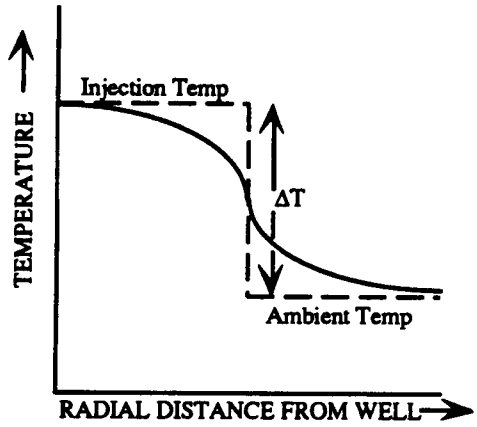

Figure 2.2: Qualitative true temperature distribution (solid line) vs. Marx-Langenheim step approximation (dashed line).

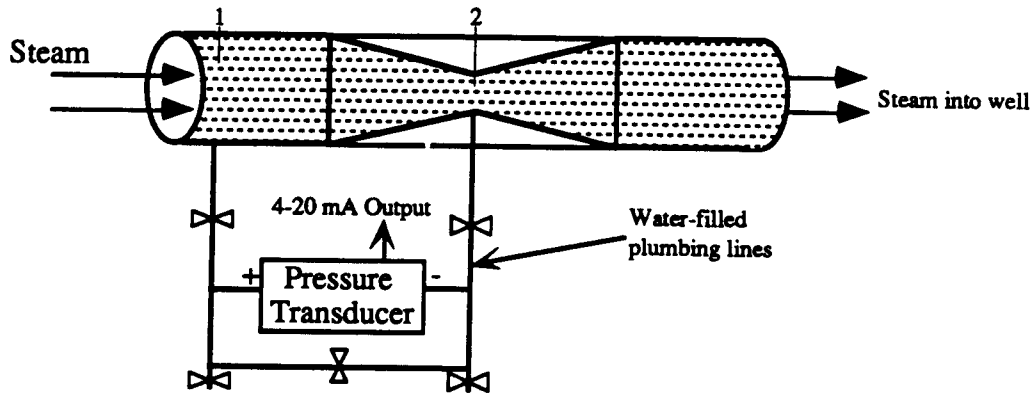

Figure 2.3: Venturi and Pressure Transducer arrangement for the injection wells.

First Pass

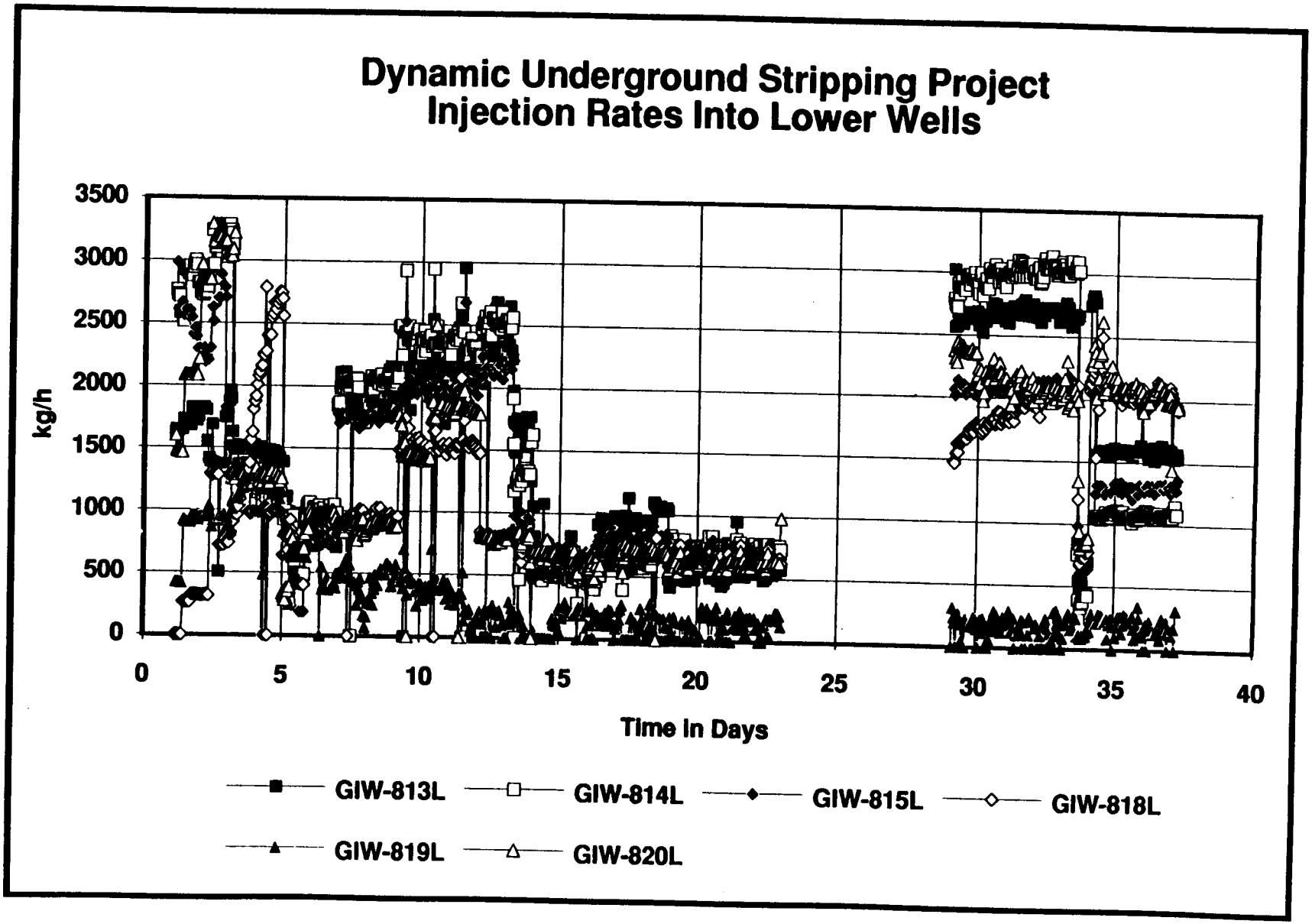

Figure 2.4: Pass 1 Injection Rates for the Lower Wells (Day 1 - Day 37)

First Pass

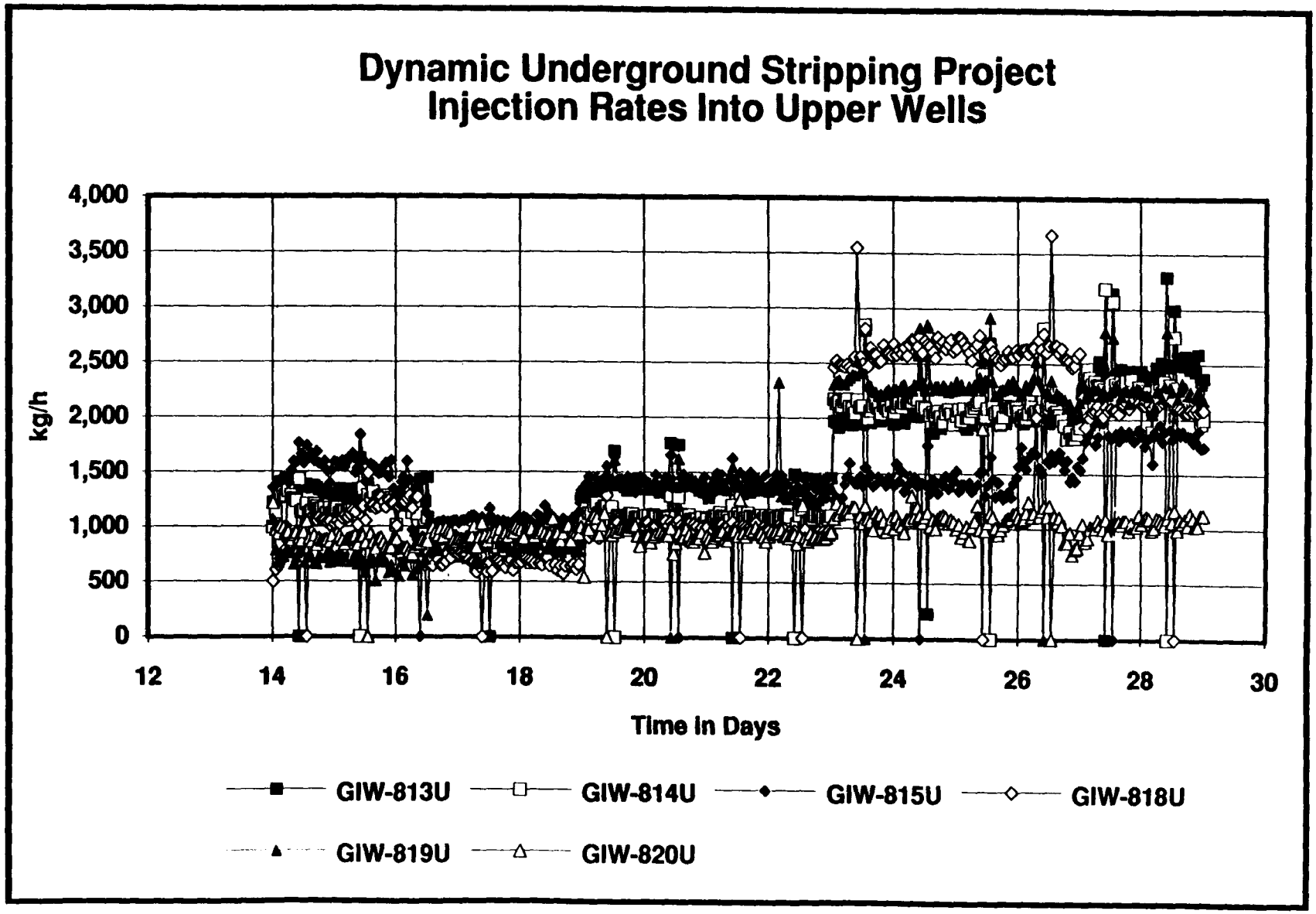

Figure 2.5: Pass 1 Injection Rates for the Upper Wells

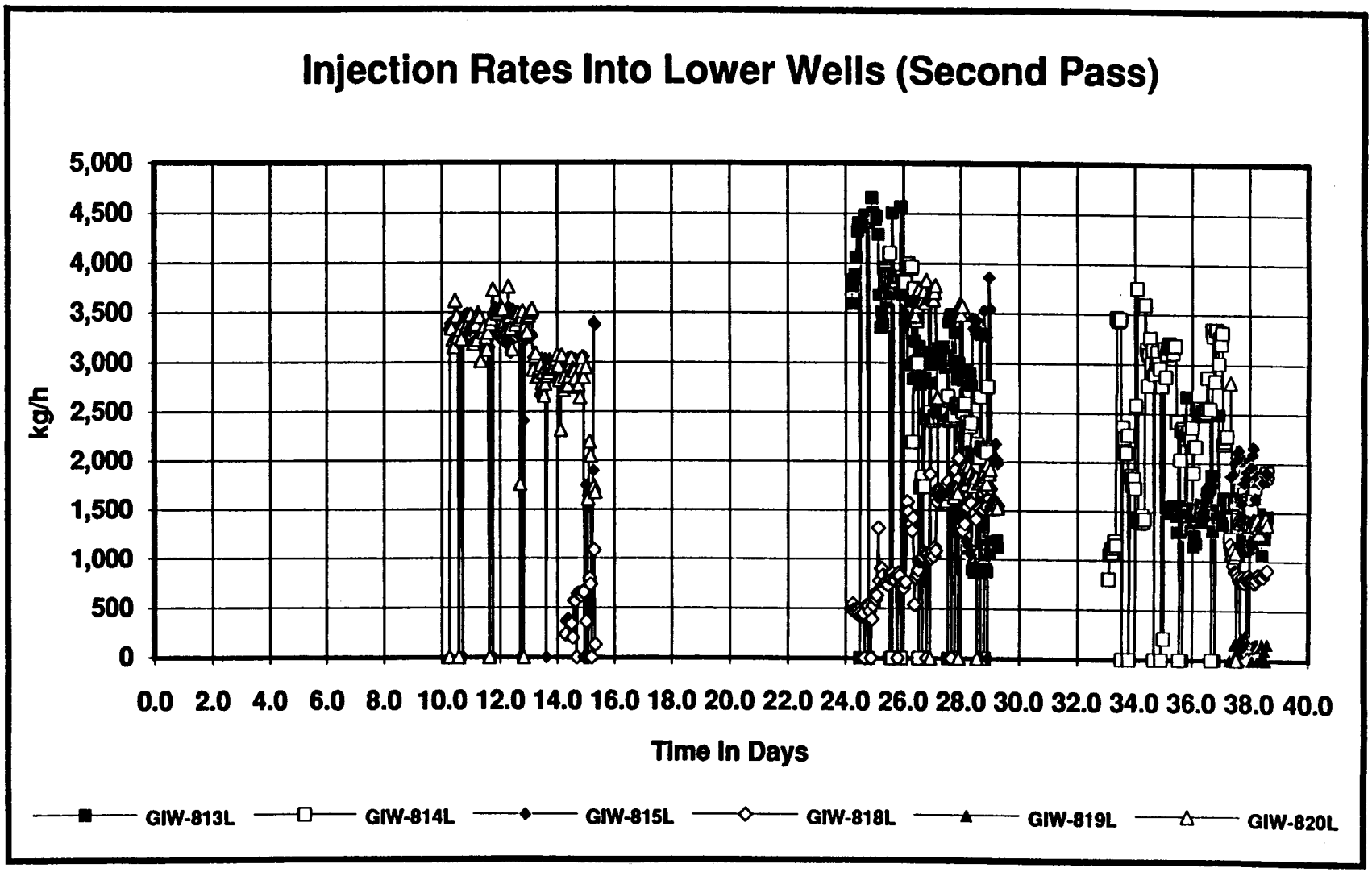

Figure 2.6: Pass 2 Injection Rates for the Lower Wells

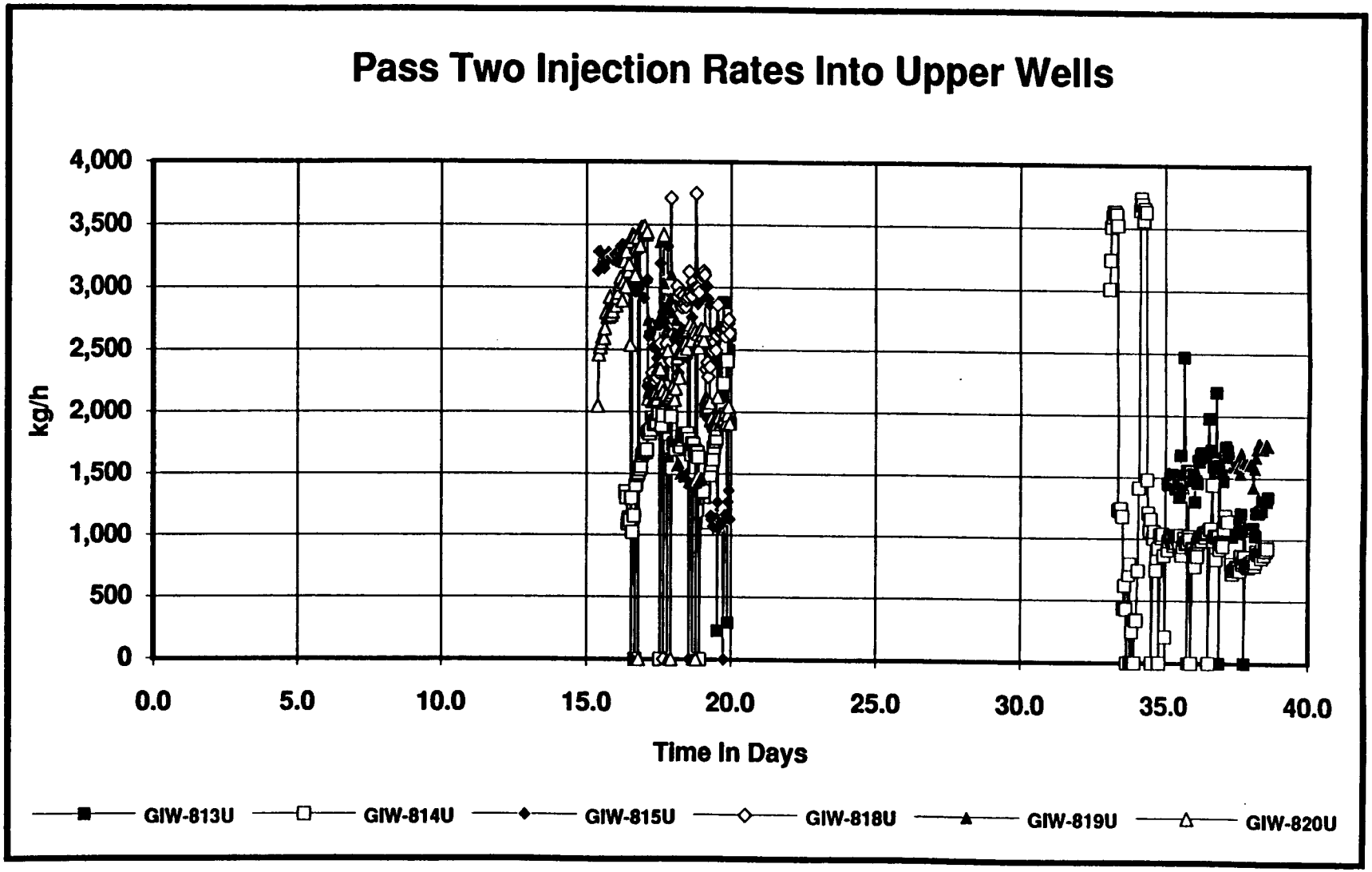

Figure 2.7: Pass 2 Injection Rates for the Upper Wells

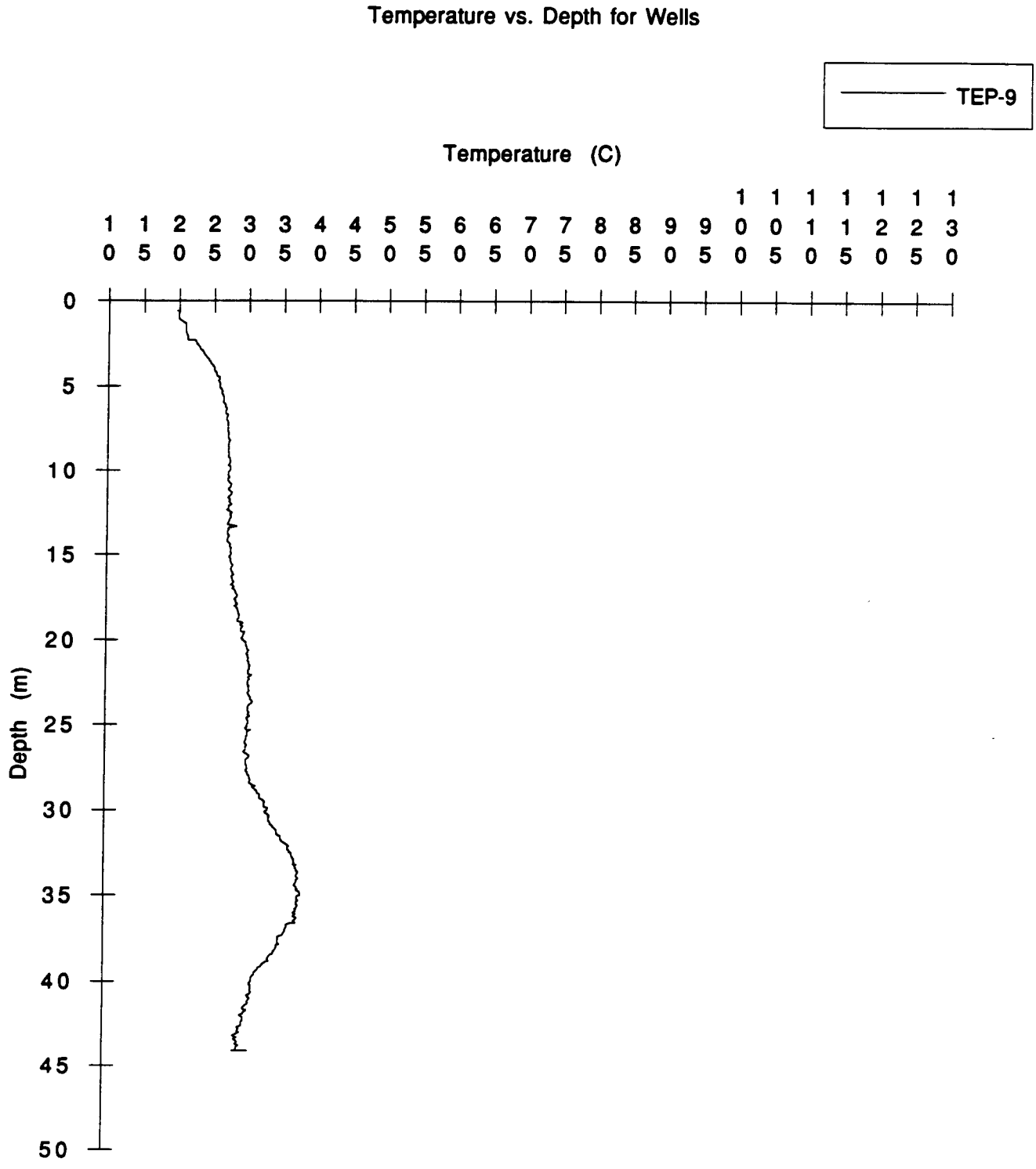

Figure 2.8: Pass 1 Day 3

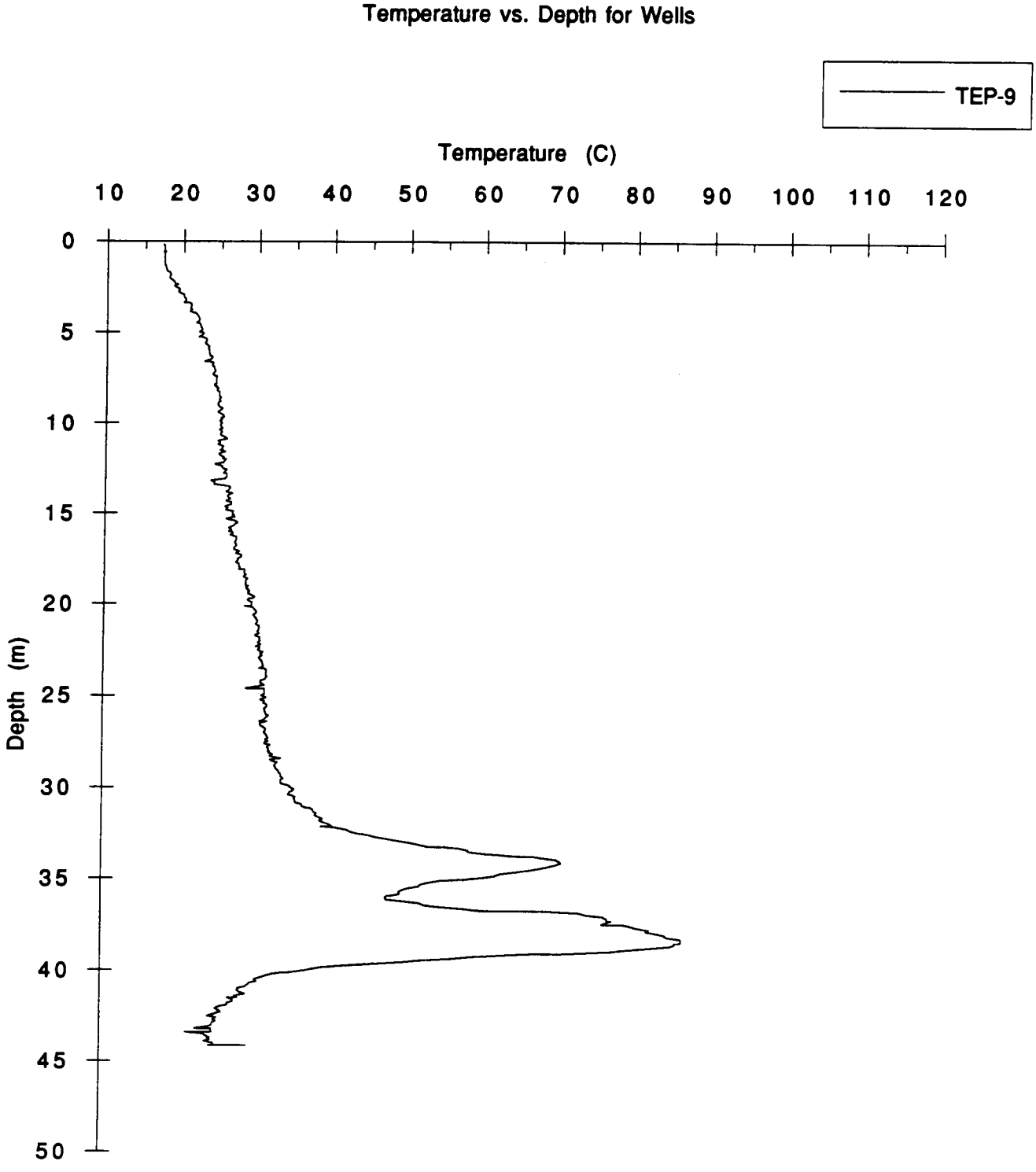

Figure 2.9: Pass 1 Day 8

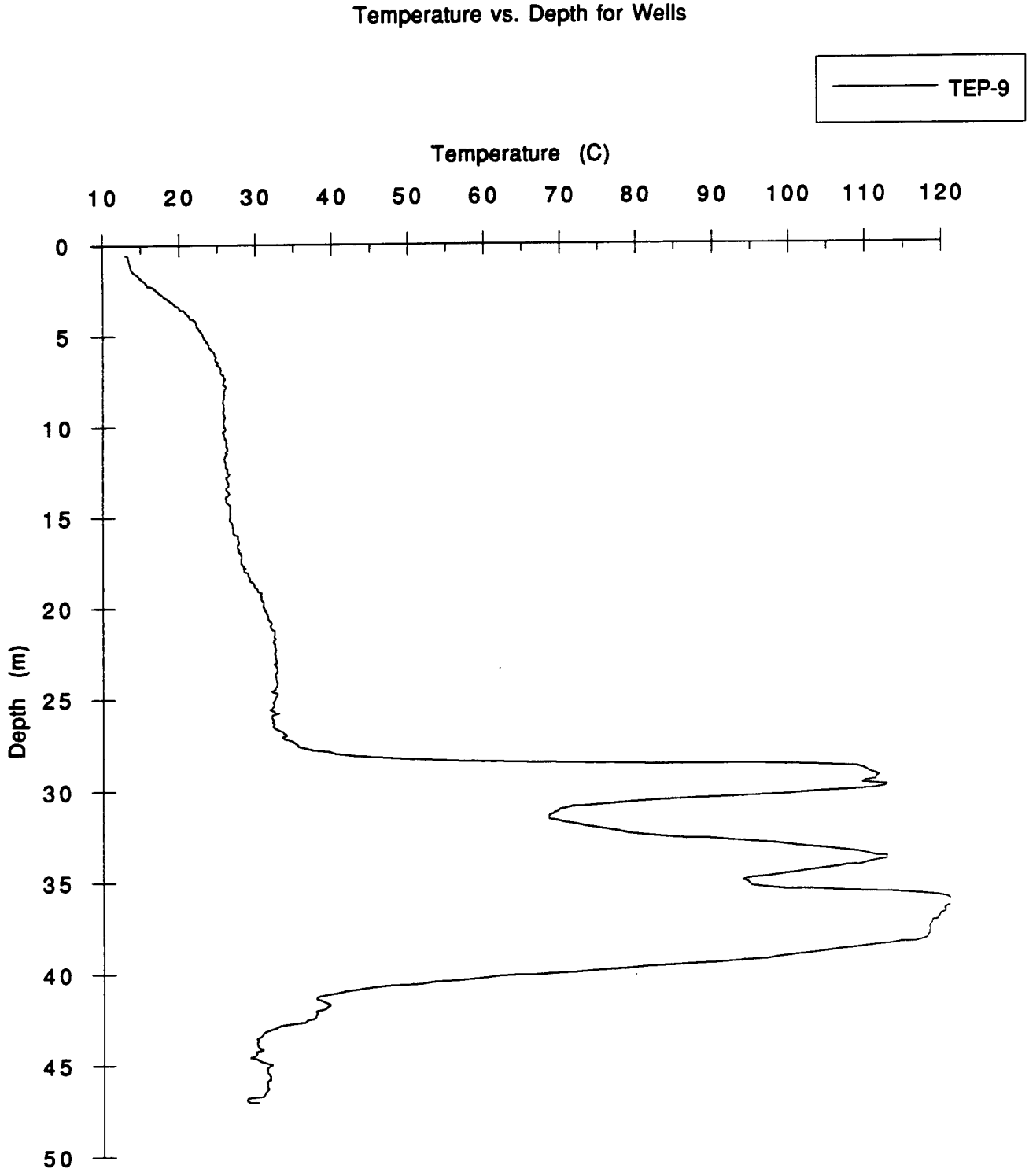

Figure 2.10: Pass 1 Day 15

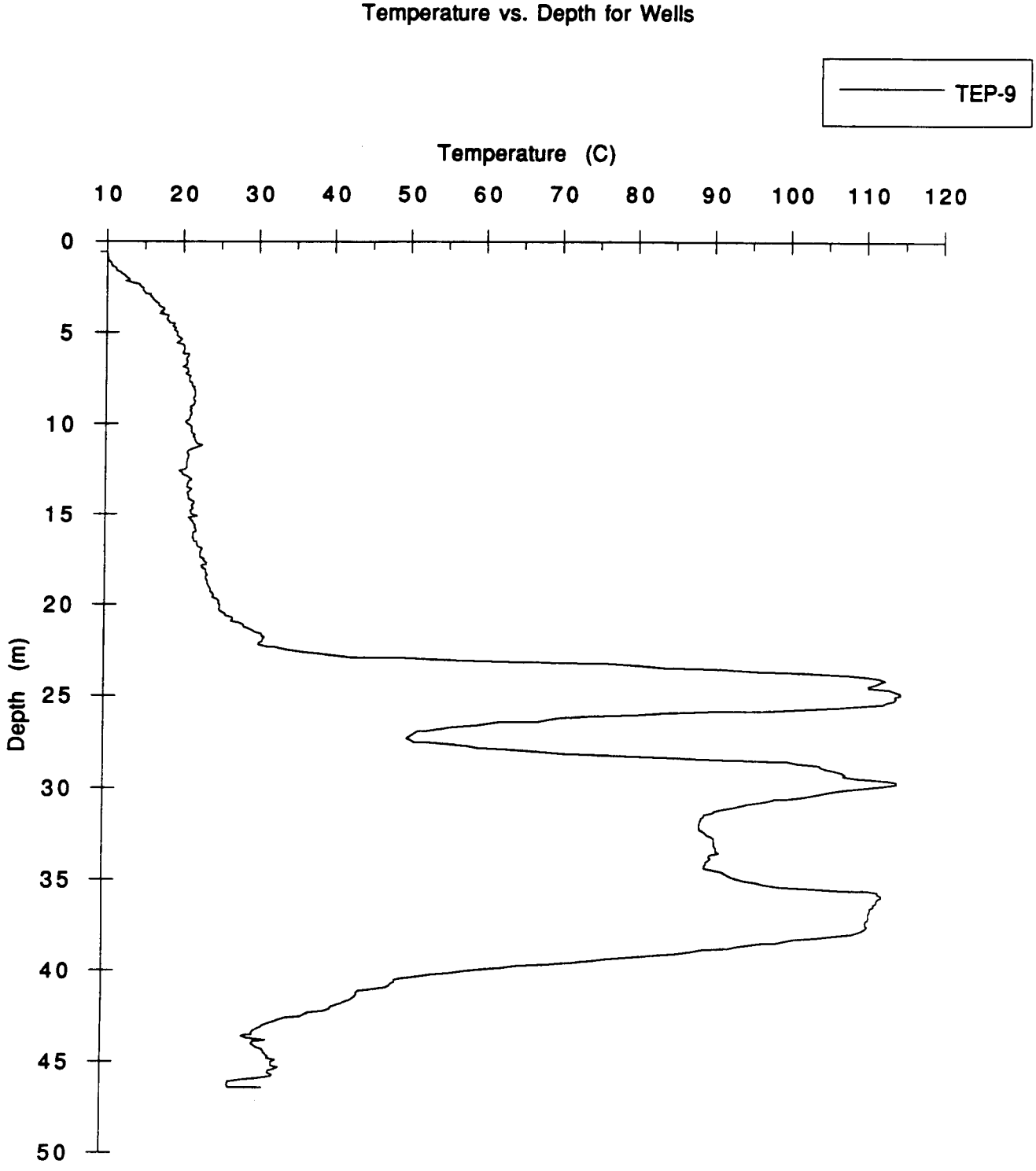

Figure 2.11: Pass 1 Day 22

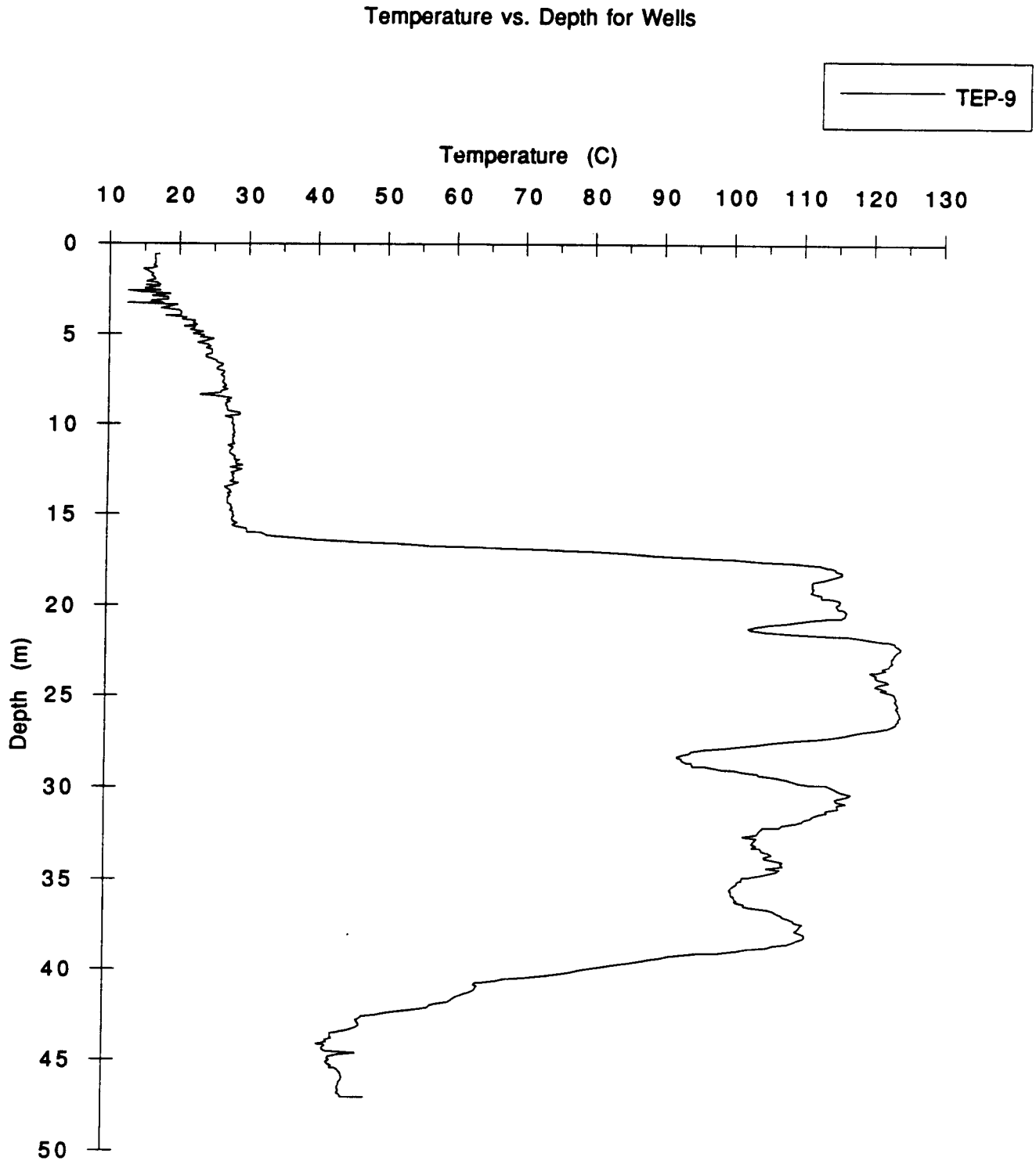

Figure 2.12: Pass 1 Day 29

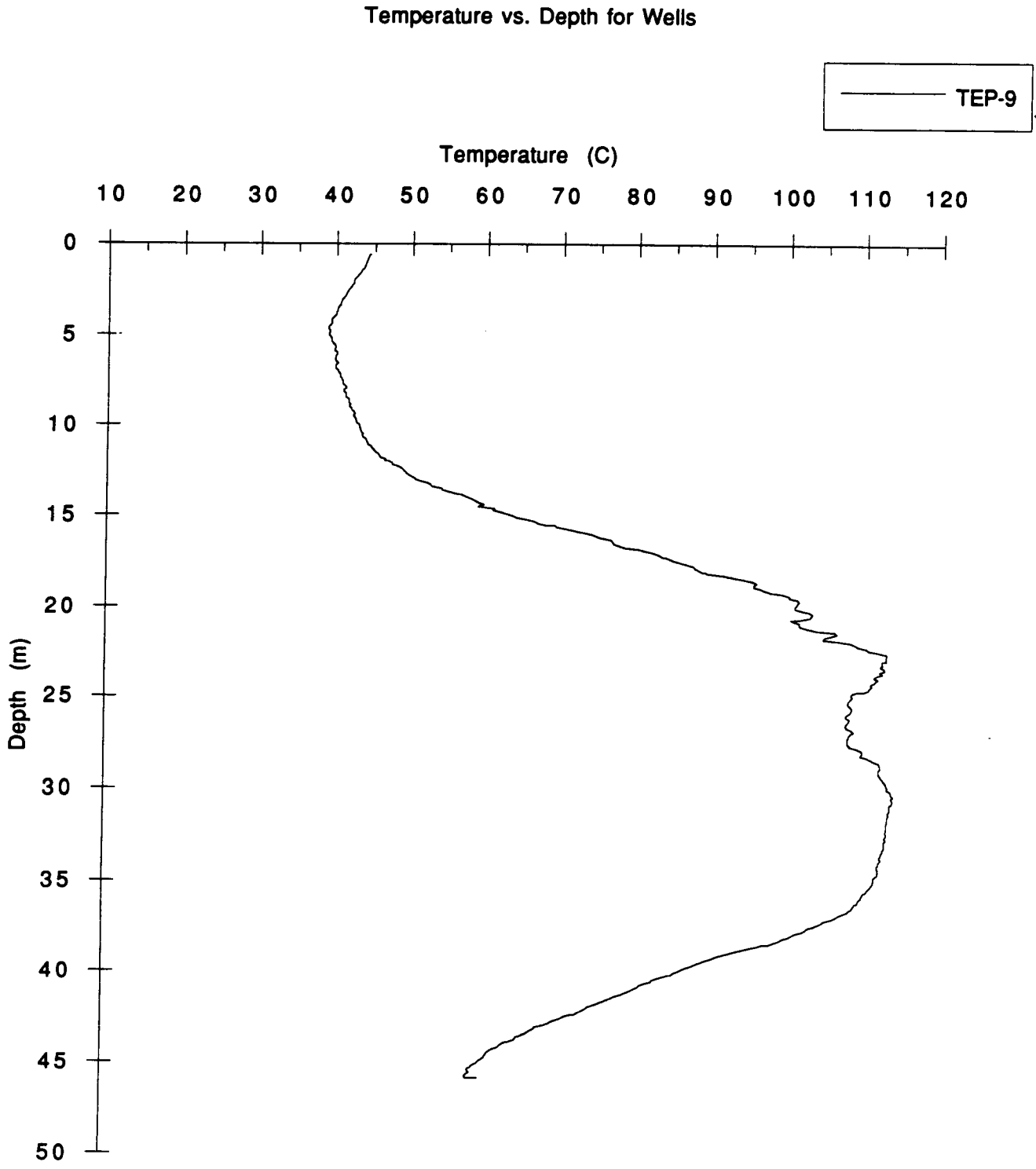

Figure 2.13: Pass 2 Day 9

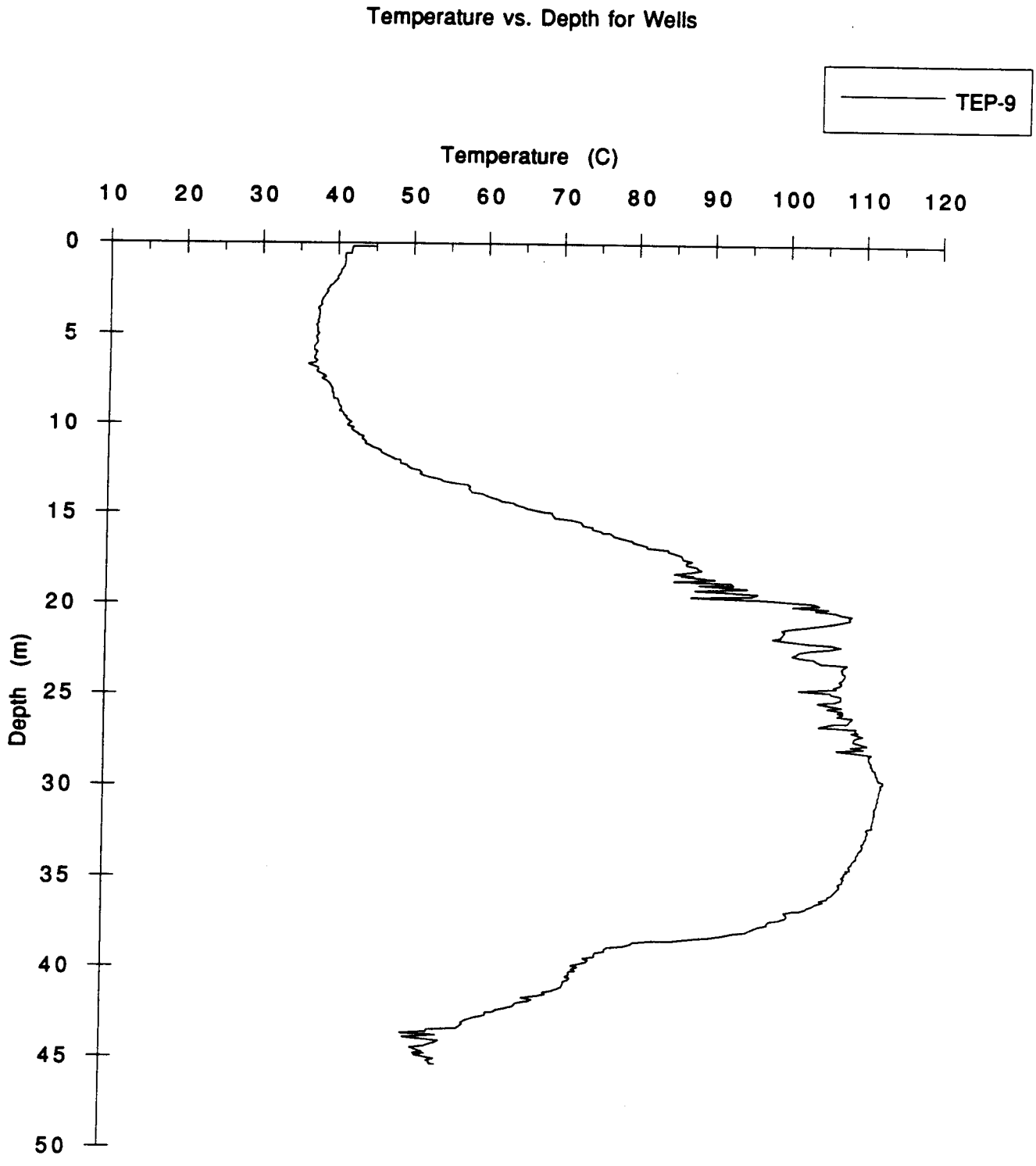

Figure 2.14: Pass 2 Day 16

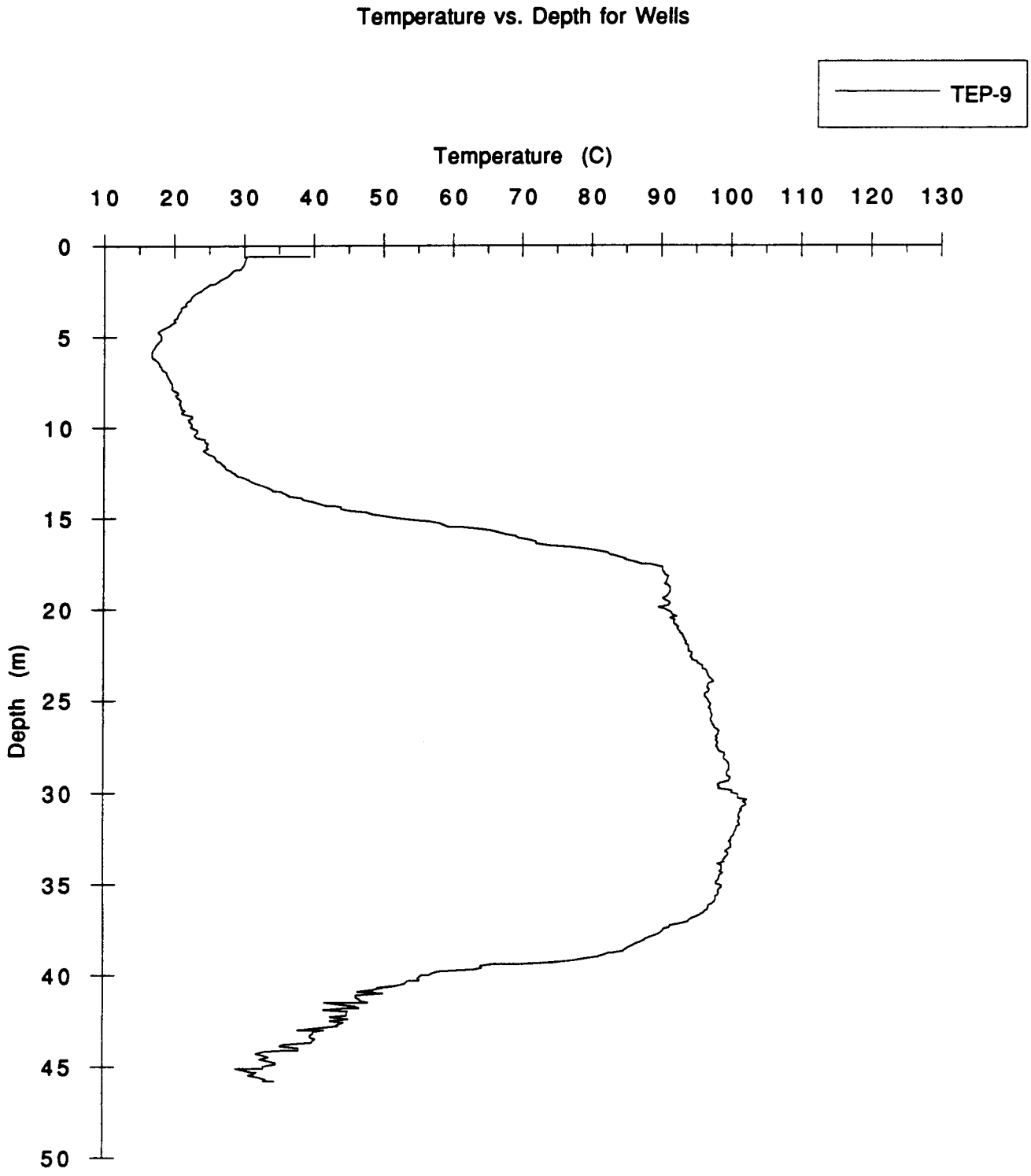

Figure 2.15: Pass 2 Day 39

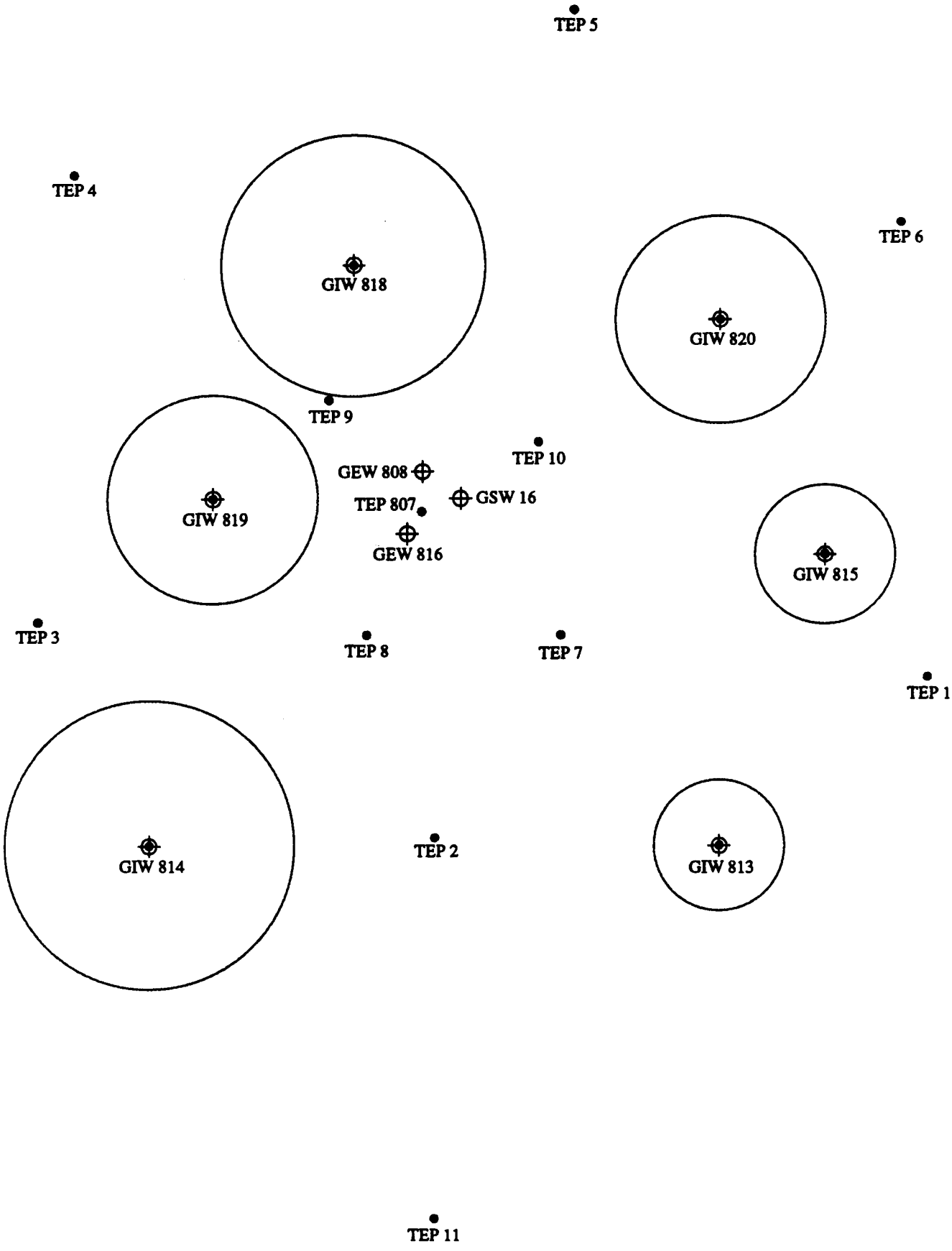

Figure 3.1: Pass 1 Lower Zone Day 2

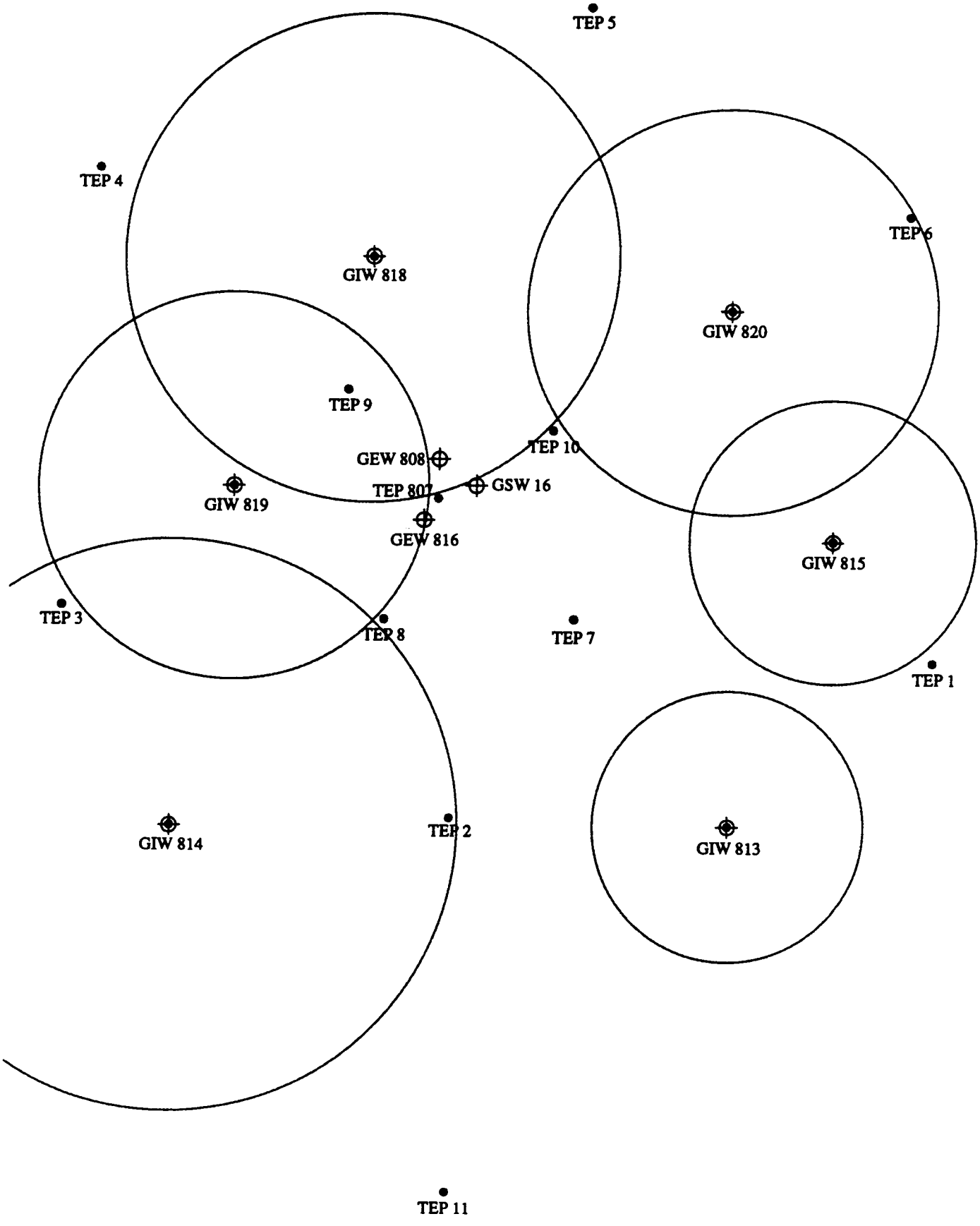

Figure 3.2: Pass 1 Lower Zone Day 6

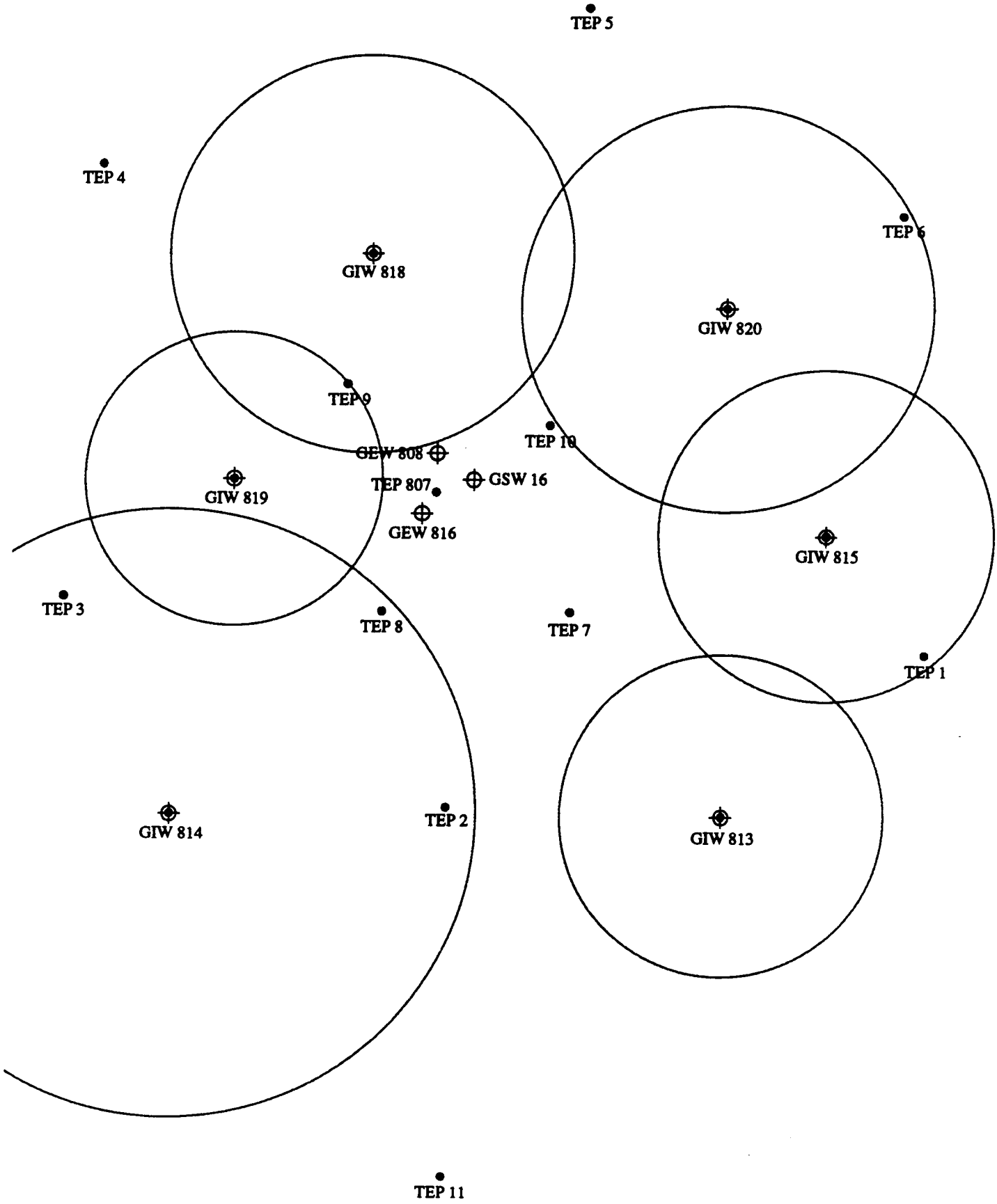

Figure 3.3: Pass 1 Lower Zone Day 10

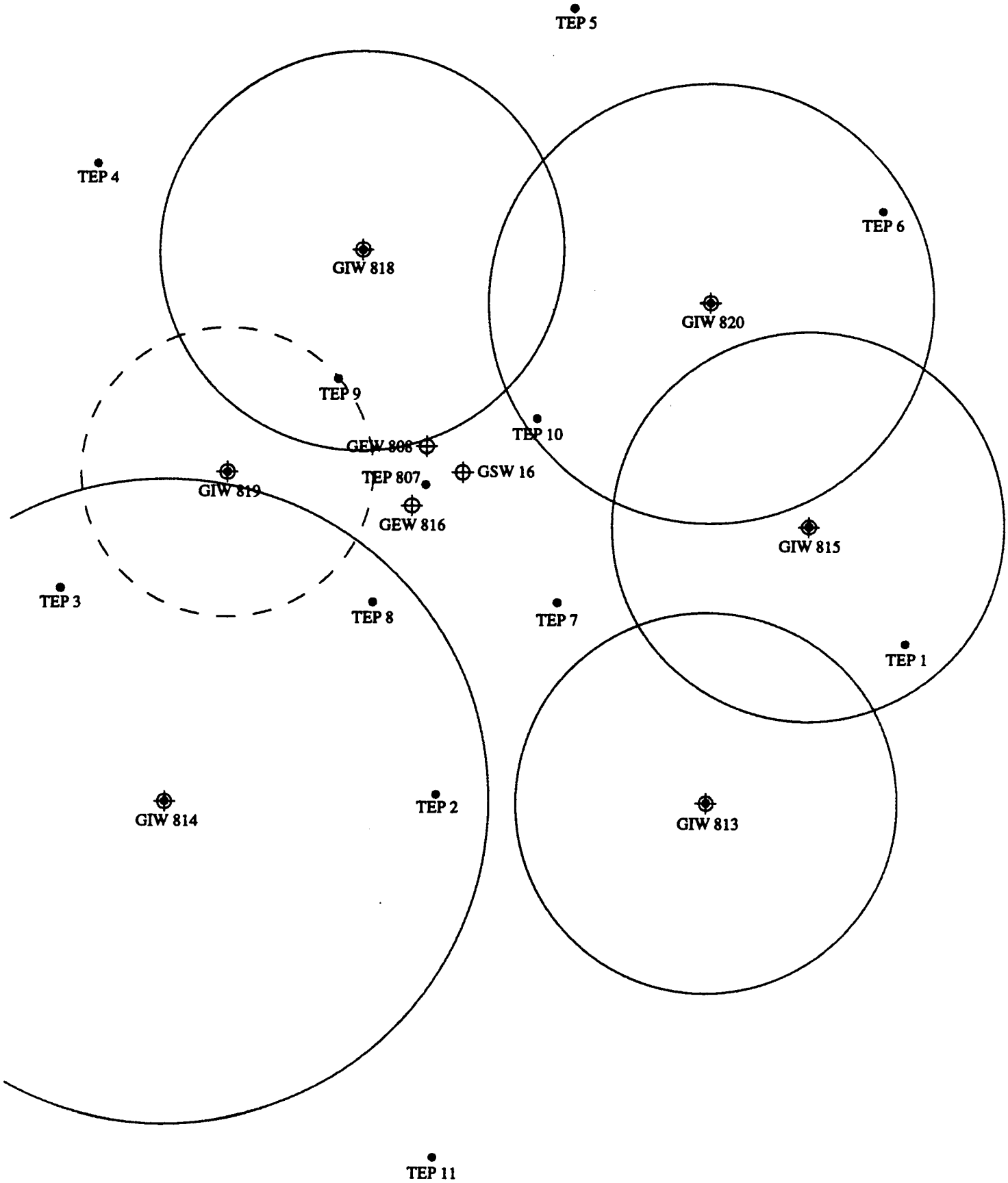

Figure 3.4: Pass 1 Lower Zone Day 14

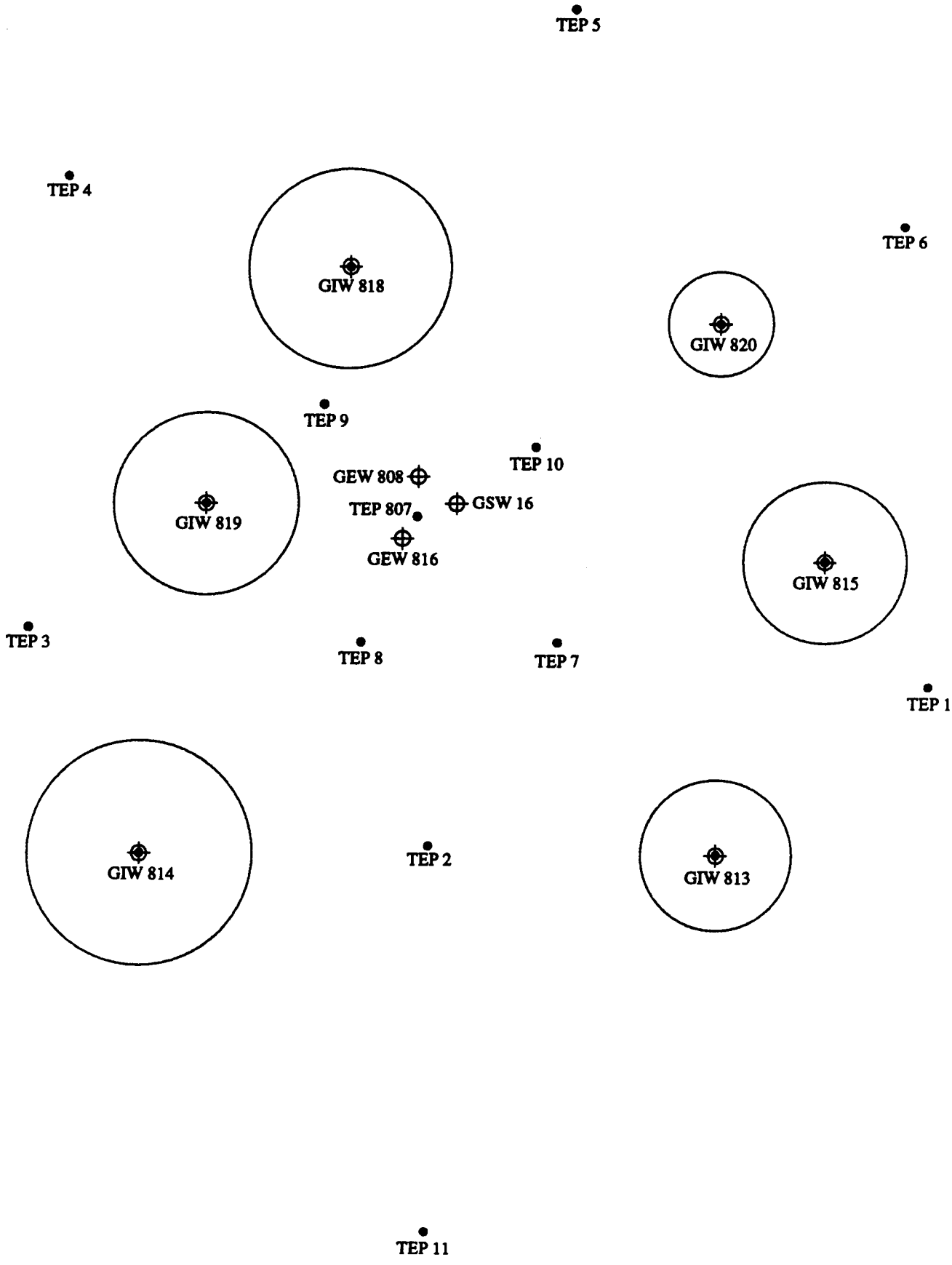

Figure 3.5: Pass 1 Upper Zone Day 15

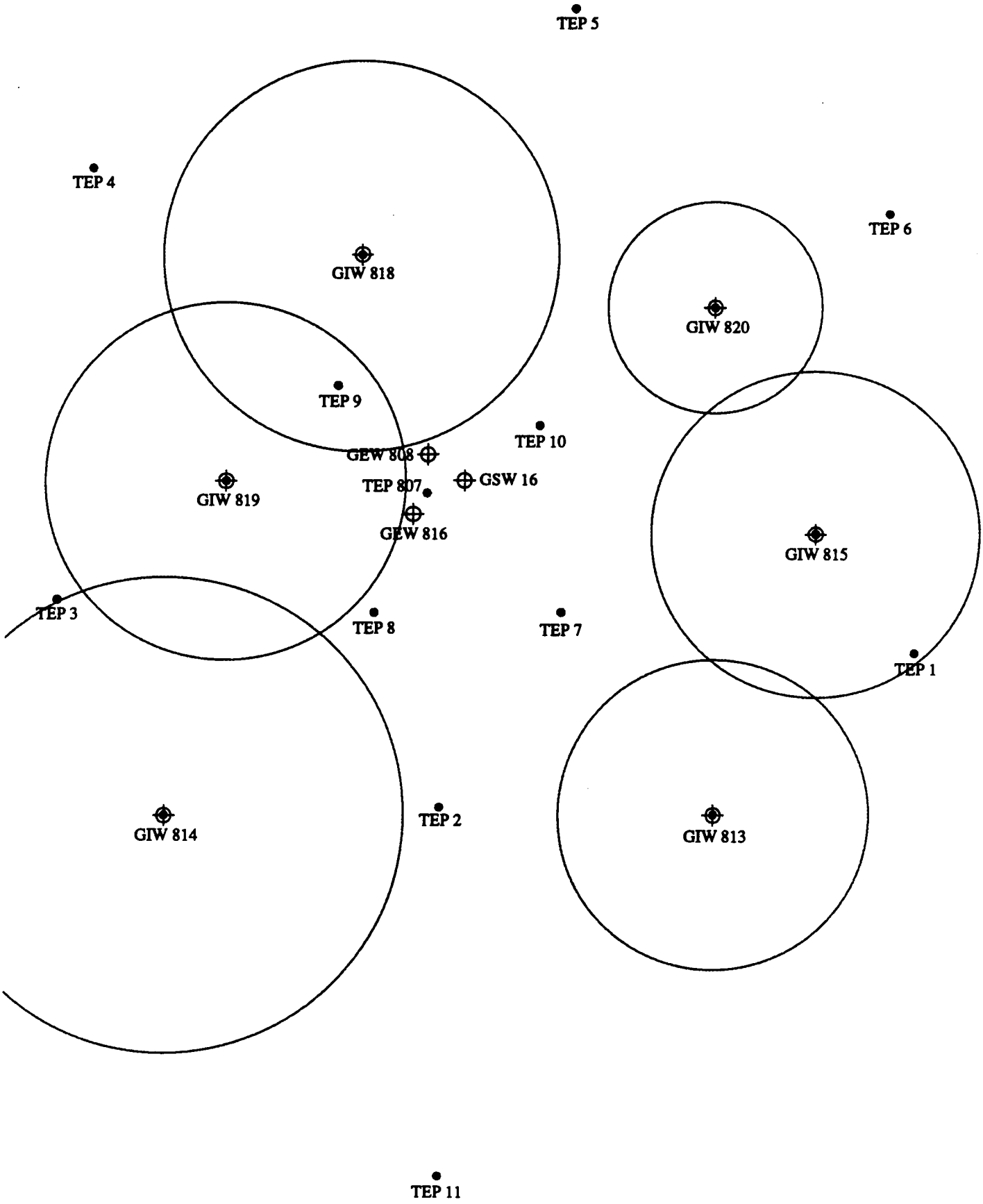

Figure 3.6: Pass 1 Upper Zone Day 19

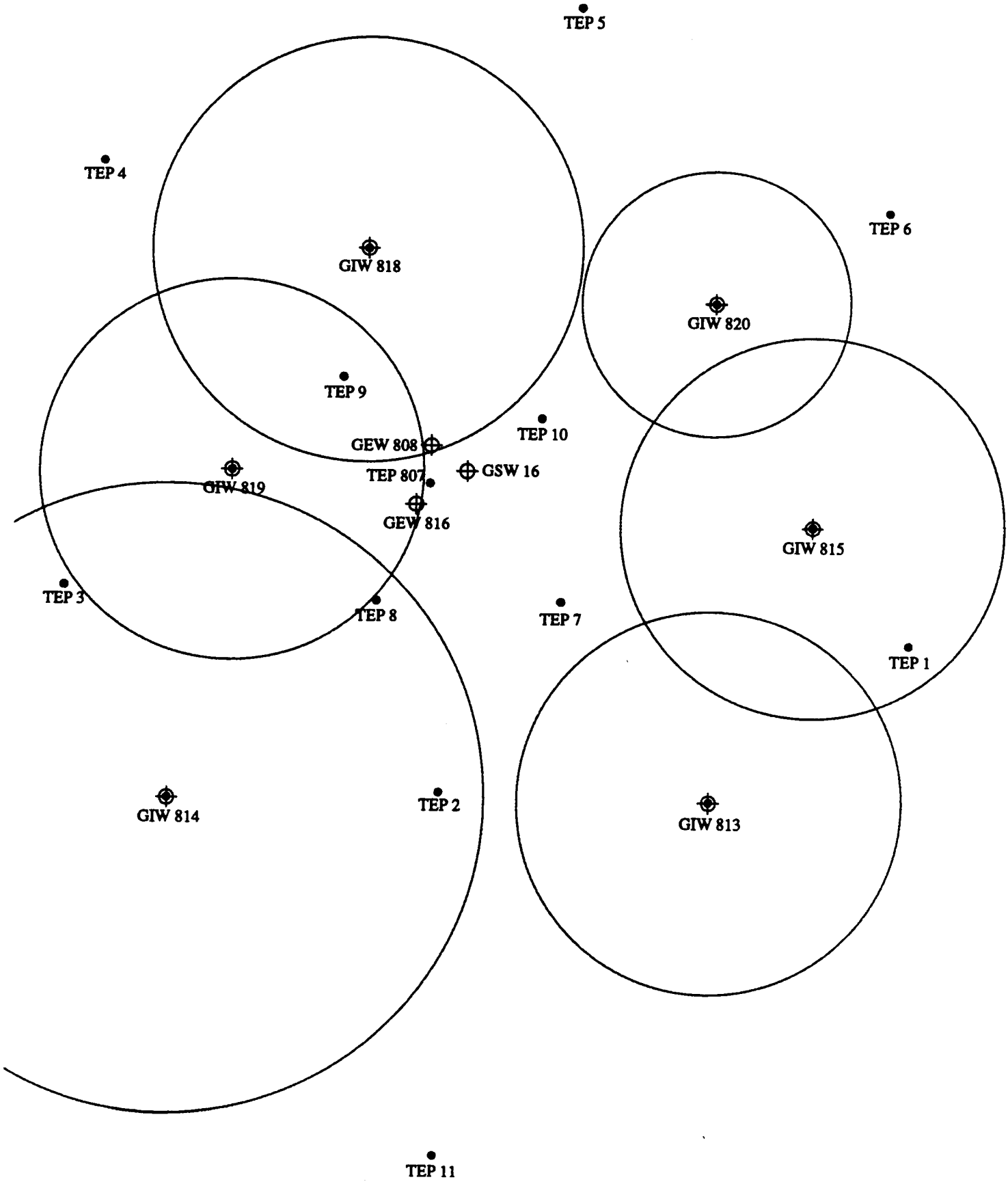

Figure 3.7: Pass 1 Upper Zone Day 23

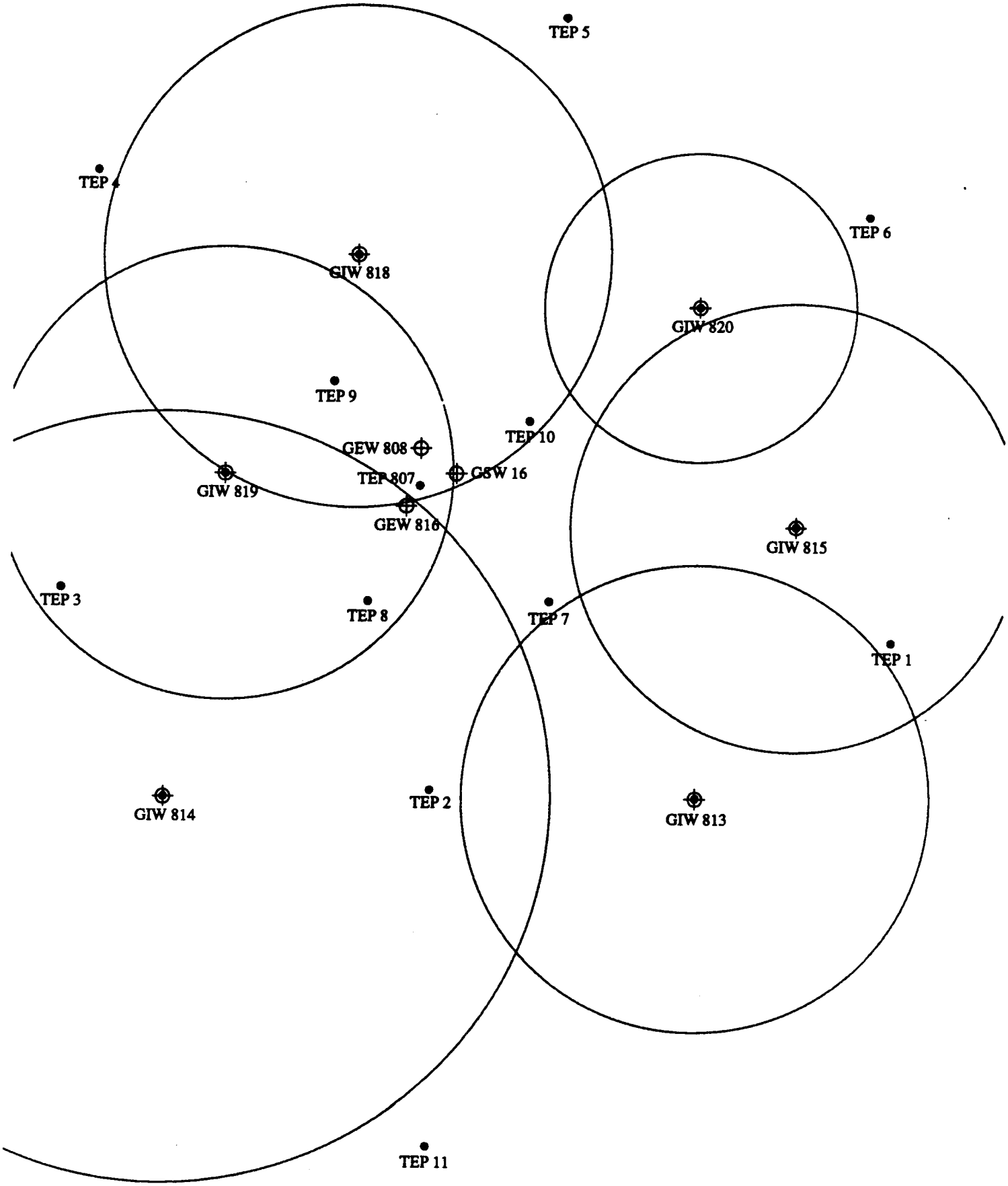

Figure 3.8: Pass 1 Upper Zone Day 28

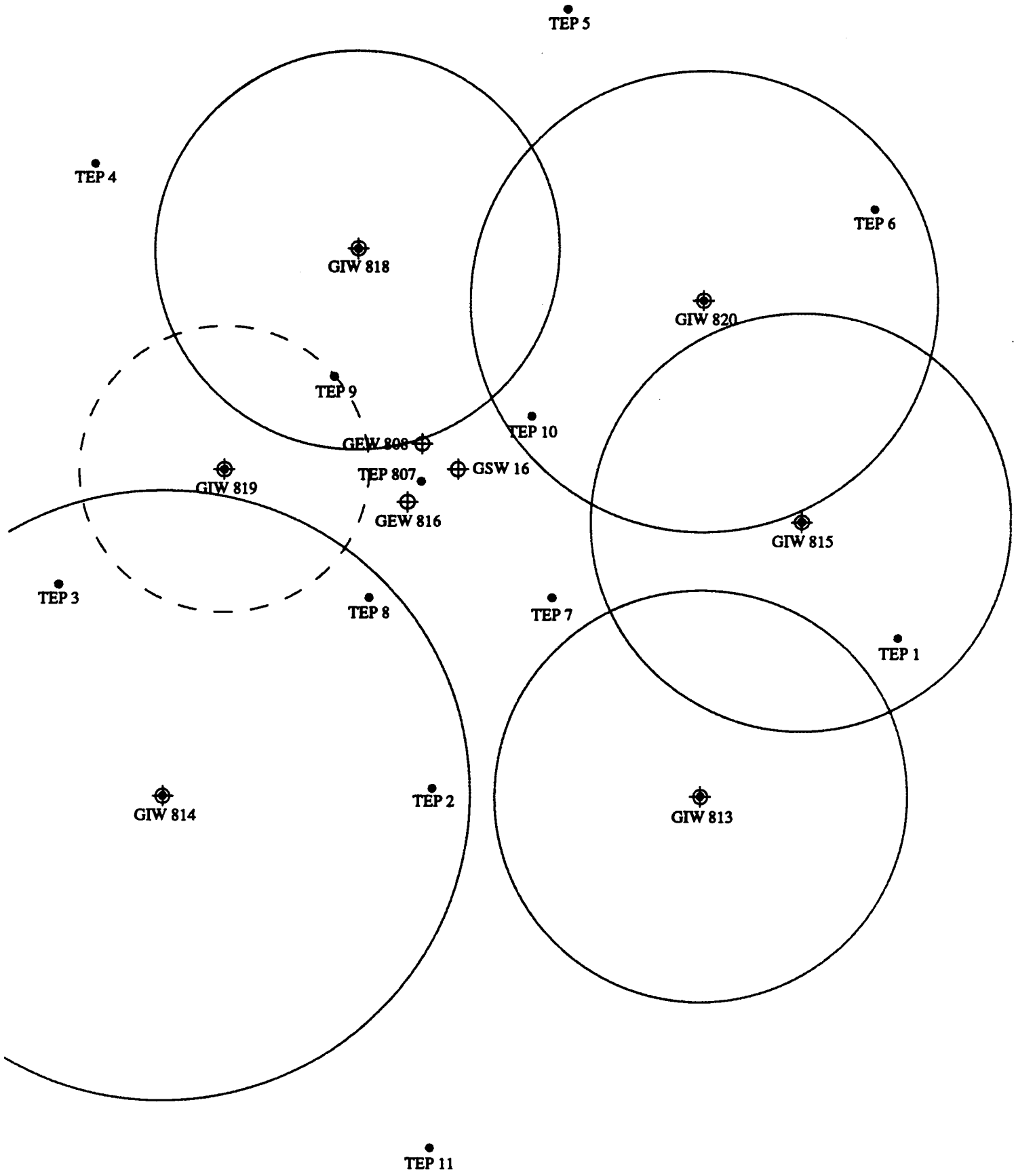

Figure 3.9: Pass 1 Lower Zone Day 29

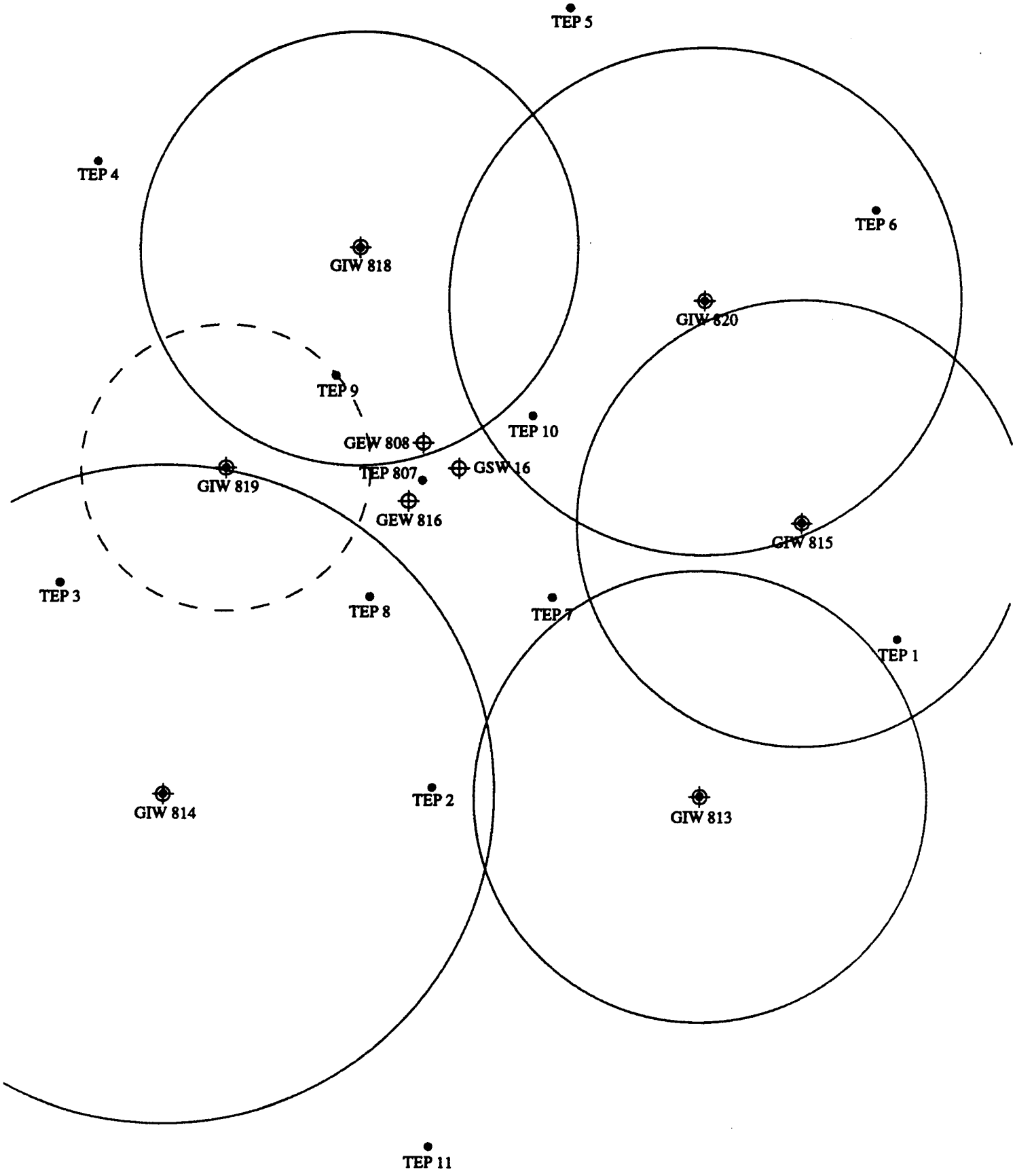

Figure 3.10: Pass 1 Lower Zone Day 33

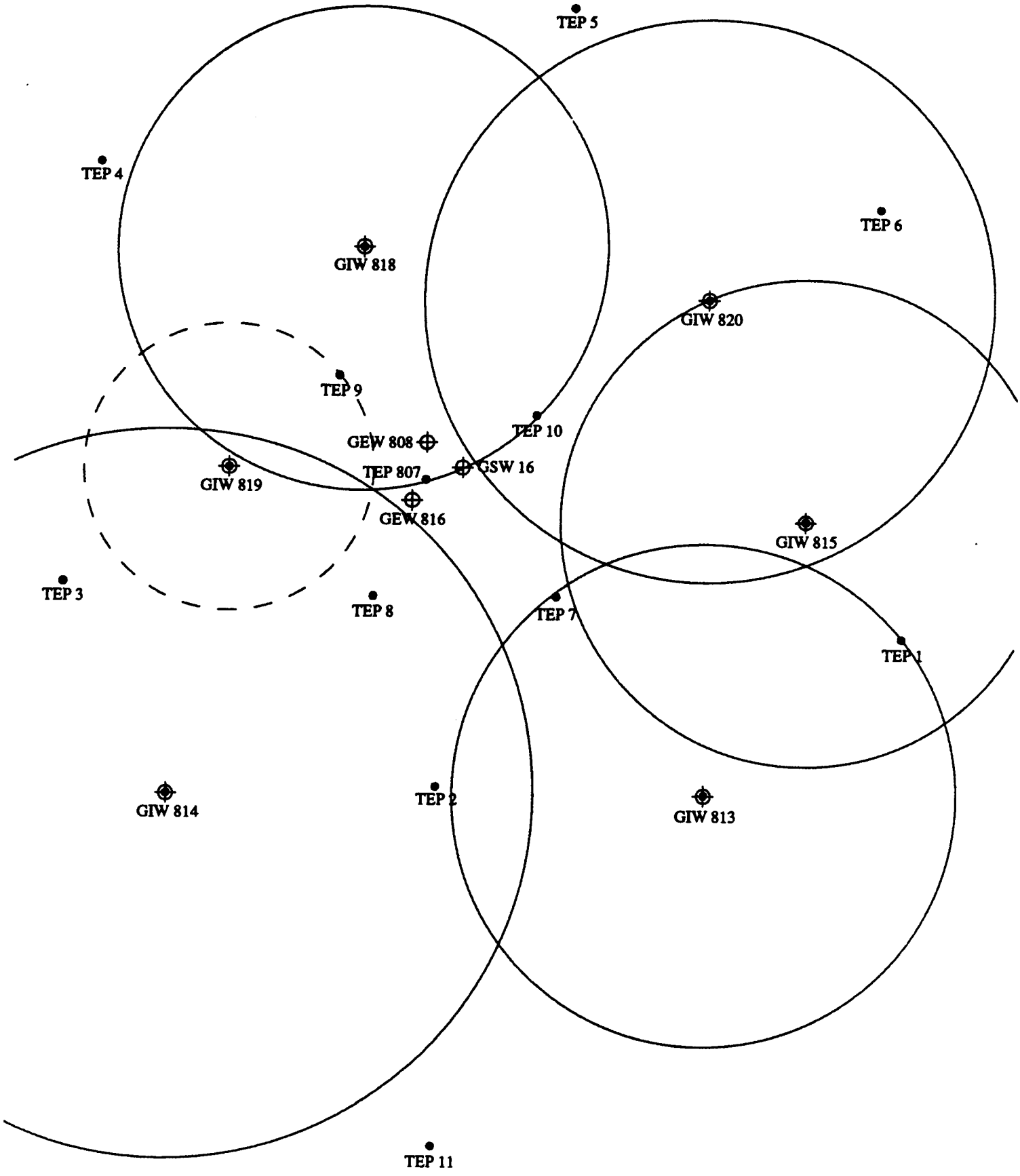

Figure 3.11: Pass 1 Lower Zone Day 37

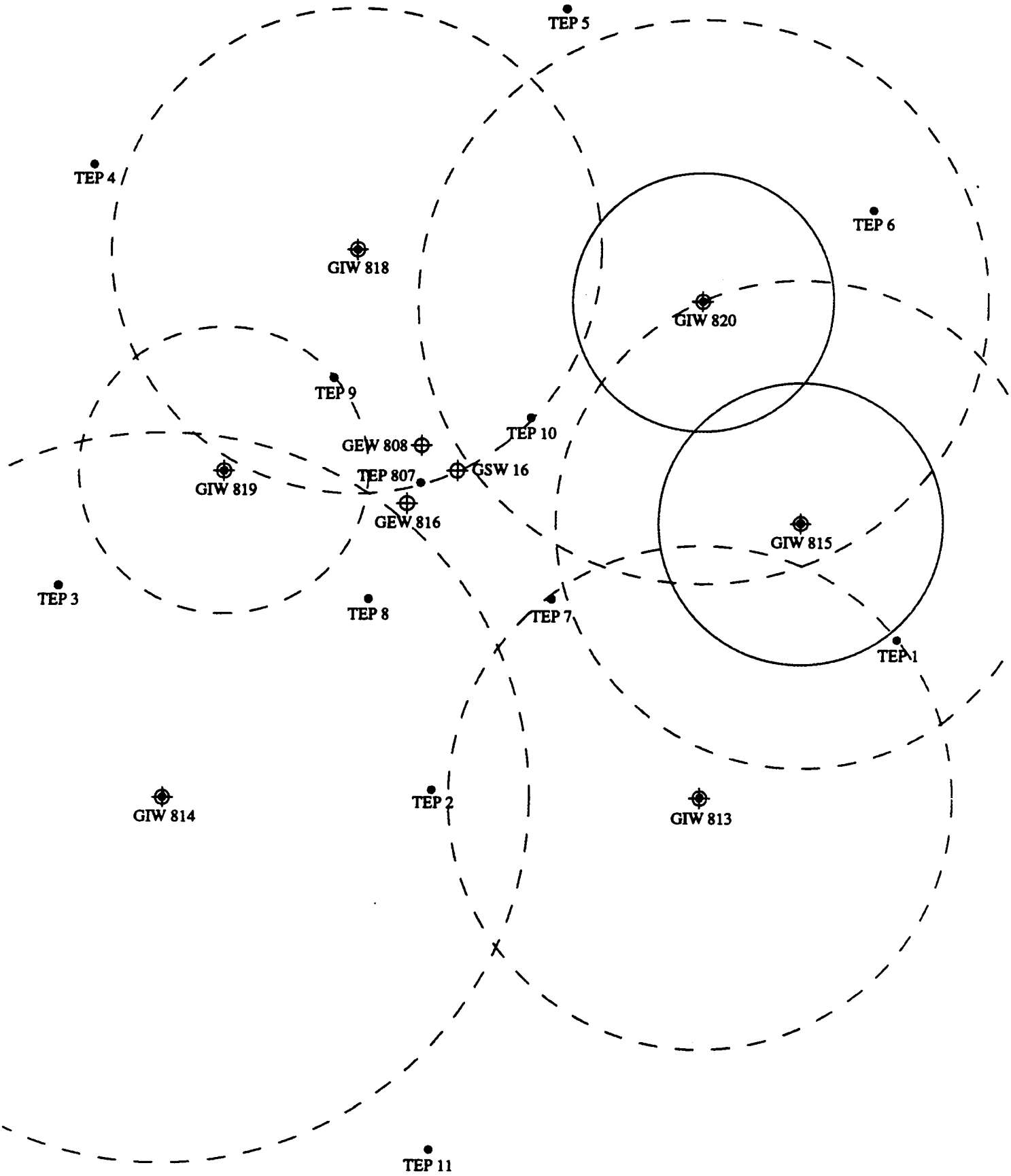

Figure 3.12: Pass 2 Lower Zone Day 11

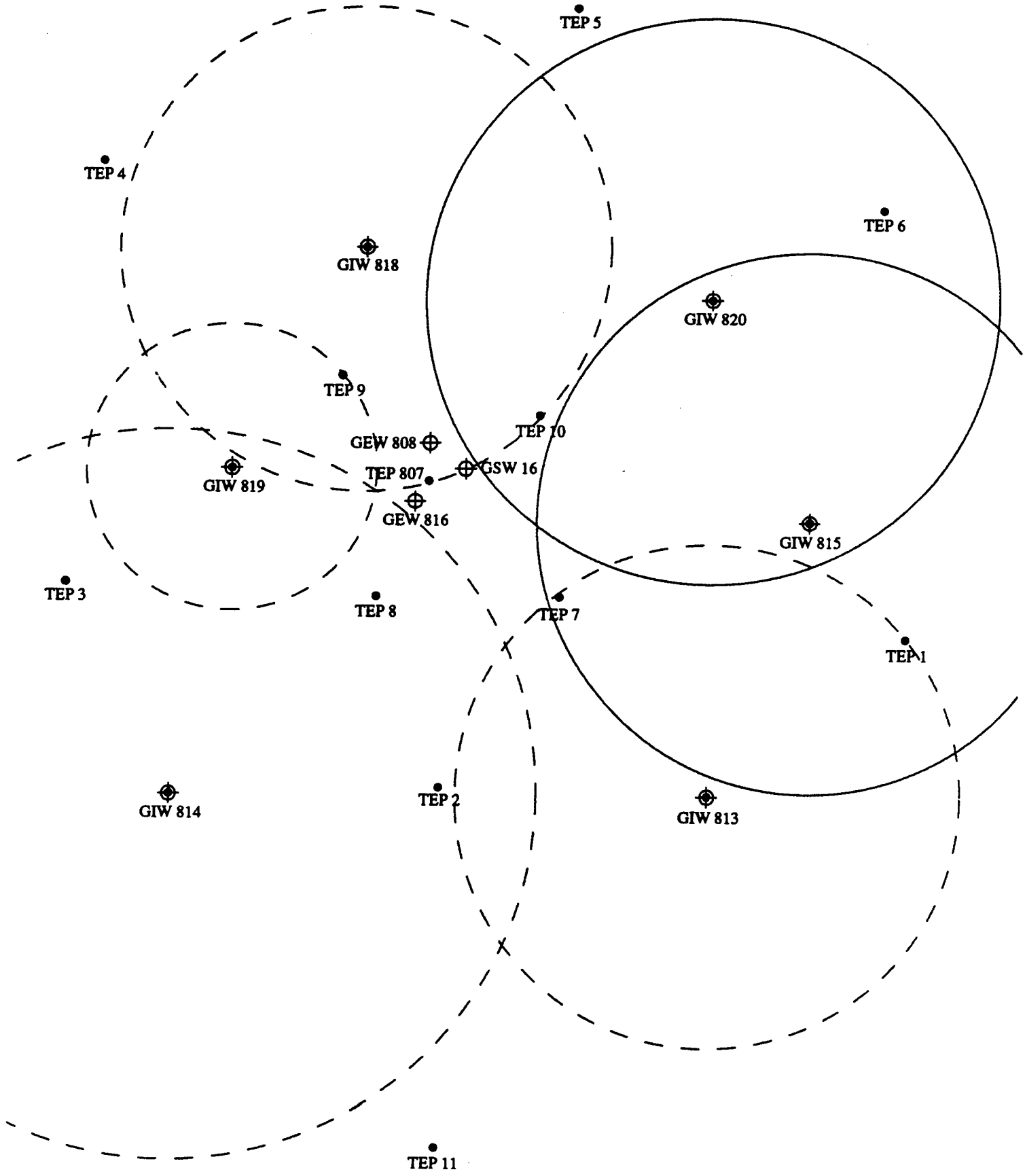

Figure 3.13: Pass 2 Lower Zone Day 15

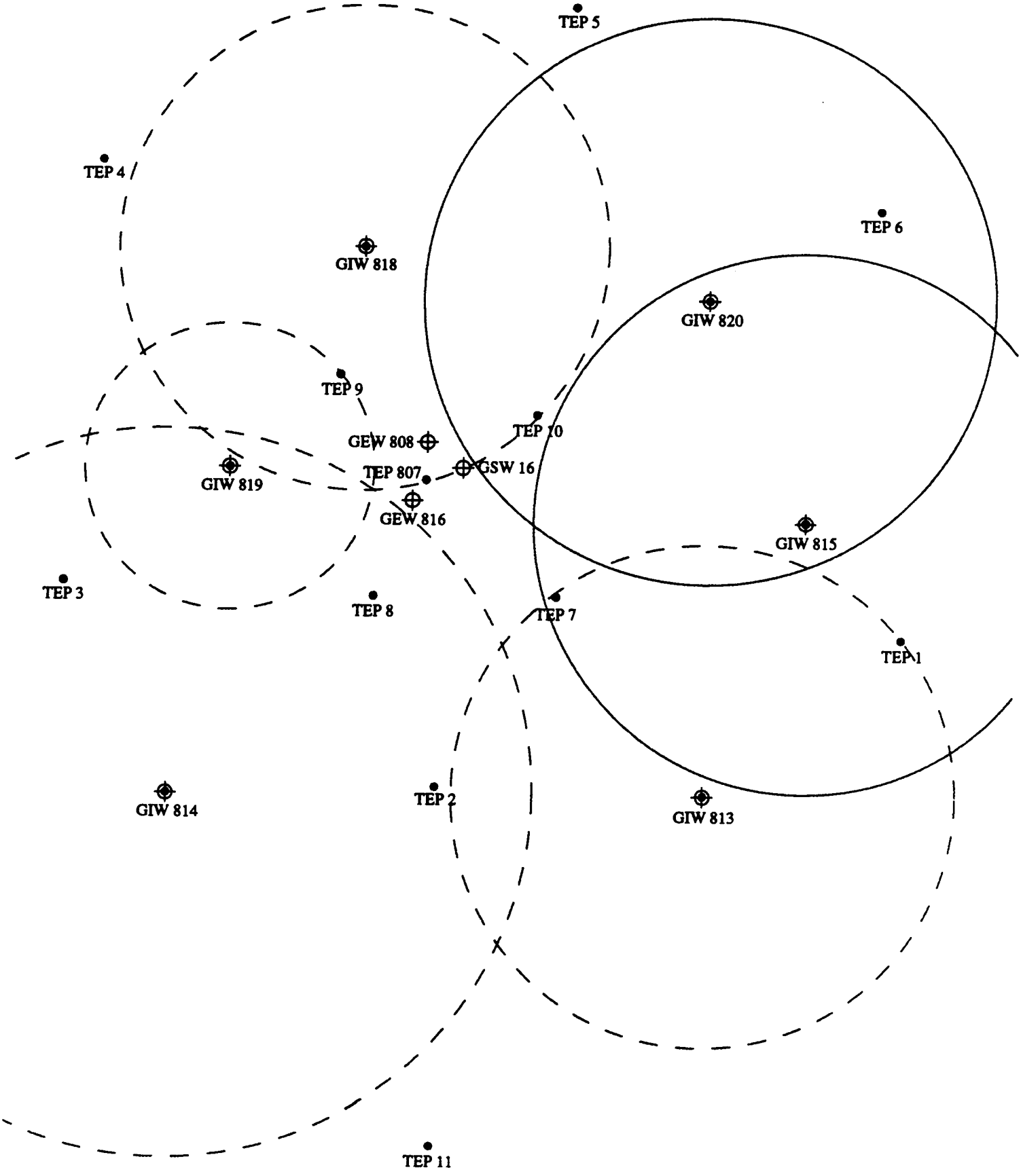

Figure 3.14: Pass 2 Lower Zone Day 20

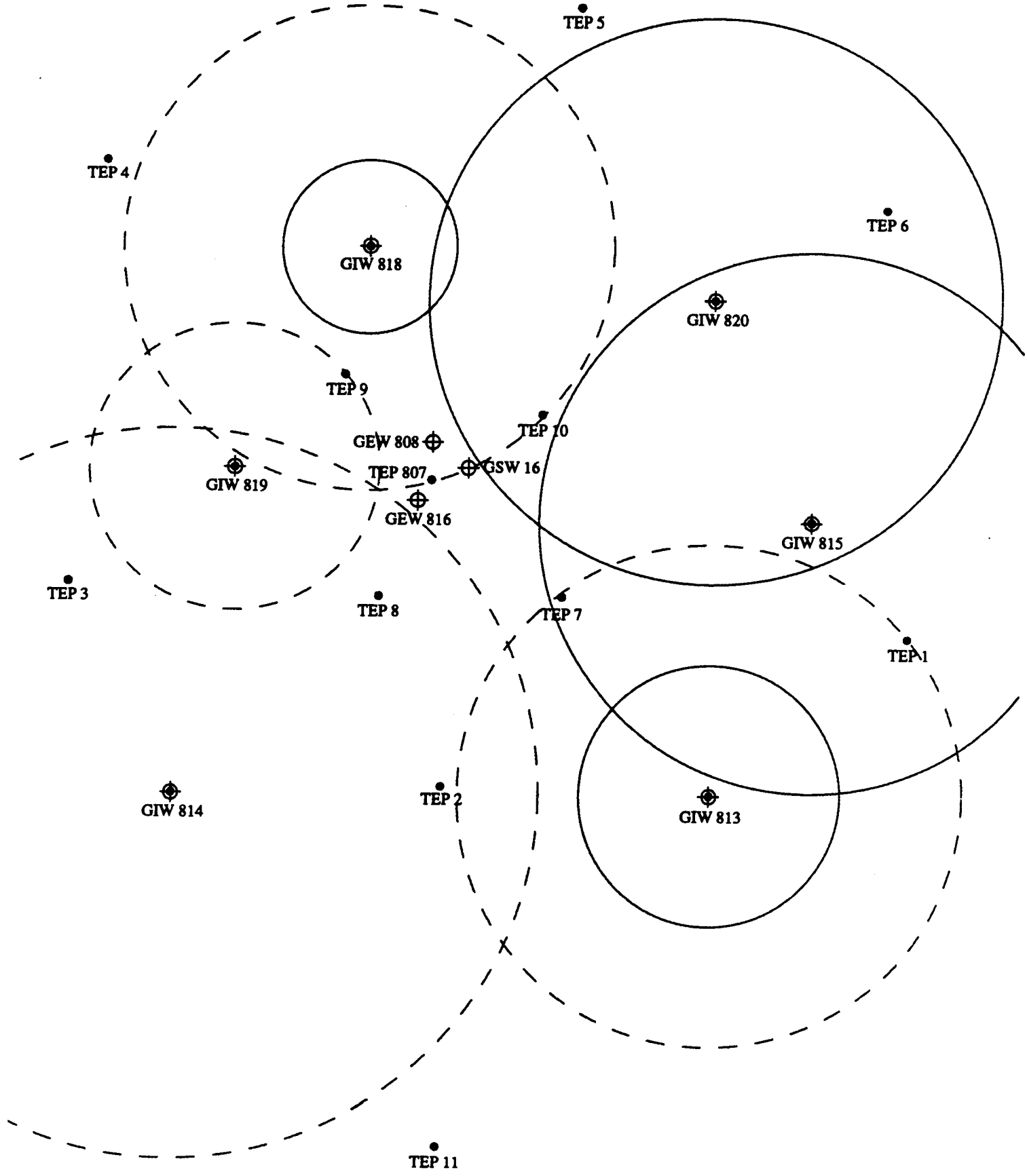

Figure 3.15: Pass 2 Lower Zone Day 25

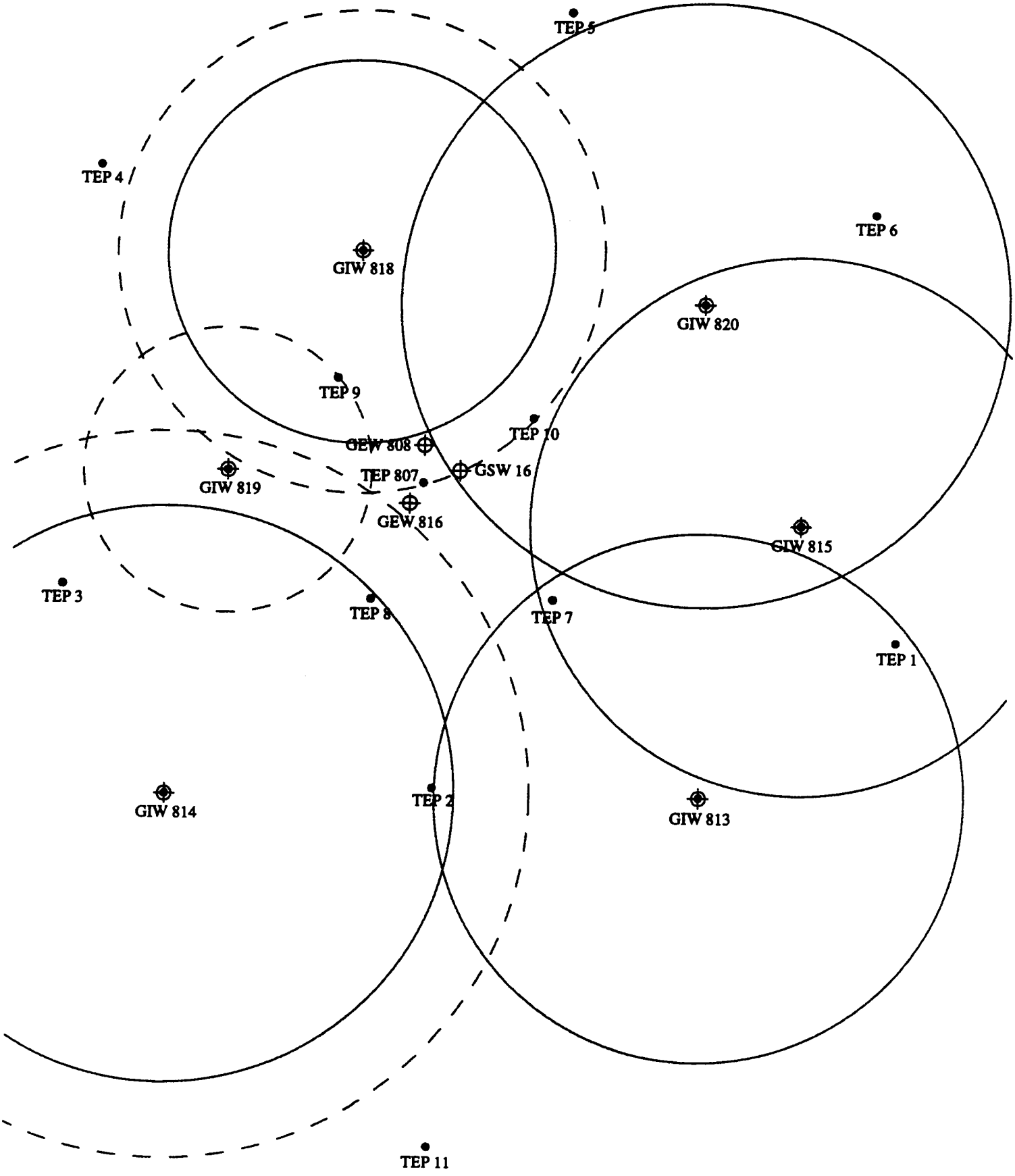

Figure 3.16: Pass 2 Lower Zone Day 30

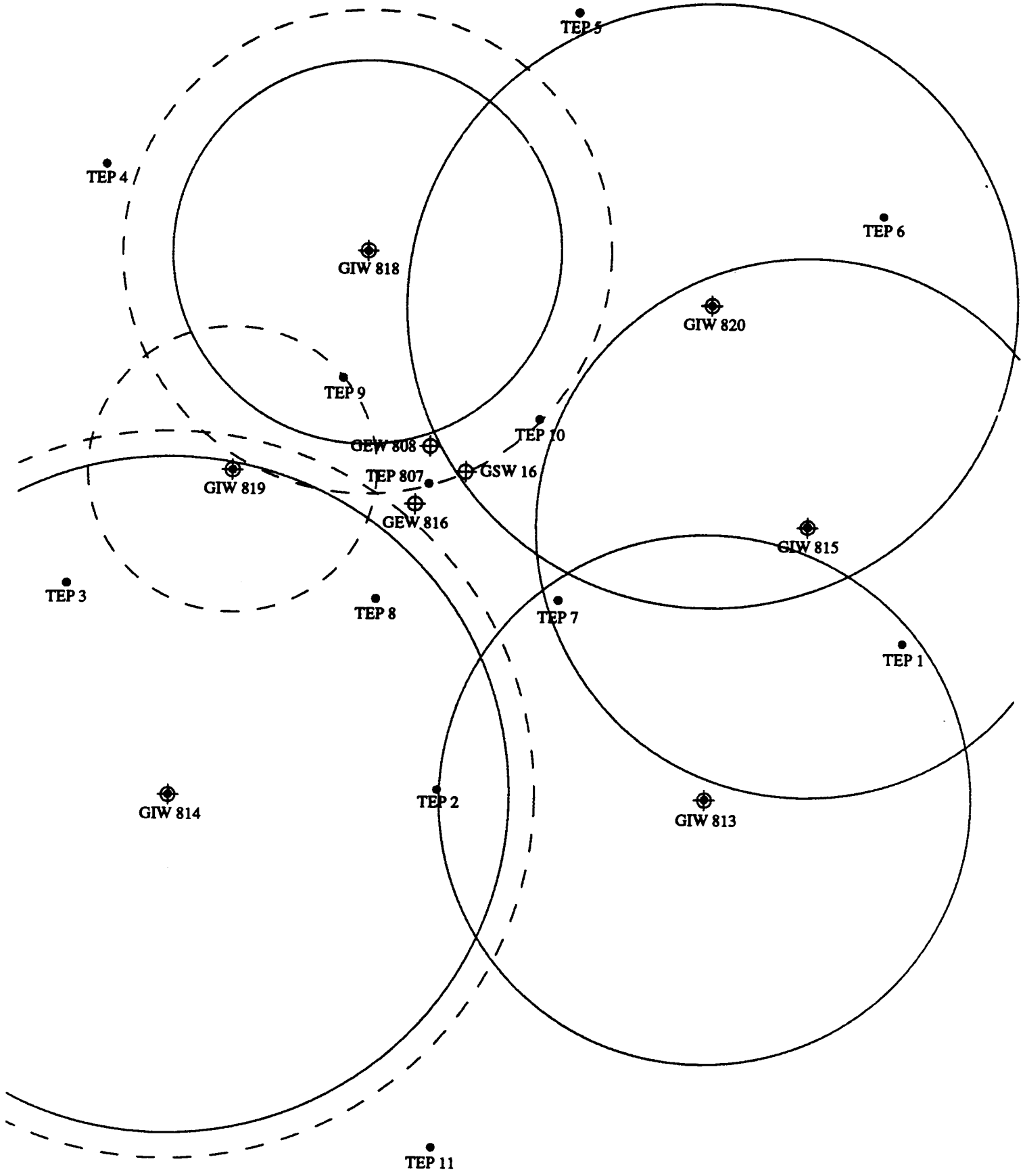

Figure 3.17: Pass 2 Lower Zone Day 35

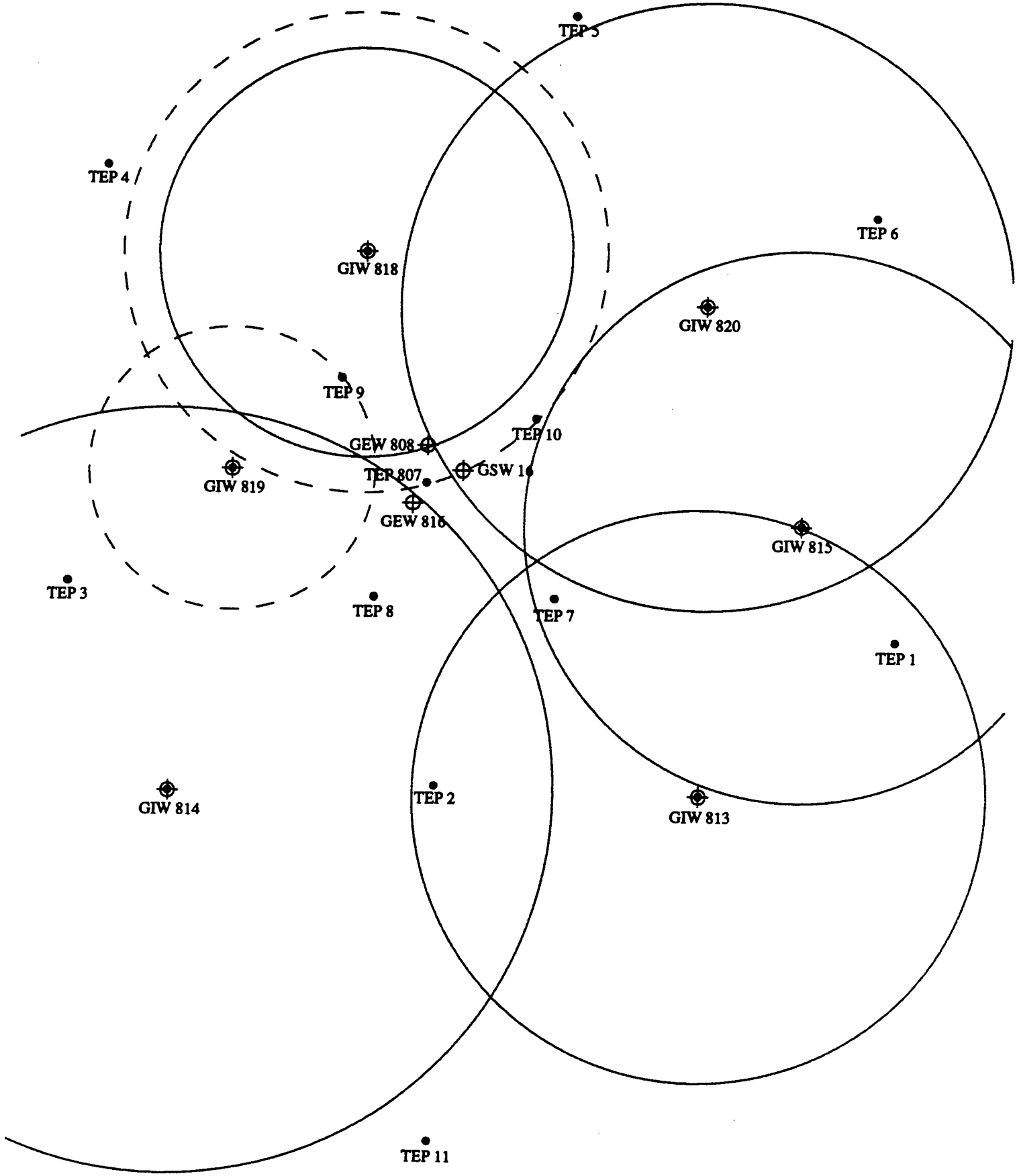

Figure 3.18: Pass 2 Lower Zone Day 39

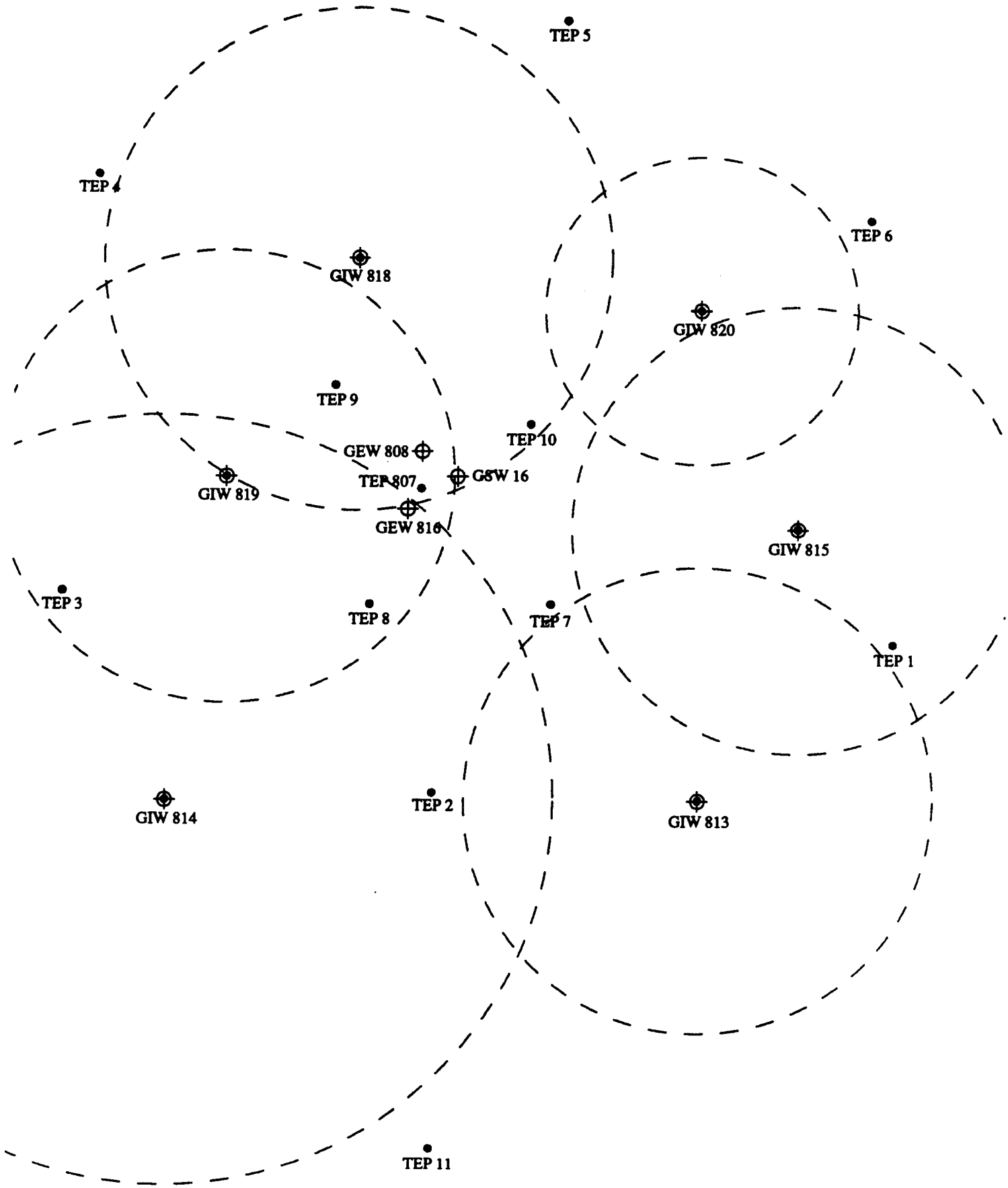

Figure 3.19: Pass 2 Upper Zone Day 15

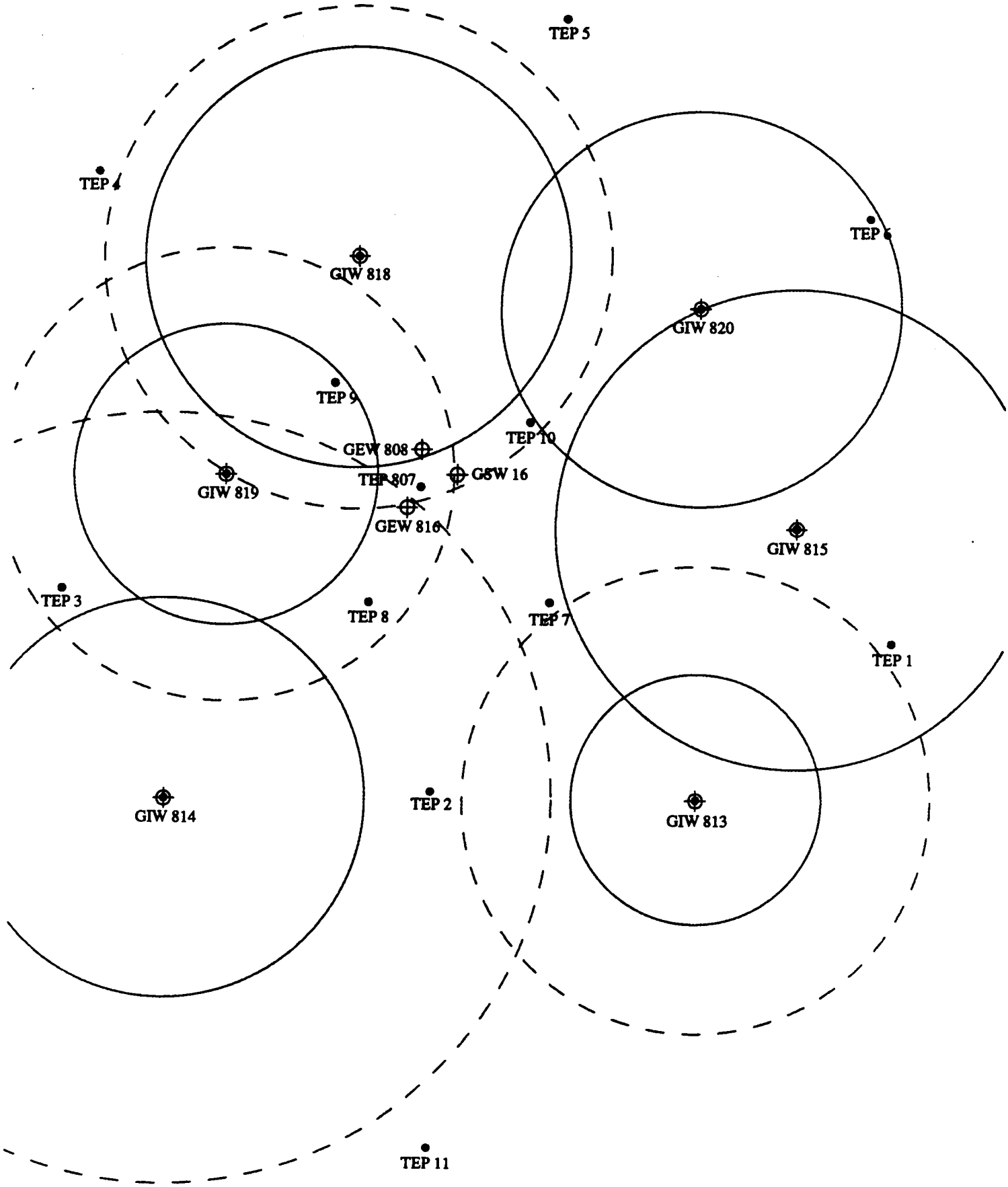

Figure 3.20: Pass 2 Upper Zone Day 20

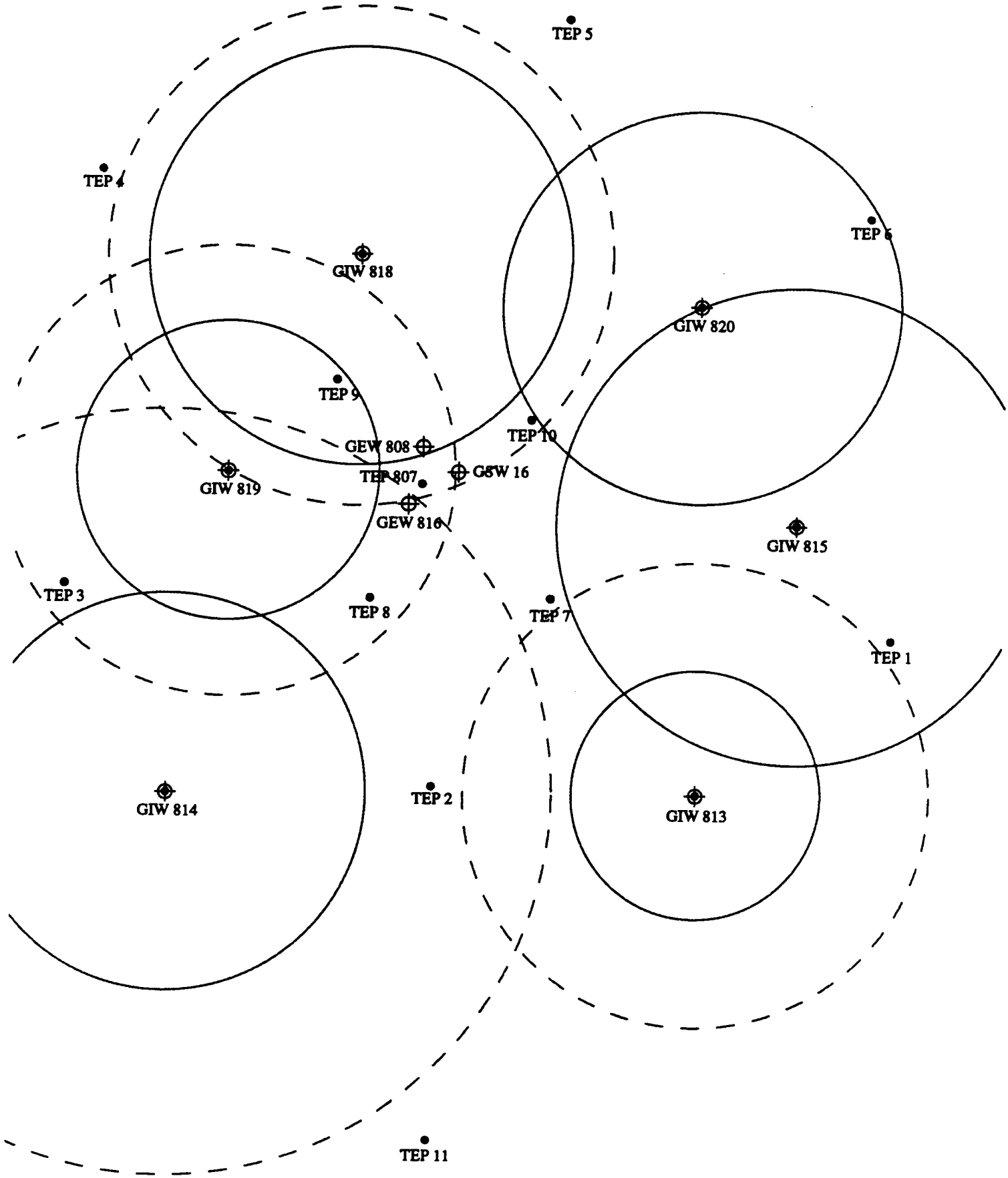

Figure 3.21: Pass 2 Upper Zone Day 25

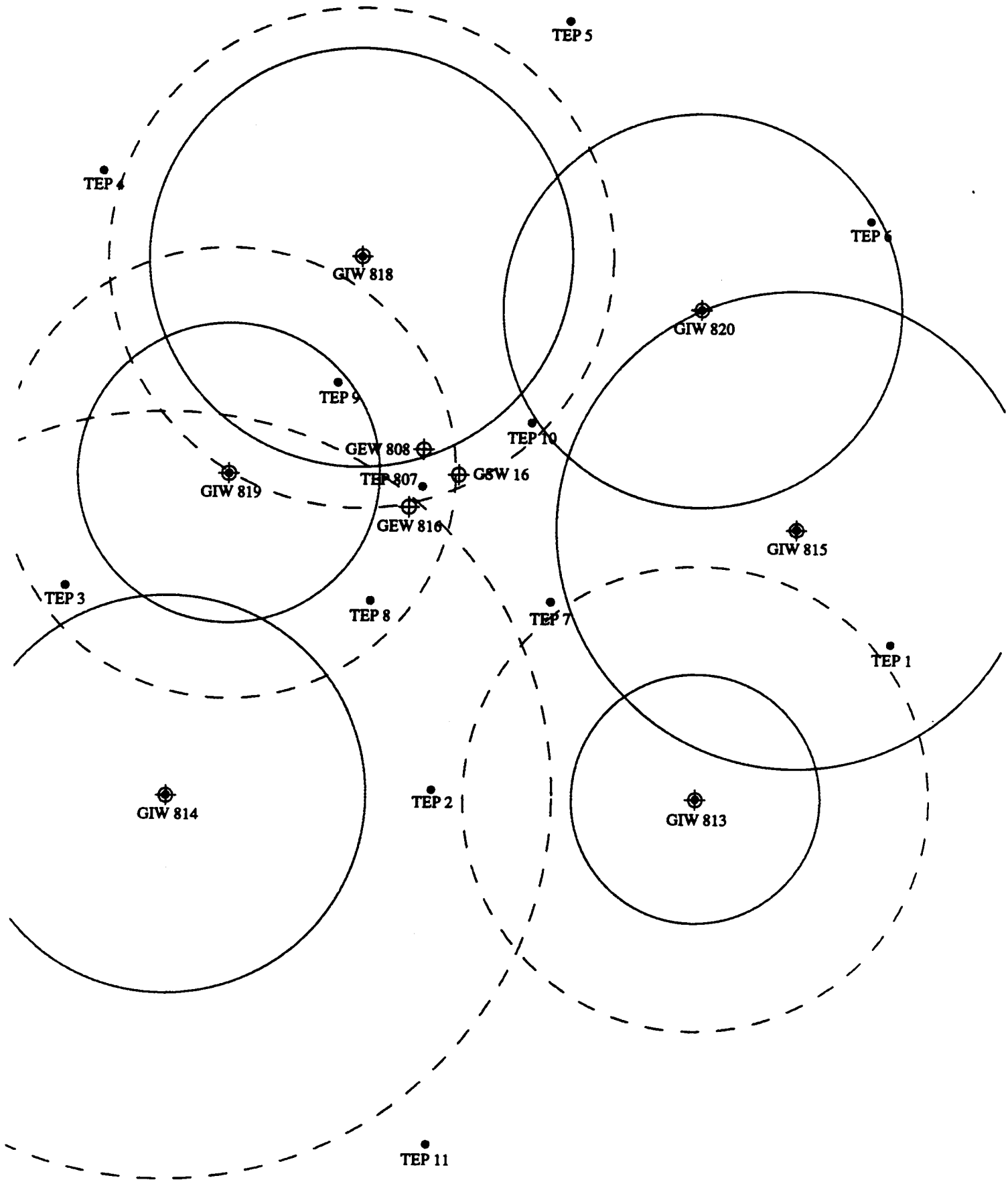

Figure 3.22: Pass 2 Upper Zone Day 30

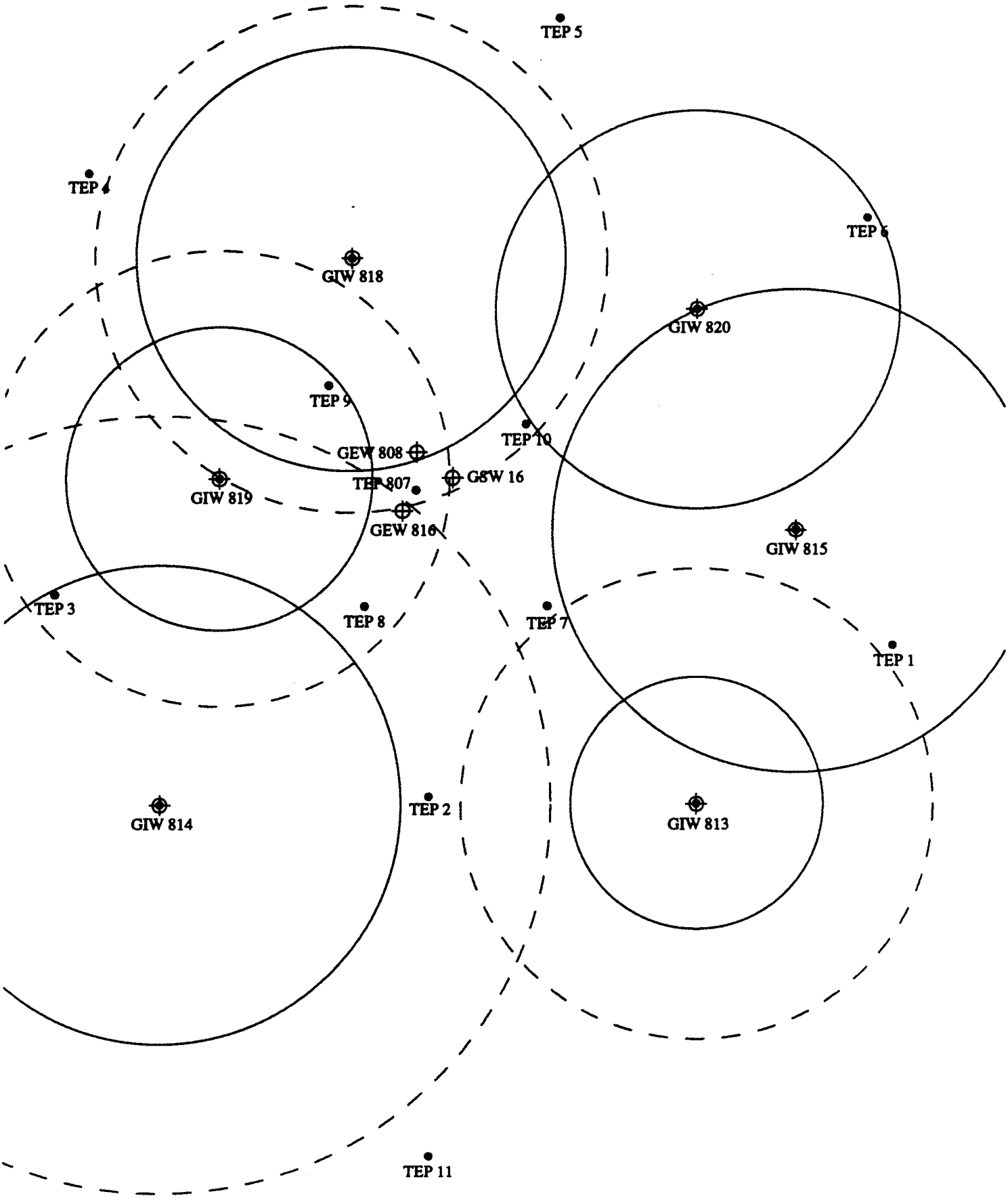

Figure 3.23: Pass 2 Upper Zone Day 35

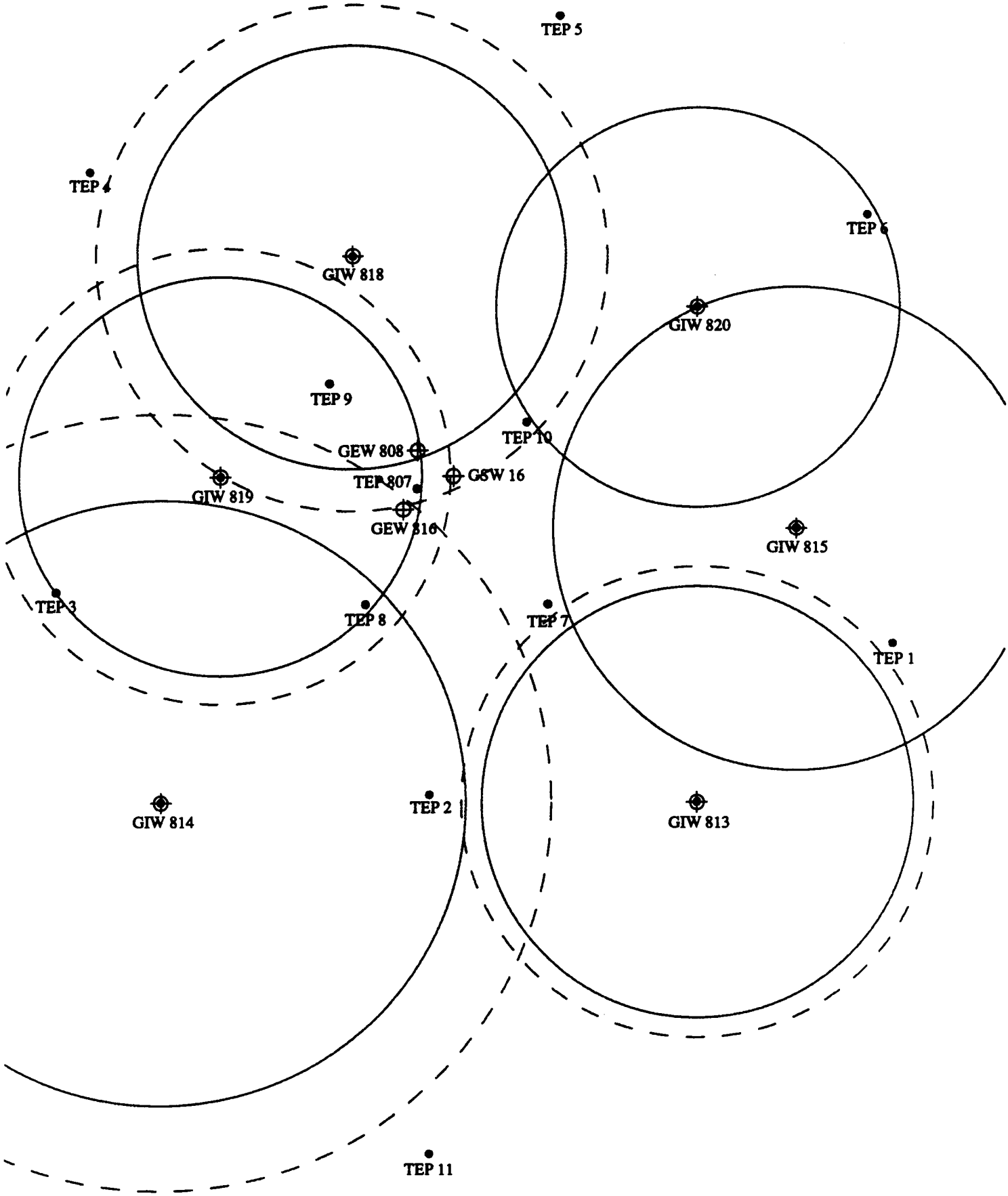

Figure 3.24: Pass 2 Upper Zone Day 39

Table 2.1: Temperature wells used to determine steam zone thickness for each injection well.

IW 813	TEP 1
IW 814	TEP 2
IW 815	TEP 1
IW 818	TEP 9
IW 819	TEP 9
IW 820	TEP 10

Table 4.1: Pass 1 comparison of the actual days steam was observed to reach the TEP wells and the days predicted to do so by the model. (Pass 1 steaming from Day 1 - Day 37).

TEP WELL	ACTUAL DAYS	PREDICTED DAYS
TEP 1	2, 12, 34	9, 19, 37
TEP 2	12, 33	6, 21
TEP 3	No Steam	5, 20
TEP 4	22	No Steam
TEP 5	No Steam	No Steam
TEP 6	24	5
TEP 7	36	37
TEP 8	8, 19	9, 22
TEP 9	11, 16, 26	3, 10, 16
TEP 10	31, 34	5, 12, 27, 37
TEP 11	No Steam	No Steam

Table 4.2: Pass 2 comparison of the actual days steam was observed to reach the TEP wells and the days predicted to do so by the model. (Pass 2 steaming from Day 10 - Day 39).

TEP WELL	ACTUAL DAYS	PREDICTED DAYS
TEP 1	11, 17	12, 17, 28
TEP 2	32, 37	29, 37
TEP 3	No Steam	28
TEP 4	18	No Steam
TEP 5	23	No Steam
TEP 6	Not Available	13, 20
TEP 7	17, 32	15, 28
TEP 8	Not Available	29, 38
TEP 9	19, 28	19, 27
TEP 10	12, 27	13, 27
TEP 11	No Steam	No Steam

Appendix

Figure A.1: Fixed Thermocouple Data for TEP1, Pass 1

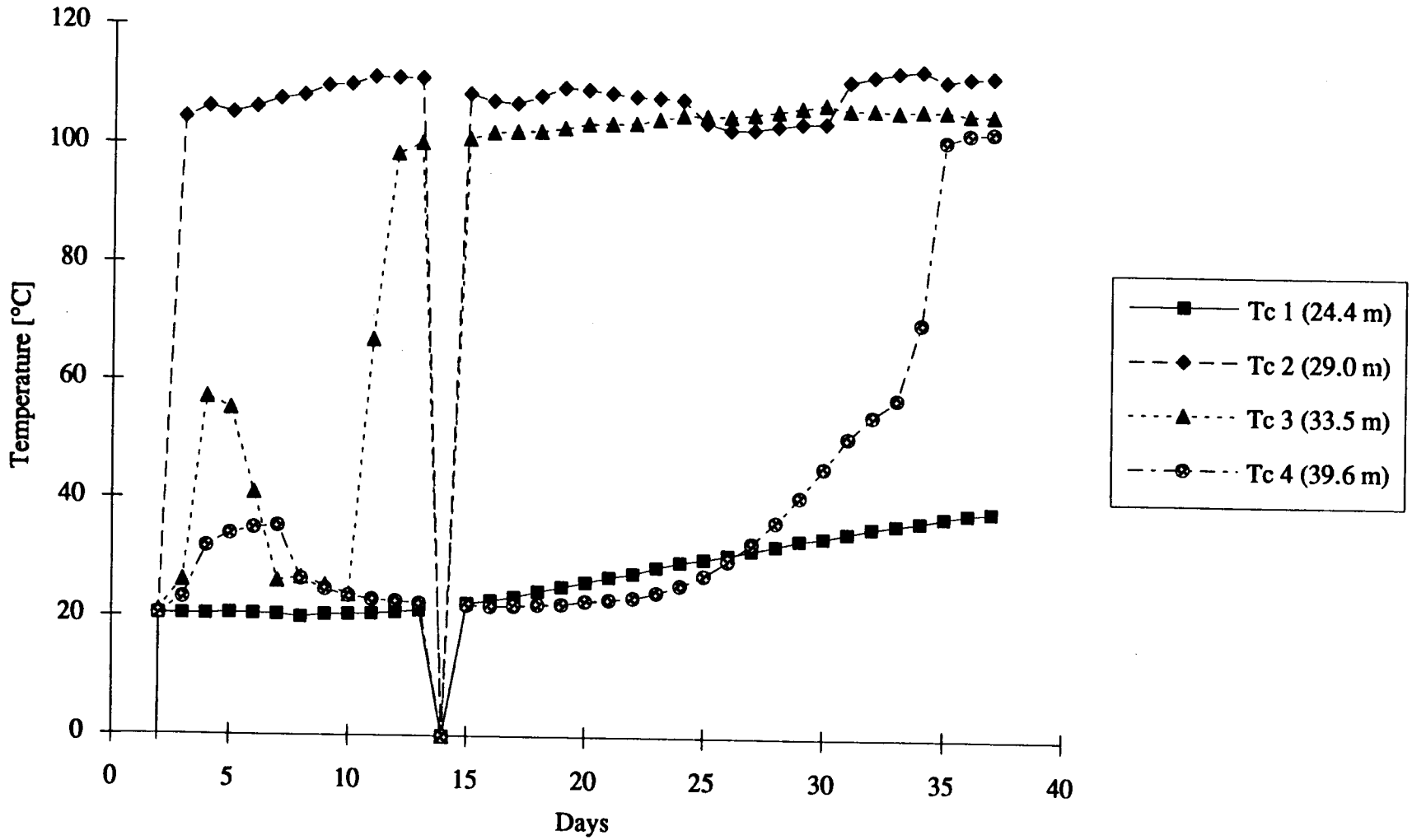

Figure A.2: Fixed Thermocouple Data for TEP2, Pass1

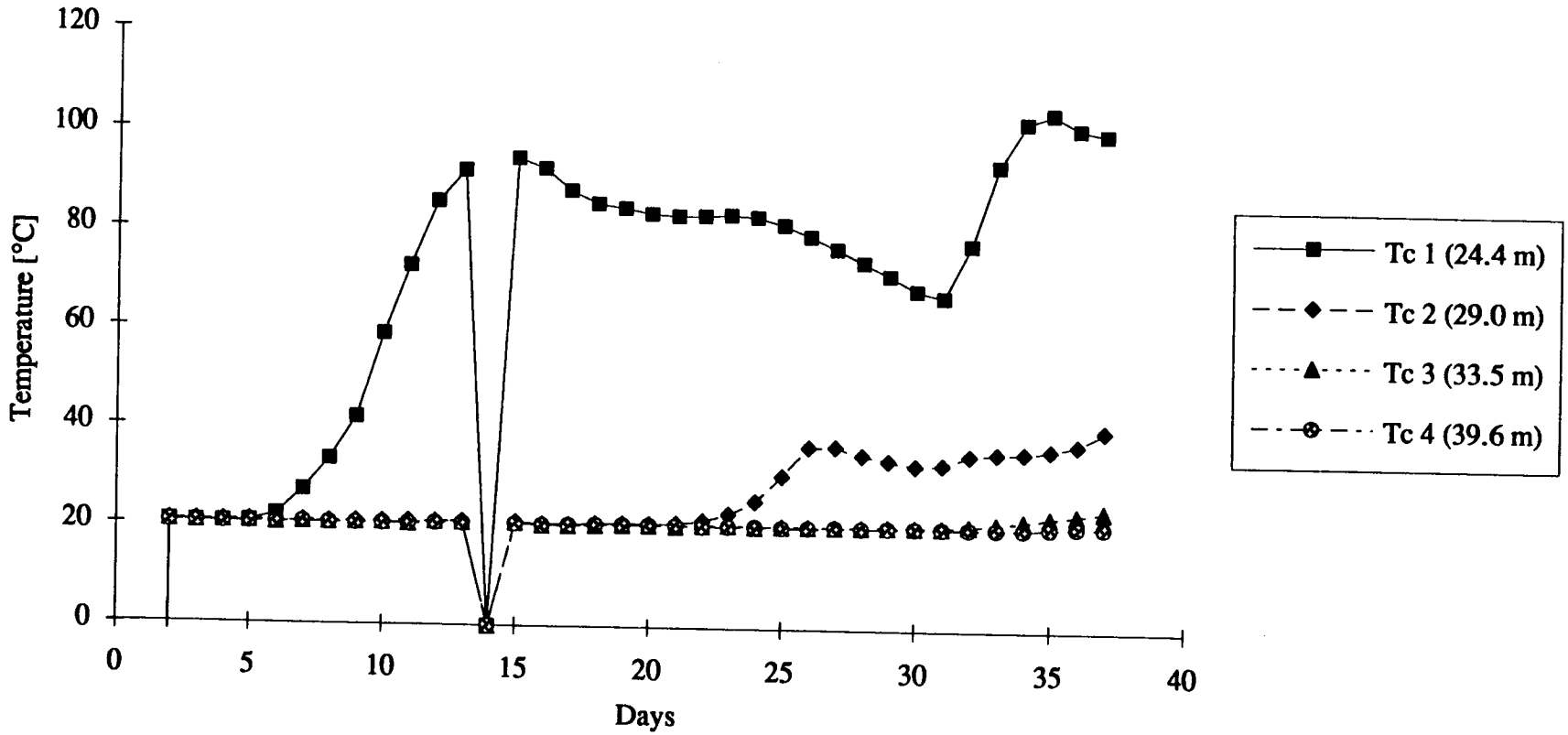

Figure A.3: Fixed Thermocouple Data for TEP3, Pass 1

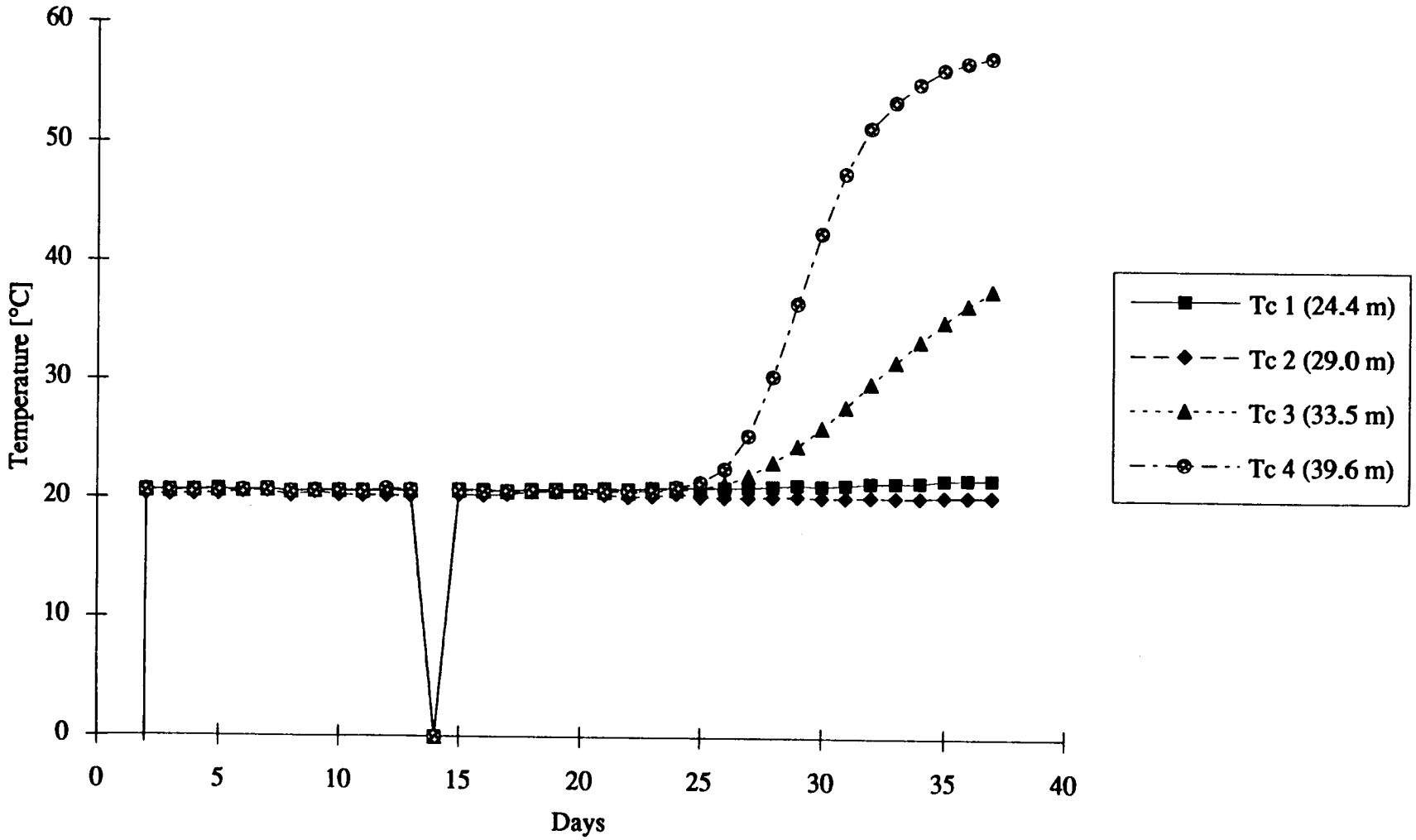

Figure A.4: Fixed Thermocouple Data for TEP4, Pass 1

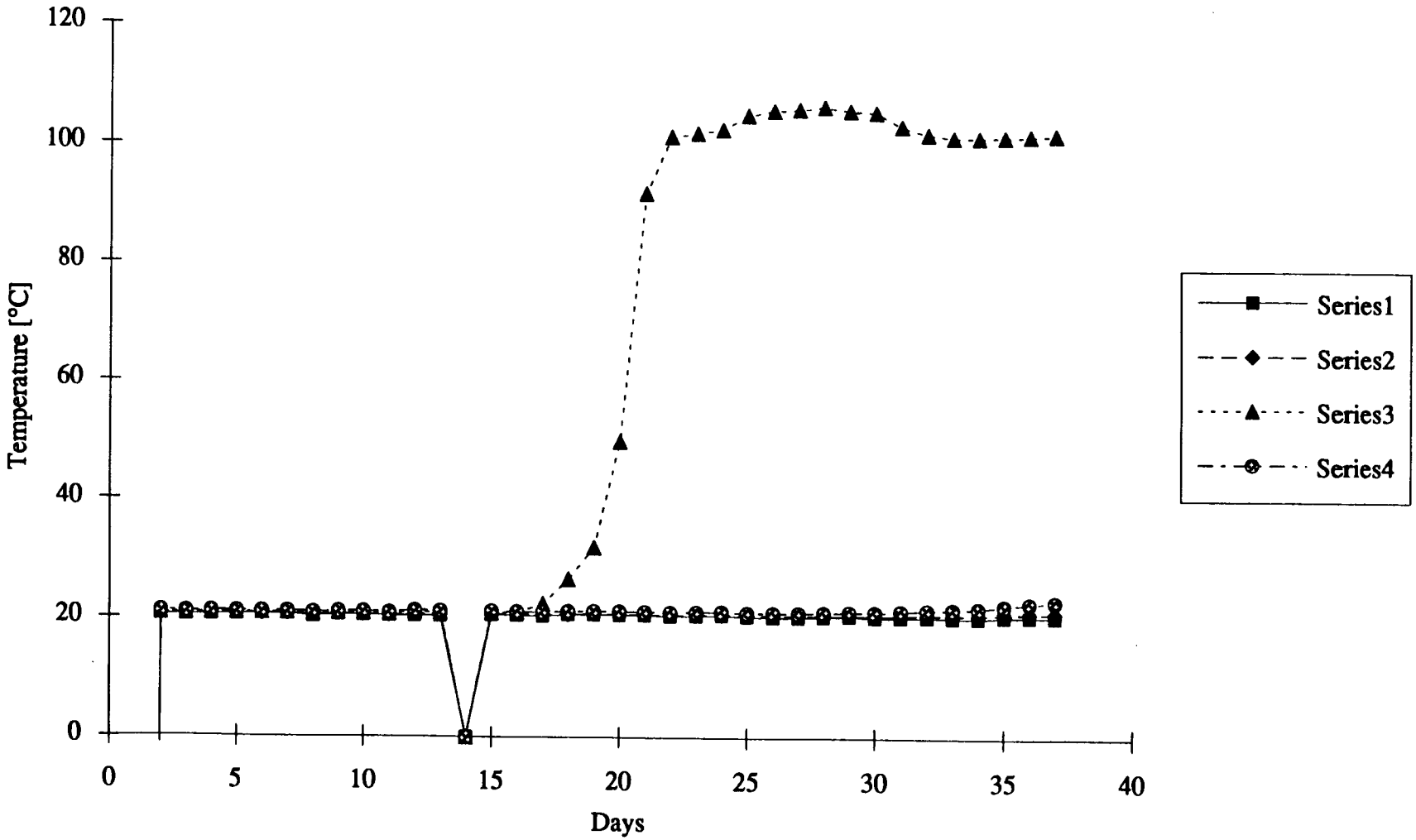

Figure A.5: Fixed Thermocouple Data for TEP5, Pass 1

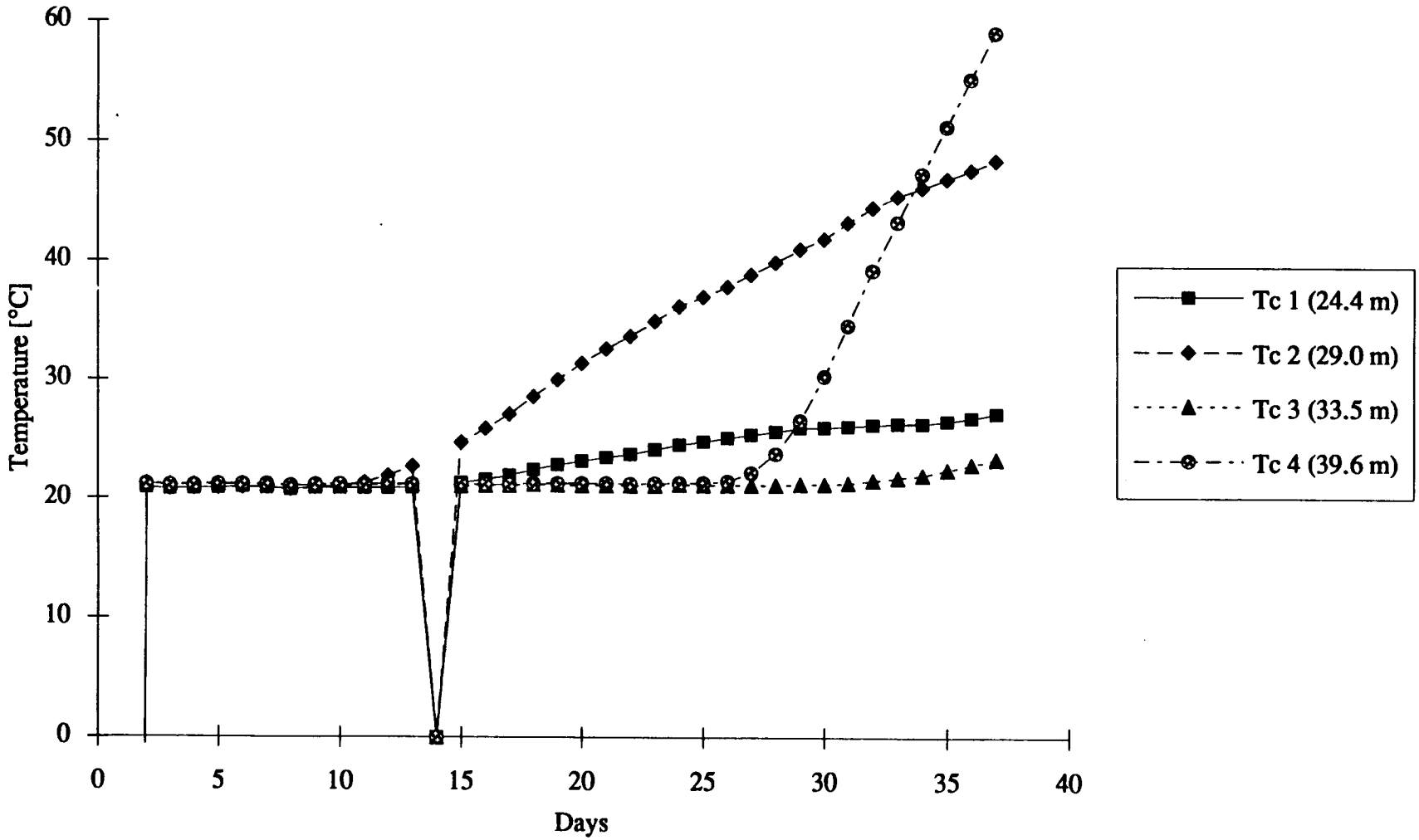

Figure A.6: Fixed Thermocouple Data for TEP6, Pass 1

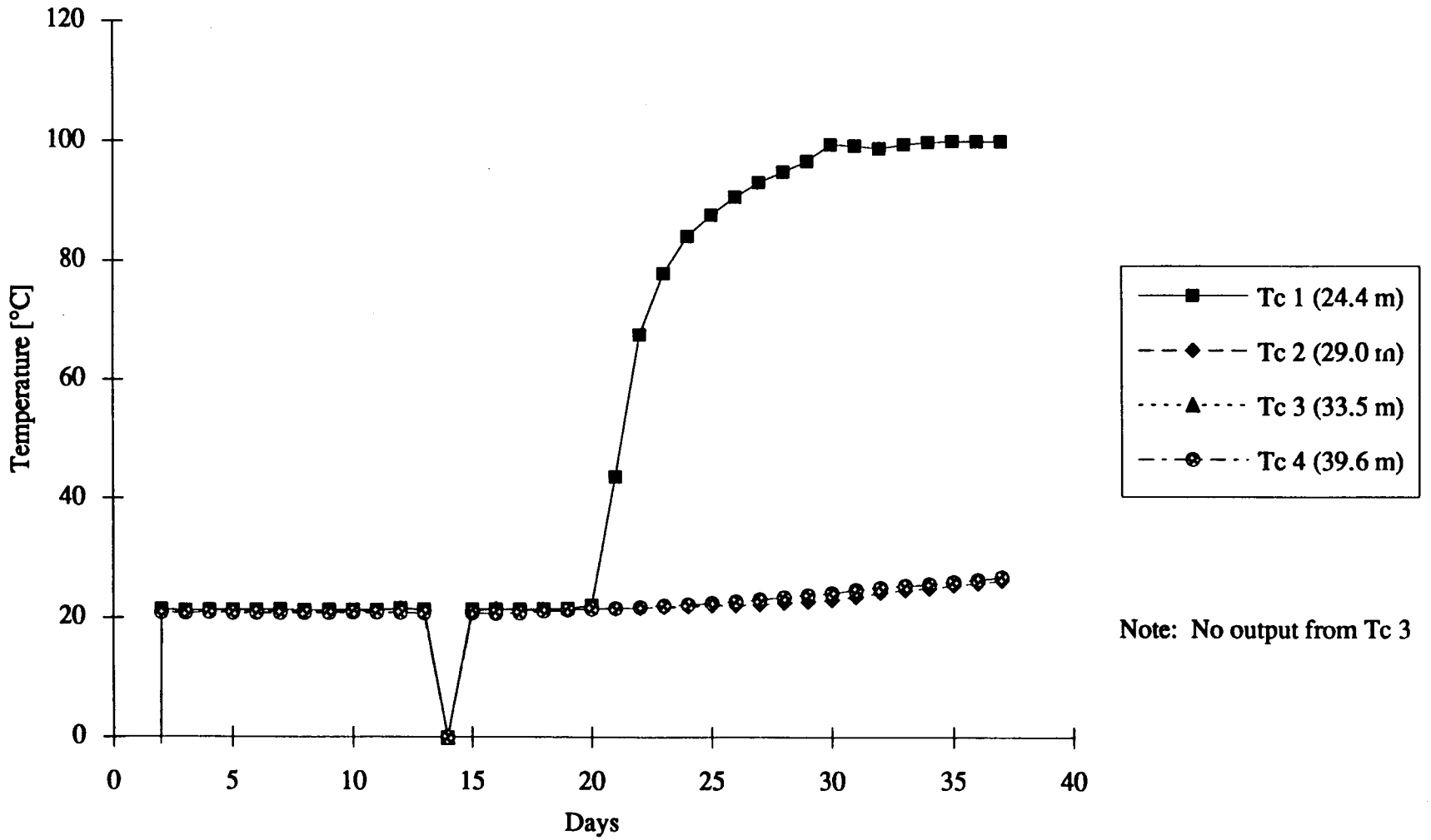

Note: No output from Tc 3

Figure A.7: Fixed Thermocouple Data for TEP7, Pass 2

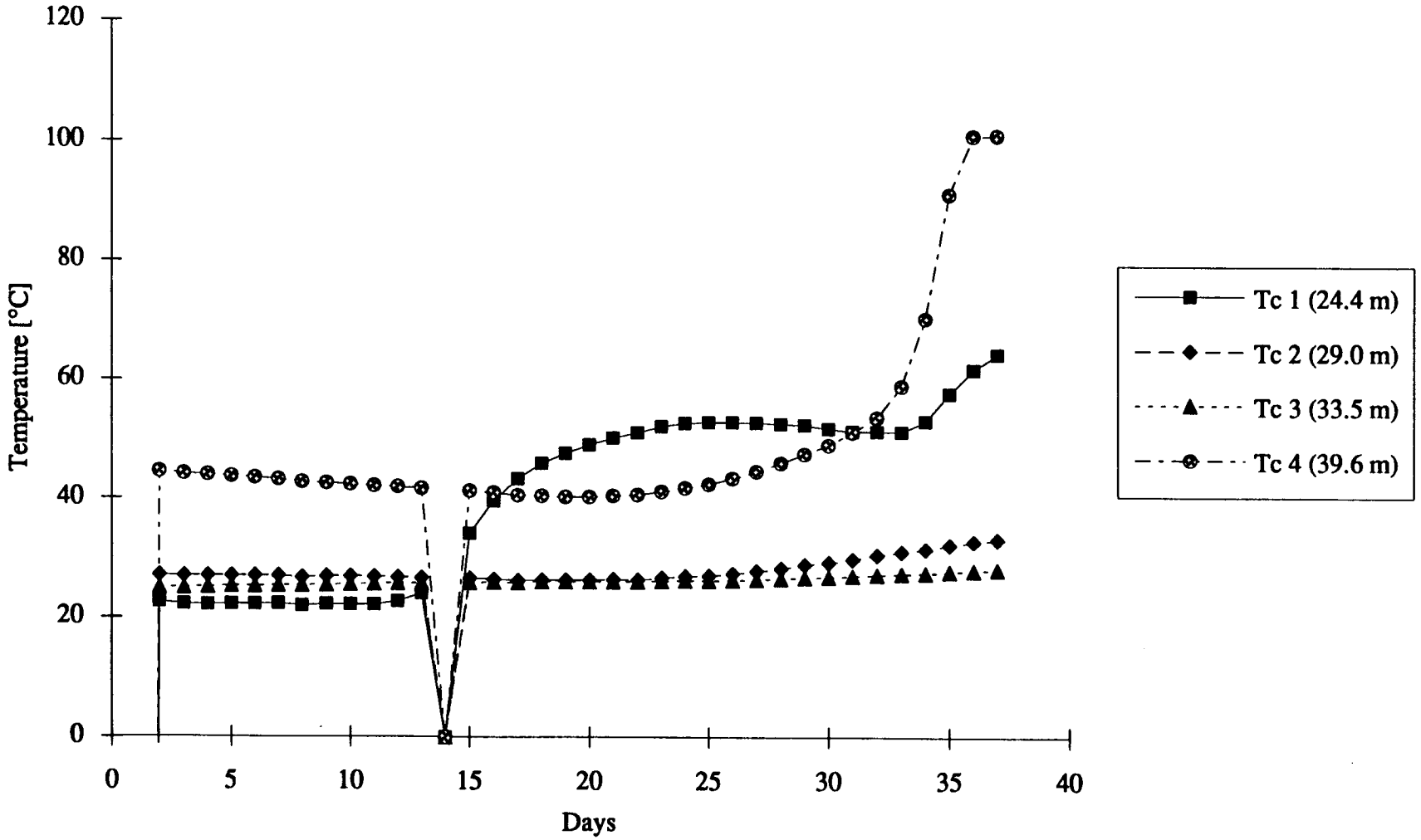

Figure A.8: Fixed Thermocouple Data for TEP8, Pass 1

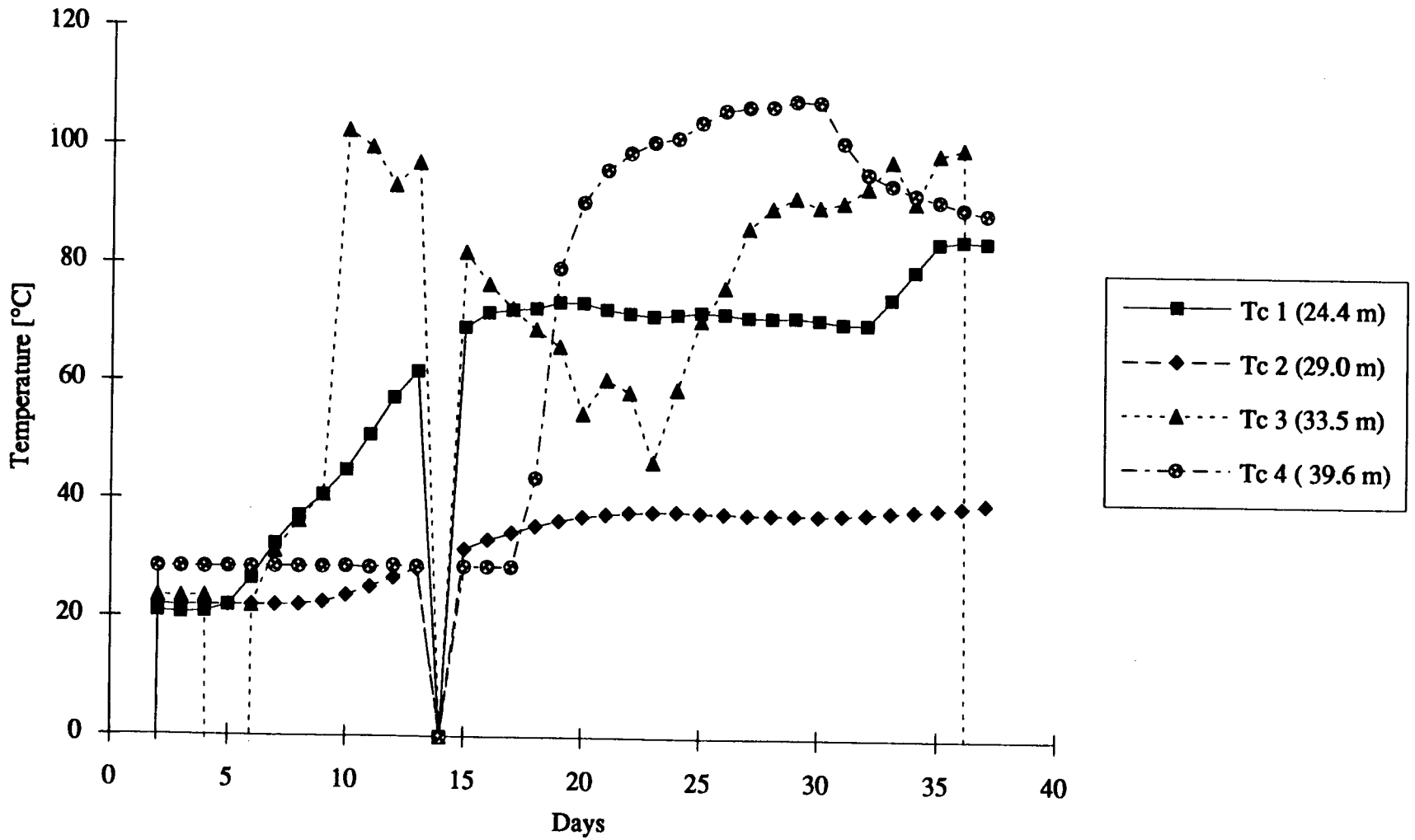

Figure A.9: Fixed Thermocouple Data for TEP9, Pass 1

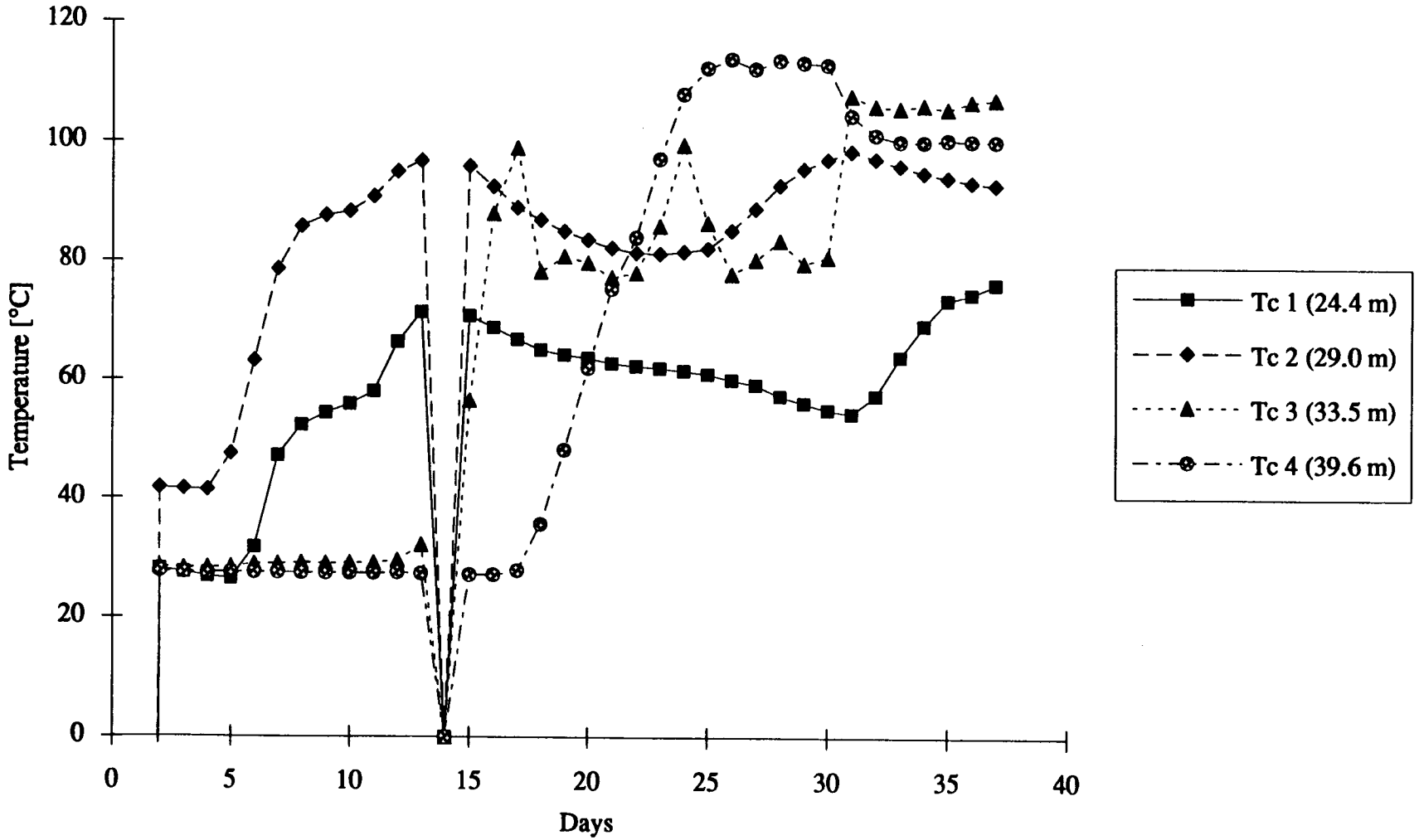

Figure A.10: Fixed Thermocouple Data for TEP10, Pass 1

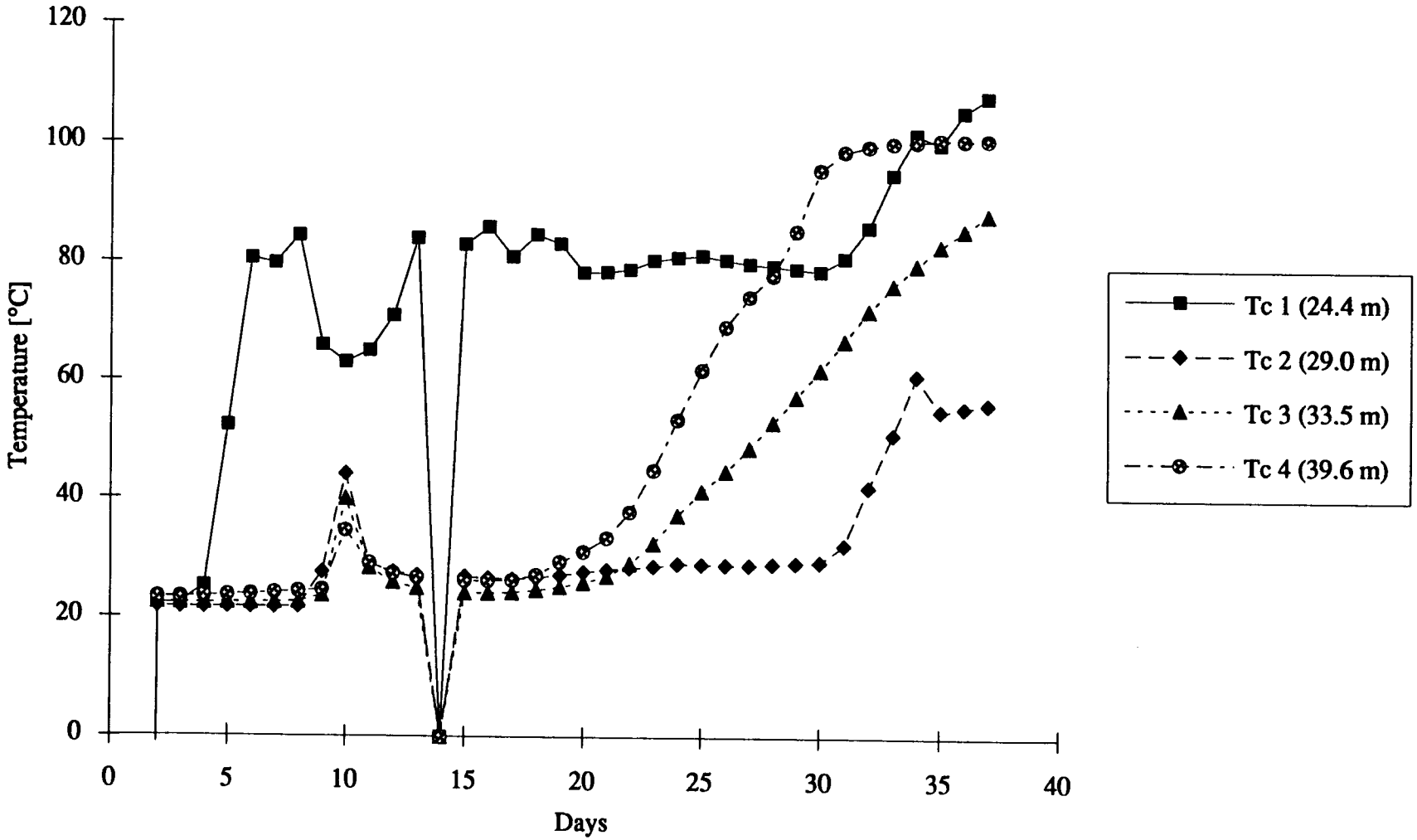

Figure A.11: Fixed Thermocouple Data for TEP11, Pass 1

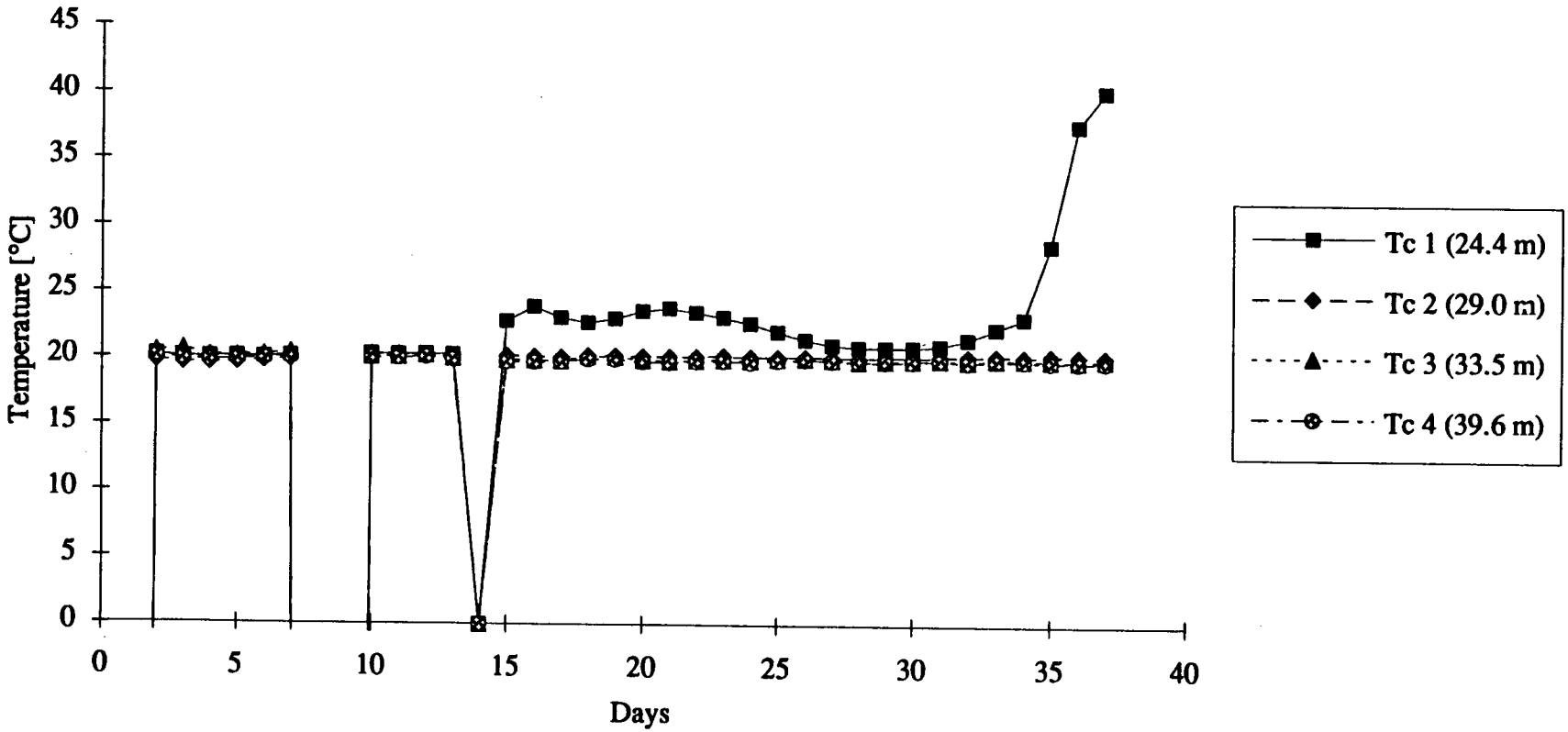

Figure A.12: Fixed Thermocouple Data for TEP1, Pass 2

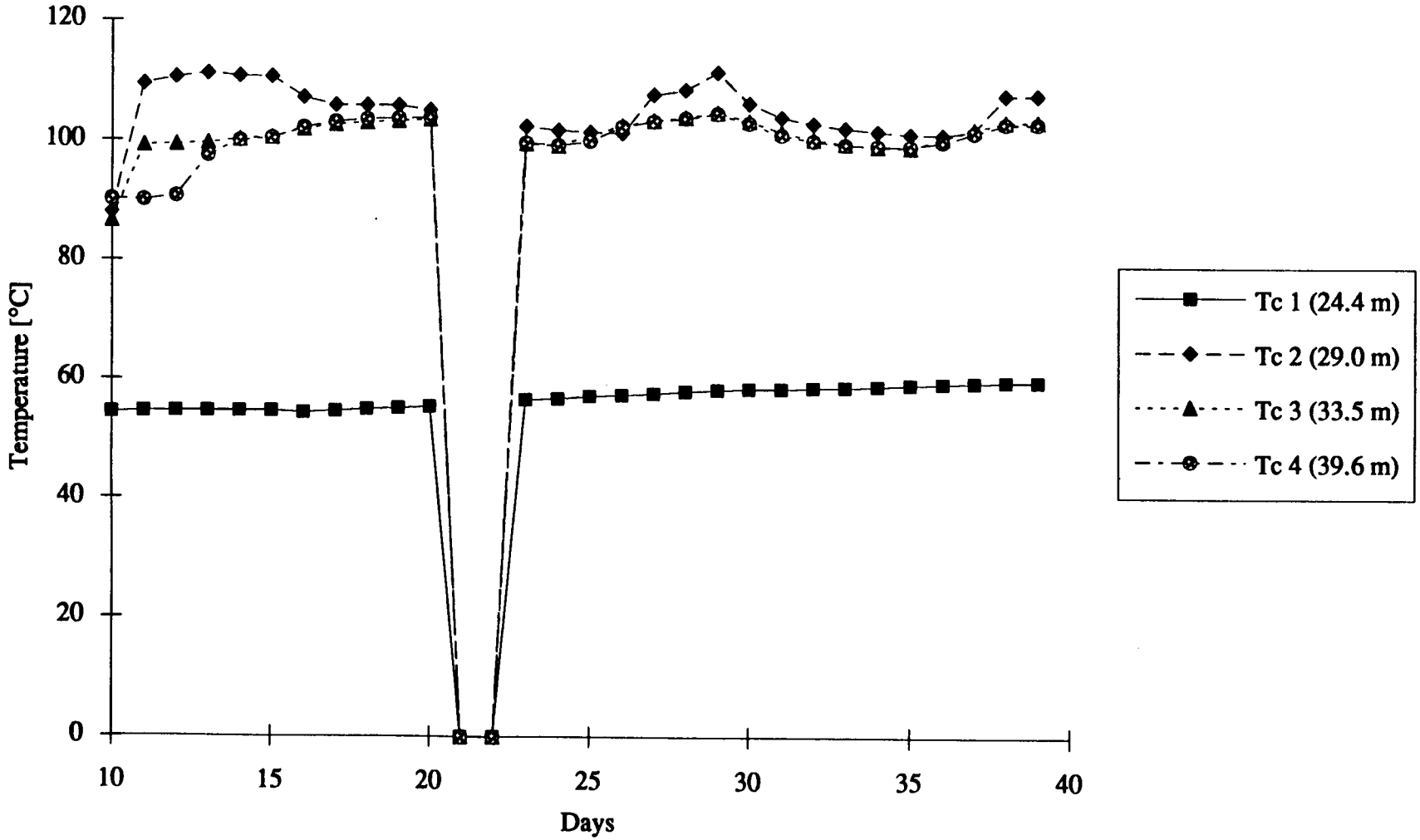

Figure A.13: Fixed Thermocouple Data for TEP2, Pass 2

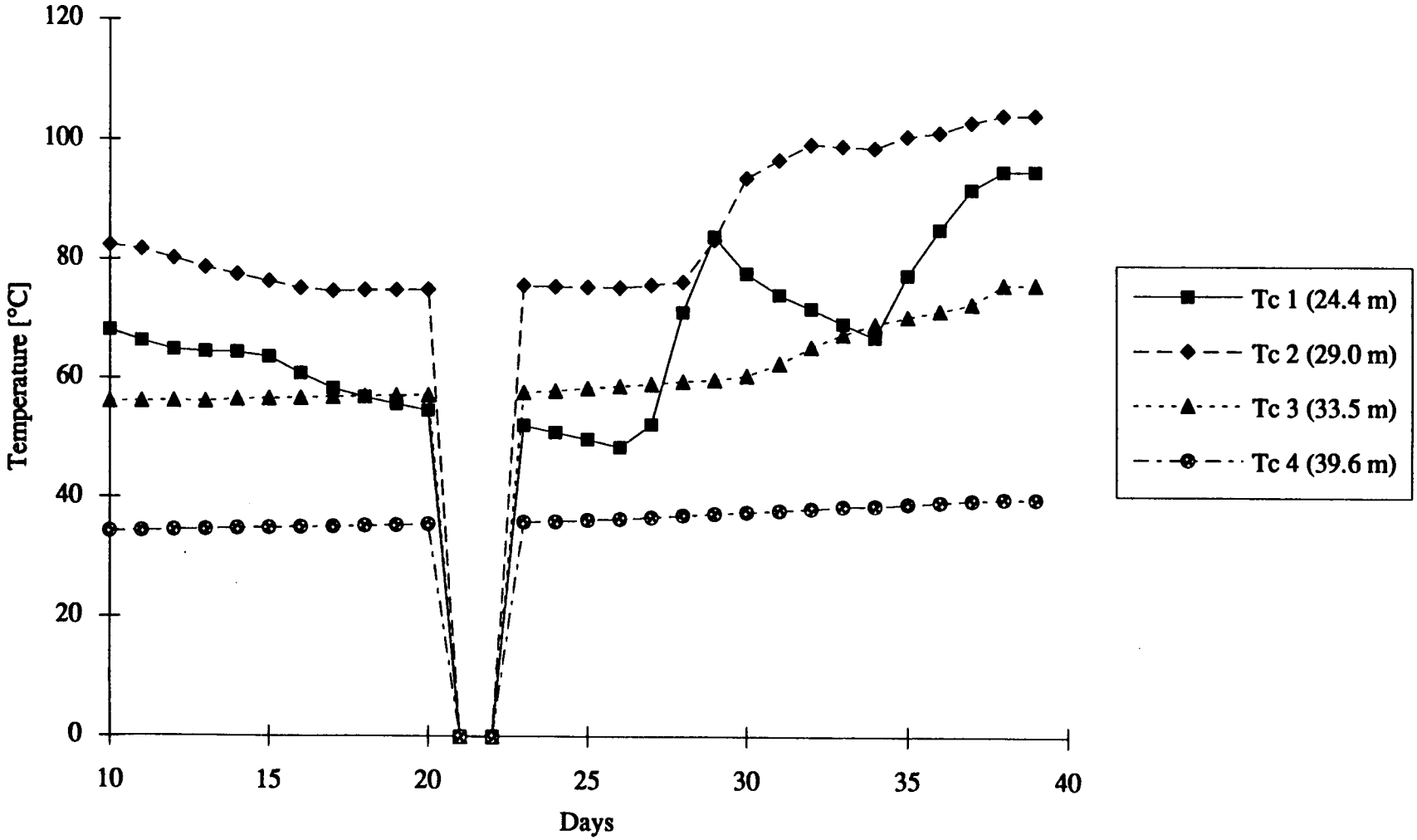

Figure A.14: Fixed Thermocouple Data for TEP3, Pass 2

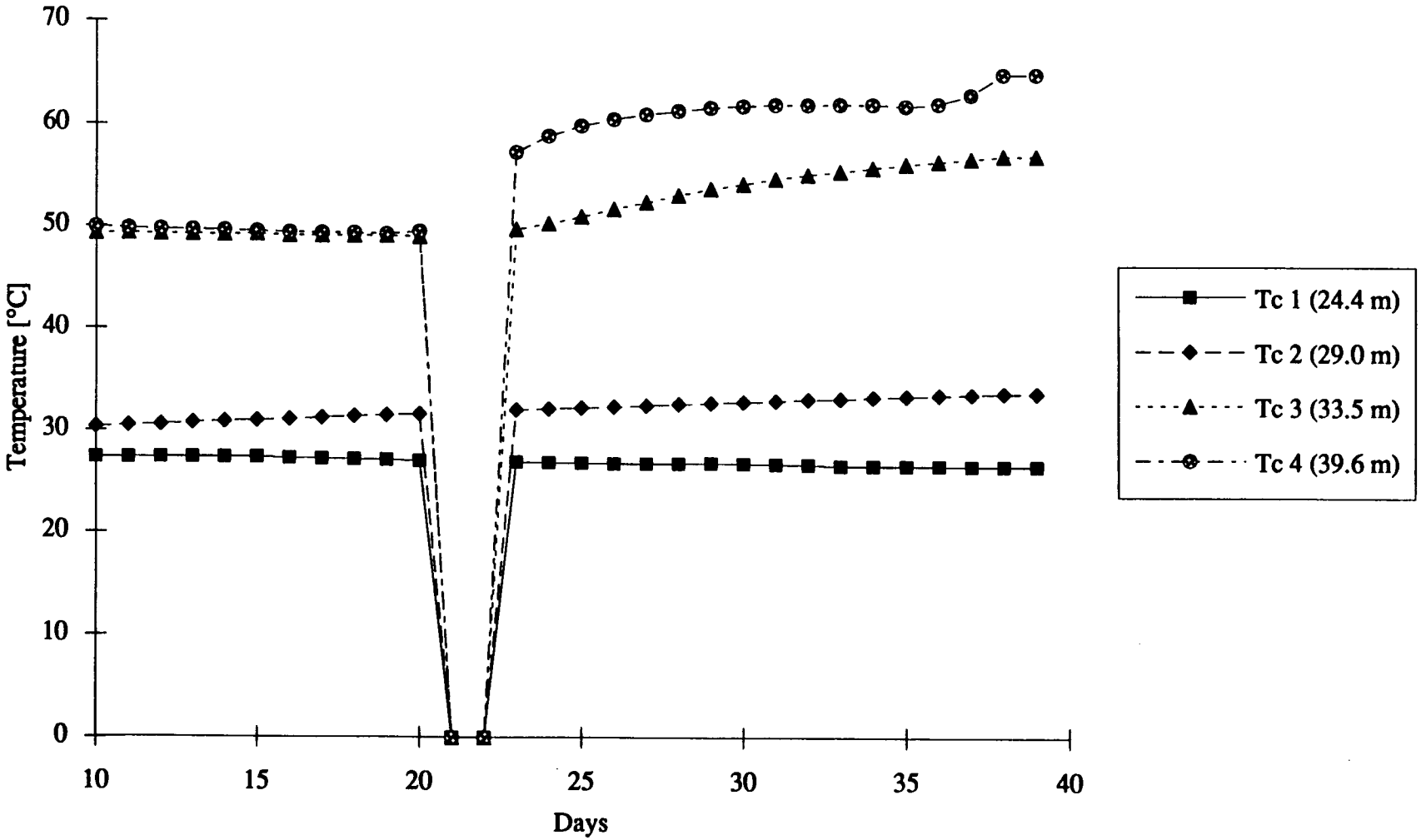

Figure A.15: Fixed Thermocouple Data for TEP4, Pass 2

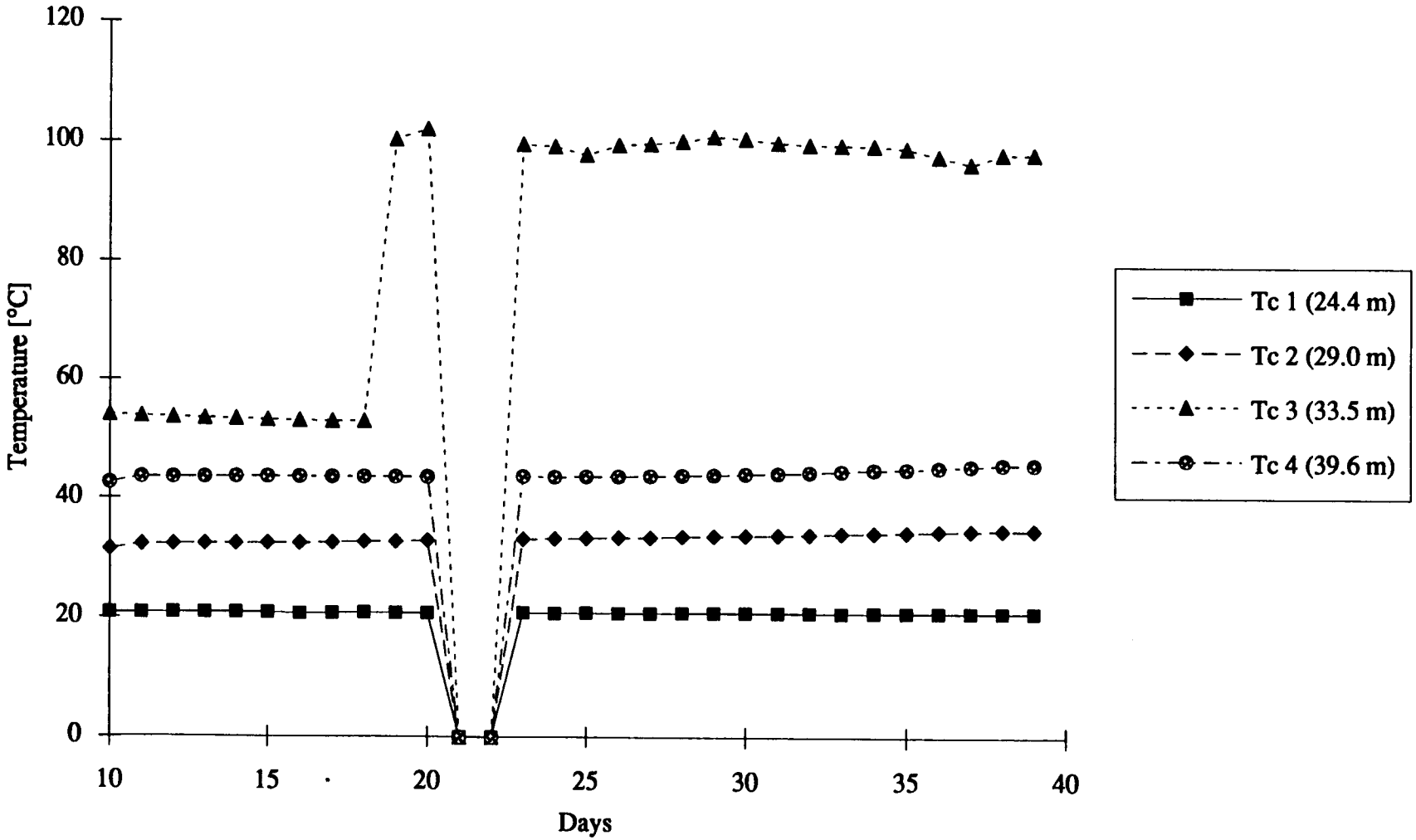

Figure A.16: Fixed Thermocouple Data for TEP5, Pass 2

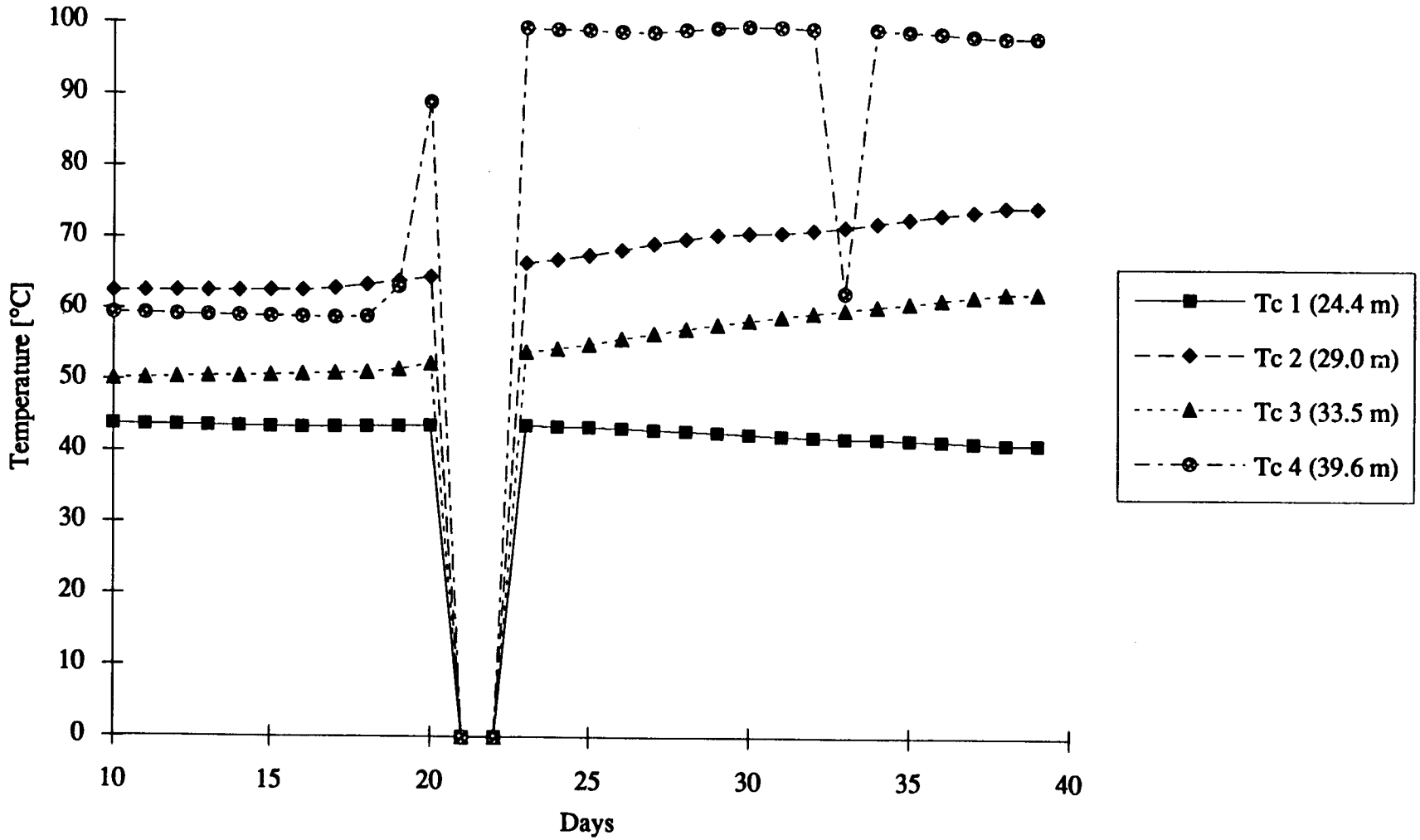

Figure A.17: Fixed Thermocouple Data for TEP6, Pass 2

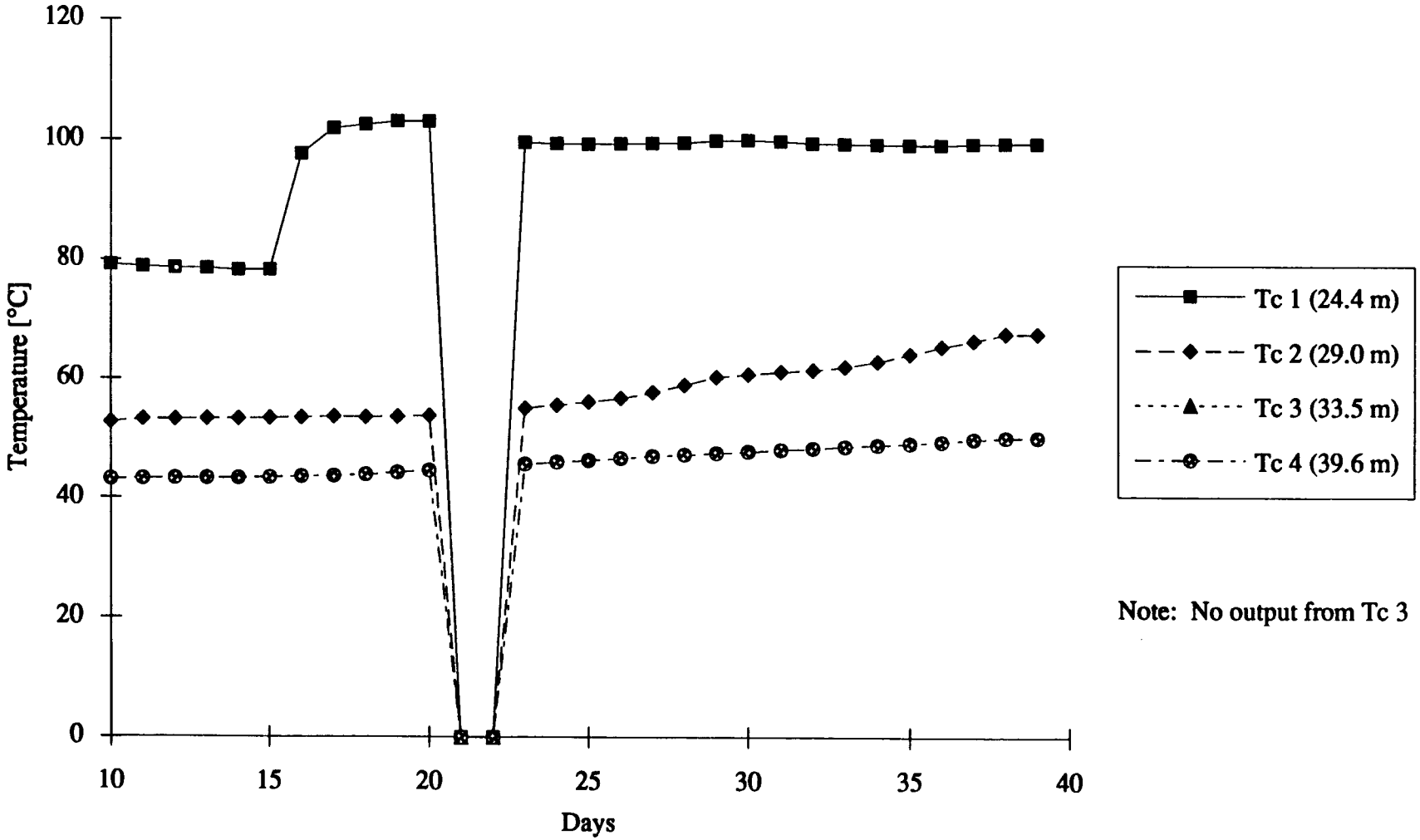

Figure A.18: Fixed Thermocouple Data for TEP7, Pass 2

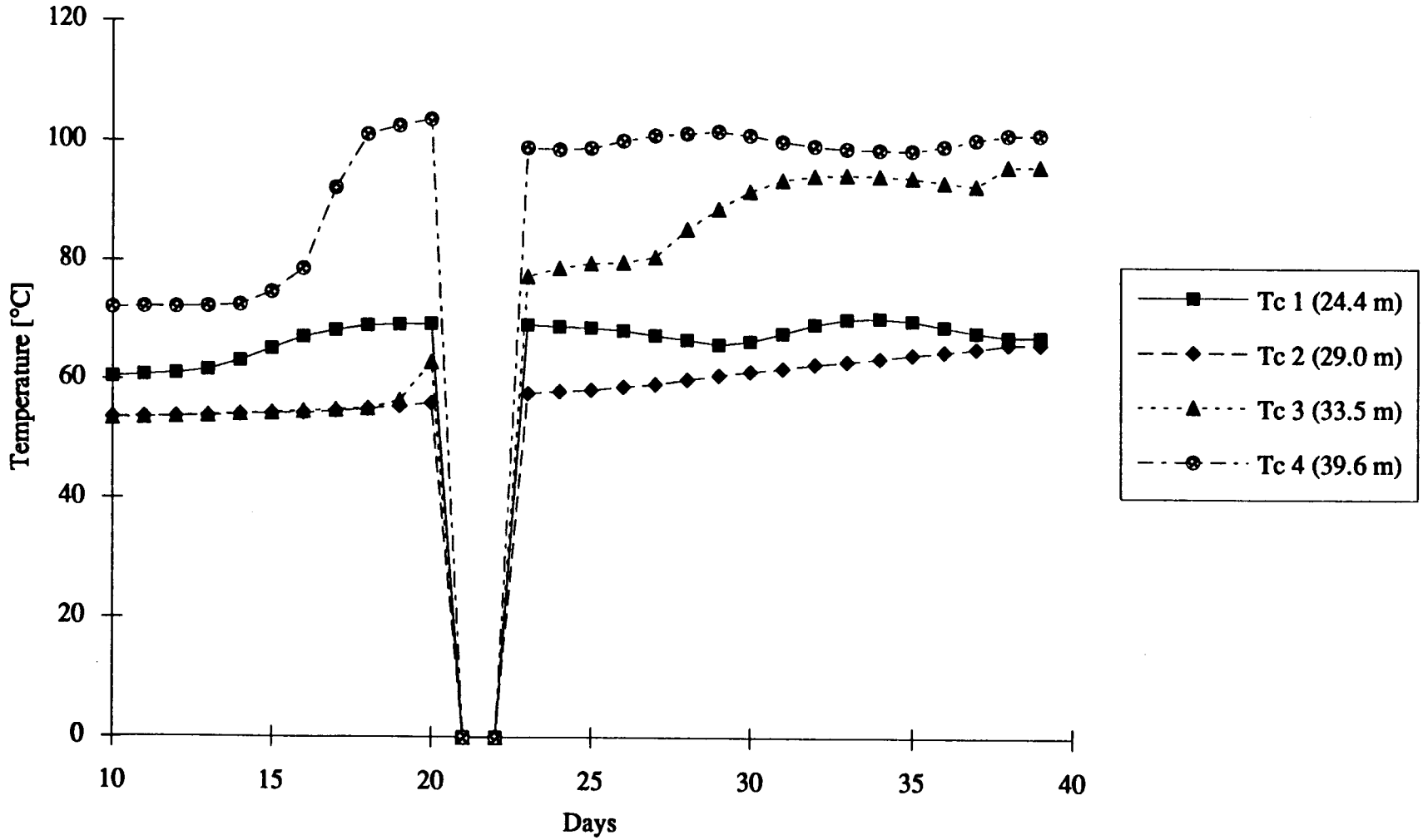

Figure A.19: Fixed Thermocouple Data for TEP8, Pass 2

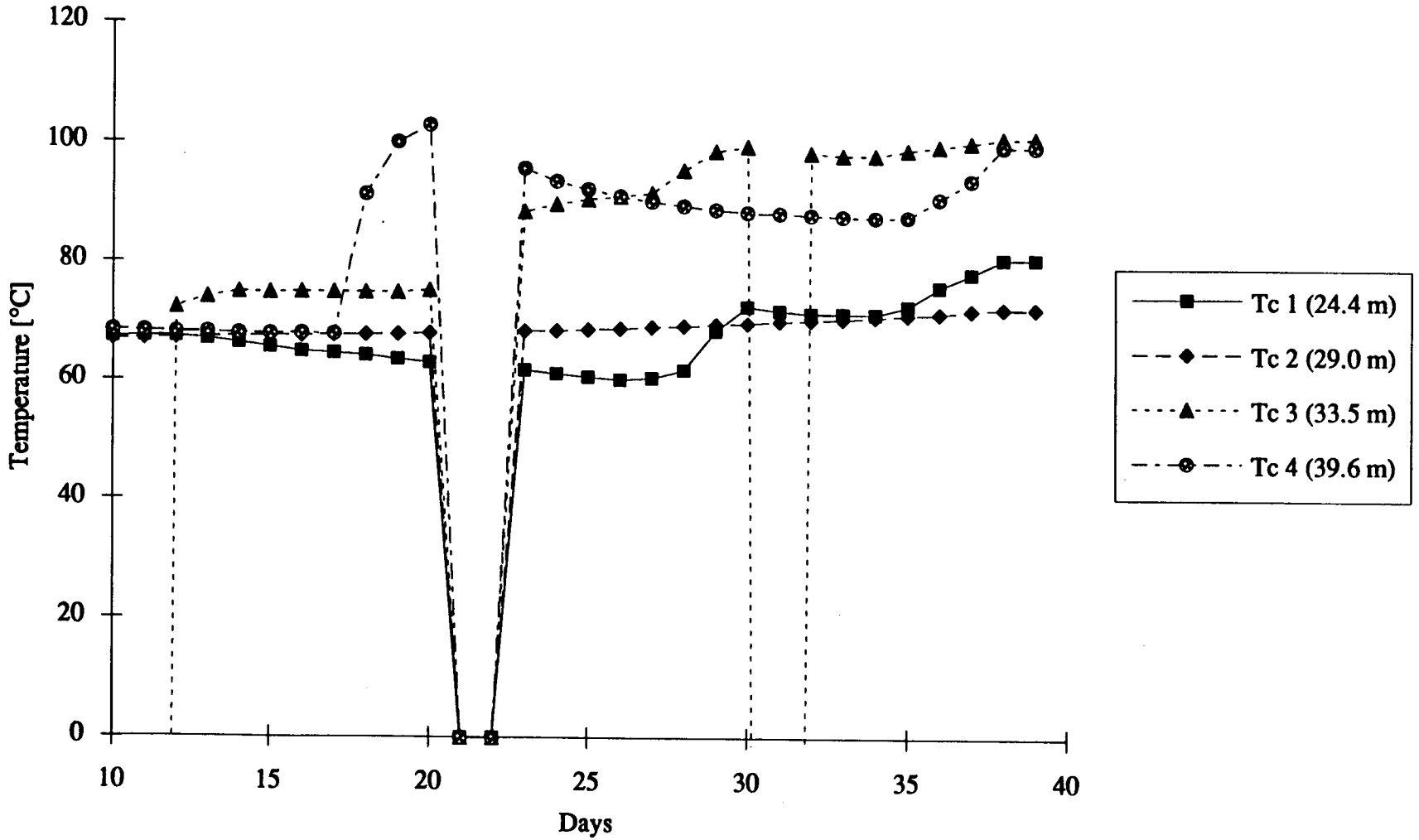

Figure A.20: Fixed Thermocouple Data for TEP9, Pass 2

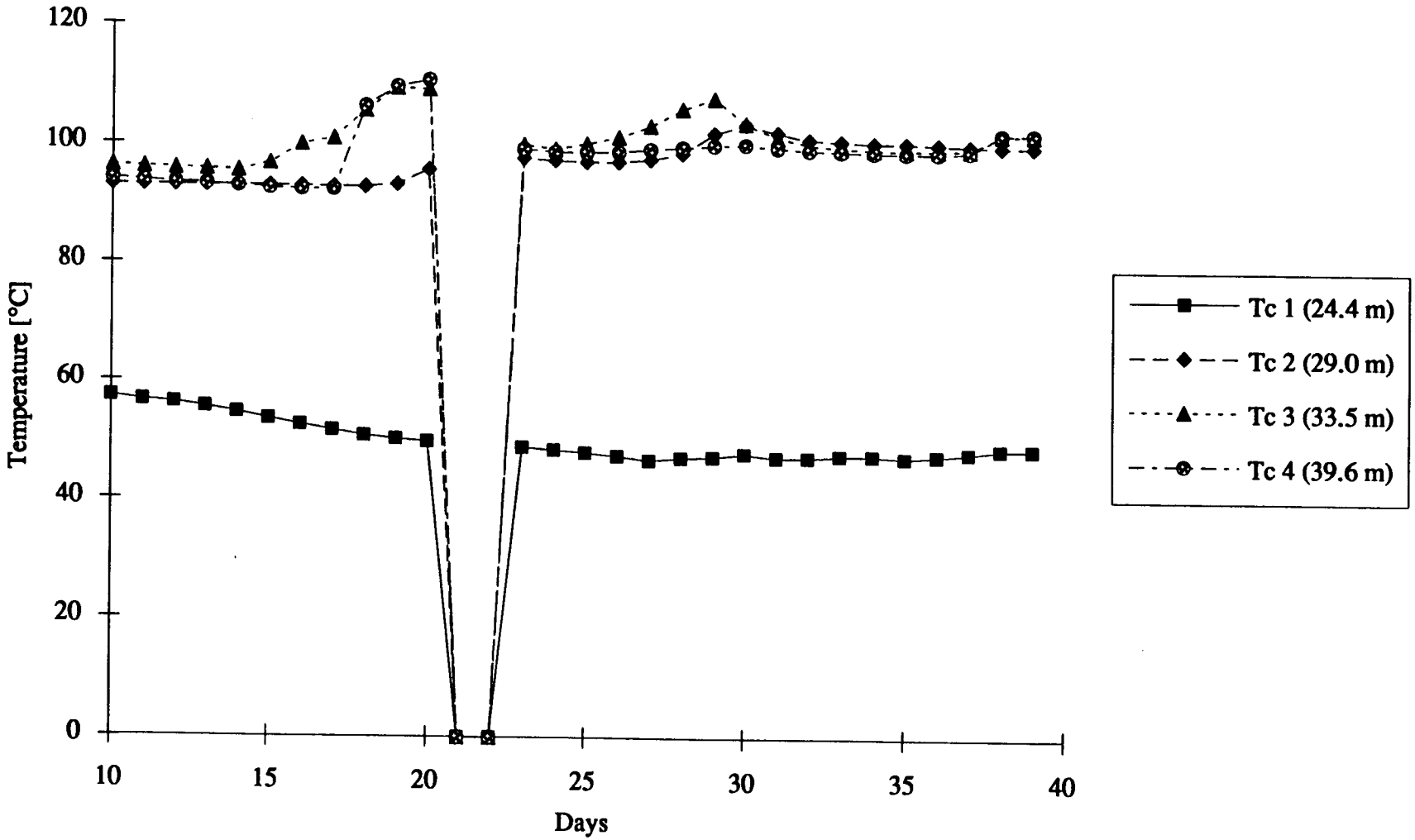

Figure A.21: Fixed Thermocouple Data for TEP10, Pass 2

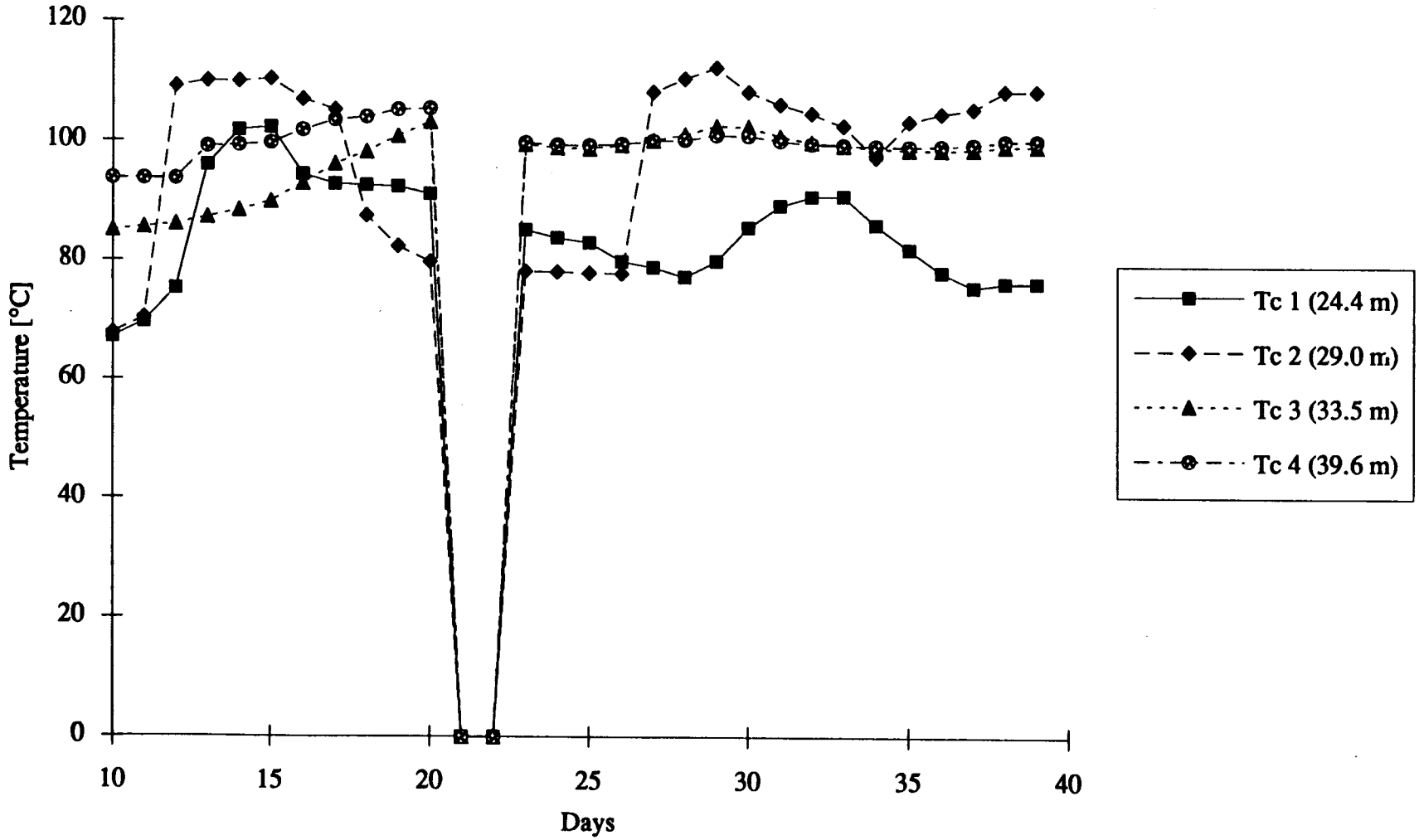

Figure A.22: Fixed Thermocouple Data for TEP11, Pass 2